TECHNISCHE UNIVERSITÄT MÜNCHEN
Lehrstuhl für Thermodynamik

Experimental Investigation of Developing Plug and Slug Flows

Edurne Carpintero Rogero

Vollständiger Abdruck der von der Fakultät für Maschinenwesen
der Technischen Universität München
zur Erlangung des akademischen Grades eines

DOKTOR INGENIEURS (DR.-ING.)

genehmigten Dissertation.

Vorsitzender: Univ.-Prof. Rafael Macian-Juan, Ph. D.
Prüfer der Dissertation:

1. Univ.-Prof. Dr.-Ing. Thomas Sattelmayer
2. Univ.-Prof. Dr.-Ing. Horst-Michael Prasser,
   Eidgenössische Technische Hochschule Zürich/ Schweiz

Die Dissertation wurde am 13.05.2009 bei der Technischen Universität München
eingereicht und durch die Fakultät für Maschinenwesen am 07.08.2009 angenommen.

A mis más admirados ejemplos de vida: a mis padres Jose y Petri.

A mi alegría diaria: a mi Andi.

Acknowledgement

Abstract

The scope of this thesis is to gain insight into gas-liquid intermittent flows. The chaotic distribution of turbulent interfaces between the different phases and a full understanding of their nature make the prediction of the flow characteristics and the numerical modelling of such flows a difficult and challenging task for researchers. In this work, particular efforts are devoted to the experimental investigation of developing intermittent flows (plug and slug flows) in horizontal pipes in order to attain a thorough physical understanding of the internal structure of these two-phase flow patterns. Experimental data is acquired with specific attention to the development of stratified and wavy flow regimes to intermittent flow regimes. The distribution of the phases, several relevant flow characteristics and the behaviour of the bubbles in the liquid phase are identified by means of wire-mesh sensor data. The main differences between plug and slug flow are elucidated and the influence of the slug void fraction on the characteristics of these flows as well as the behaviour of the dispersed bubbles in the slug body are analysed in detail. The simultaneous use of the Particle Image Velocimetry (PIV) technique and the Pulsed Shadowgraph (PS) technique for the acquisition of experimental data enables the calculation of the velocity field of the liquid phase. These techniques are adapted for horizontal two-phase pipe flows within this work, allowing the study of the kinematics of stratified, wavy, plug and slug flows. Turbulent quantities of these flows are also analysed.

Contents

List of Figures

List of Tables

Nomenclature

Roman Symbols

A	Pipe cross sectional area	[m^2]
B_0	Distribution parameter used by Zuber and Findlay	[-]
c	Speed of light	[m/s]
C	Shedding rate coefficient	[-]
C_0	Weighted velocity/liquid fraction distribution parameter	[-]
C_1	Weighted mean drift velocity proportionality constant	[-]
C_{Abd}	Coefficient used by Abdul-Majeed	[s/m]
C_{Chis}	Coefficient used by Chisholm	[-]
C_D	Drag coefficient	[-]
C_{DT}	Parameter used by Tomiyama	[-]
C_{int}	Interfacial shear stress coefficient	[kg/m^4]
C_{Maln}	Coefficient used by Malnes	[m/s]
D	Pipe diameter	[m]
E_w	Fraction of non-stratified liquid	[-]
f_W	Wall friction force	[N/m^3]
$f_{W,G}$	Gas wall friction factor	[-]
$f_{W,L}$	Liquid wall friction factor	[-]
g	Acceleration due to gravity	[m/s^2]
h	Liquid height	[m]
I	Relative intensity	[-]
j	Superficial velocity	[m/s]
k	Turbulent kinetic energy	[m^2/s^2]
l	Length	[m]
n	Current number of measurements/image/bubbles	[-]
n_{RI}	Refractive index	[-]
N	Total number of measurements/images/bubbles	[-]
p	Pressure	[Pa]
P	Perimeter	[m]
Q	Volumetric flow rate	[m^3/s]
r	Generic position	[m]
R	Radius	[m]
R_{corr}	Correlation coefficient	[-]
s	Sheltering coefficient	[-]
S	Slip ratio	[-]

t	Time	[s]
T	Period or time of passage	[s]
T_G	Gas temperature	[K]
T_L	Liquid temperature	[K]
u	Velocity	[m/s]
u_{mf}	Velocity below which no bubbles are present in the slug	[m/s]
u_{m0}	Term used by Andreussi and Bendiksen	[m/s]
u_r	Relative velocity	[m/s]
U_M	No-slip velocity, mixture velocity	[m/s]
V	Volume	[m^3]
x	Quality	[-]
$X_{Lock-Mart}$	Lockhart-Martinelli parameter	[-]
x, y, z	Coordinates	[m]

Greek Symbols

α	Volumetric phase fraction	[-]
β	Angle of pipe inclination	[°]
Δ	Difference	[-]
λ_L	No-slip hold-up	[-]
μ	Dynamic viscosity	[Pa $\cdot$ s]
ν	Frequency	[Hz]
ϕ	Lockhart and Martinelli two-phase multiplier	[-]
ρ	Density	[kg/m^3]
σ	Surface tension	[N/m]
τ	Interfacial friction	[N/m^3]
θ	Angle of incidence	[°]
θ^*	Angle of refraction	[°]

Superscripts

n	n-th iteration	
$\rightarrow$	Vector	
'	Fluctuation	
-	Mean value	

Subscripts

b	Slug tail
Bub	Bubble
$Chis$	Chisholm´s
CL	Collapsed liquid level
$crit$	Critical
d	Drift

f	Liquid film, film region
G	Gas phase
h	Hydraulic
i	Generic index
int	Interfacial
j	Generic index
k	Generic index
L	Liquid phase
Lock − Mart	Lockhart´s and Martinelli´s
M	Mixture phase
m	Average
n	Generic index, number of the current measurement/image/bubble
p	Generic index for slug tail or slug nose
r	Relative quantity between the phases
rms	Root mean square
s	Slug body, slug region
sample	Sampling
t	Slug front
Trans	Transition
tur	Turbulent
u	Slug unit
w	Wall

Dimensionless Numbers

Bo	Bond number
Eo	Eötvös number
Fr	Froude number
Re	Reynolds number
We	Weber number

Abbreviations

ATHLET	**A**nalysis of **TH**ermal-hydraulics of **LE**aks and**T**ransients
BWR	**B**oiling **W**ater **R**eactor
CFD	**C**omputational **F**luid **D**ynamics
CMFD	**C**omputational **M**ulti-**F**luid **D**ynamics
DNS	**D**irect **N**umerical **S**imulation
GRS	**G**esellschaft für Anlagen- und **R**eaktor**S**icherheit
IT	**I**nterface **T**racking
LED	**L**ight **E**mitting **D**iode
LES	**L**arge **E**ddy **S**imulation
LOCA	**L**oss **O**f **C**oolant **A**ccident

ODE	**O**rdinary **D**ifferential **E**quation
PIV	**P**article **I**mage **V**elocimetry
PMMA	**P**oly**M**ethyl **M**eth**A**crylate
PS	**P**ulsed **S**hadowgraph
PWR	**P**ressurized **W**ater **R**eactor
RANS	**R**eynolds **A**veraged **N**avier-**S**tokes
3D	Three **D**imensional
WMS	**W**ire-**M**esh **S**ensor

Mathematical Operators

d	Differential
∂	Partial differential
σ_i	Standard deviation

1 Introduction

1.1 Background

The study of two-phase flows has great significance for several technological applications. In particular, gas-liquid two-phase flows are often encountered in a wide range of industrial applications, such as condensers, evaporators, distillation towers, nuclear power plants, boilers, crude oil transportation and chemical plants among others. Gas-liquid flow is not only the most common of the two-phase flows, it is also the most complex since it combines the characteristics of a deformable interface with those of a compressible phase. The transportation of gas and liquid in conducts can lead to several topological configurations called flow patterns or flow regimes.

The use of numerical flow simulation has increased in the last years. Numerical predictions of the transient behaviour of two-phase flows become more affordable and more indispensable. Open questions regarding the optimization, interpretation and security of two-phase flow technical plants and components, especially for nuclear reactor systems and chemical technology, can be answered using this approach. However, the development of computational codes for the simulation of two-phase flows relies heavily on the physical understanding of the two-phase flow phenomena, such as phase distribution, interfacial structure development, bubble interactions, two-phase flow turbulence, boiling and condensation, etc. To gain insight into these phenomena and to further enhance the capabilities of numerical simulation, detailed and critical observations of the flow structure and its evolution are essential. Local and temporal high resolution information about two-phase flows is needed for a successful detailed modelling.

1.2 Two-Phase Flows in Horizontal Pipes

Several authors have written books about two-phase flows in the last decades, e.g. Wallis [1969], Mayinger [1982], Chisholm [1983] or more recently Kolev [2007]. Part of the definition of the flow regime is a description of the morphological arrangement of the components, or flow pattern. Gas and liquid flow in horizontal pipes shows a number of different interfacial configurations. Classification and description of the flow distributions into different patterns are frequently very subjective. The more common air-water flow patterns which are encountered in co-current horizontal flow are shown in figure 1.1.

At high liquid flow rates and for a wide range of gas flow rates, small gas bubbles are dispersed throughout the continuous liquid phase (bubble flow or also called dispersed flow). These bubbles tend to concentrate in the upper part of the tube due to buoyancy.

For relatively low gas and liquid rates, a stratified configuration occurs, whereby the liquid flows along the bottom of the pipe and the gas flows above it. An increase of the gas flow rate at a constant liquid flow rate causes this stratified flow to change to a wavy flow. At still higher liquid velocities, the waves can grow to the top of the pipe and, intermittently, form liquid blockages. This intermittent pattern is subdivided into plug and slug flow patterns. When the liquid slug body is almost free of gas bubbles, the pattern is termed as plug flow (or also called elongated bubble flow). It occurs at very low gas velocities and consists of elongated gas bubbles that move along the top of the pipe. Slug flow is found at higher gas velocities; it is a stratified flow with the intermittent appearance of high-velocity liquid slugs, which bridge the whole pipe and which can be highly aerated. The intermittent regime is often extended to include semi-slug flow in which there are
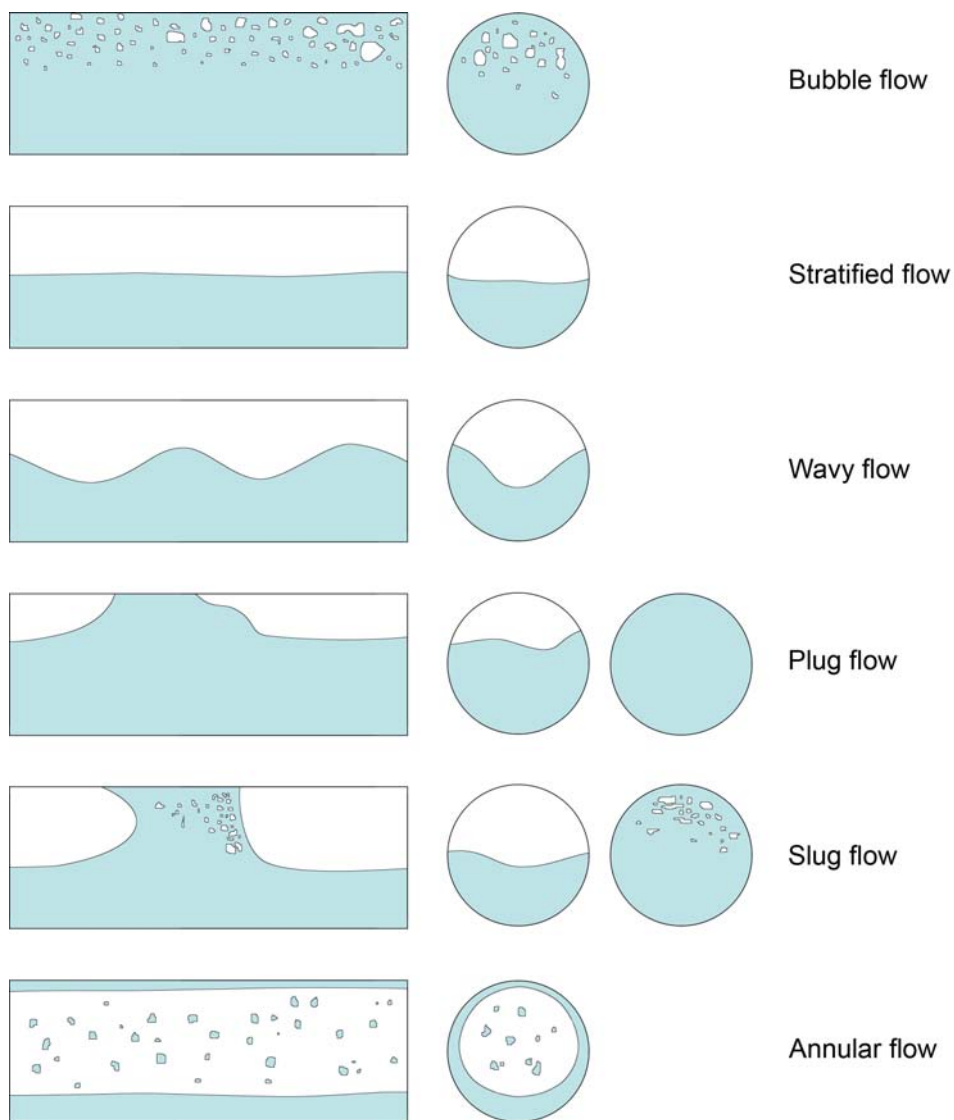
Figure 1.1: Flow patterns in horizontal pipes.

large surges of liquid that do not fill the whole pipe cross section. For higher gas flow rates, the liquid tends to form a ring or annulus around the tube wall. Due to gravity, the liquid film at the bottom of the tube may be much thicker than the film at the top. Small droplets entrain into the gas core.

Several flow regime maps have been developed to describe two-phase flow patterns and flow transitions. The probably first flow map for horizontal pipes was proposed by Baker [1954]. In the following years, different flow maps purely based on experimental observations were developed, for example the flow maps of Mandhane et al. [1974] and Barnea [1987] among others for horizontal co-current flow. A mechanistic model to predict flow pattern transitions in horizontal pipes was first made by Taitel and Dukler [1976]. Many of these flow maps have wide industrial applications; although extremely useful, they are not adequate to define the regime completely because of additional distinguishing criteria, such as the difference between laminar and turbulent flow or the relative importance of various forces. Figure 1.2 shows the flow map according to Mandhane et al. [1974], where the superficial velocities (see section 2.1 for definition) of the gas and liquid phase are represented by the abscissa and the ordinate, respectively. Depending on these velocities, the flow pattern which occurs can be identified. By the use of such maps, on which only the boundary lines appear, it is important to note that a few experimental points may lie on the wrong side of these lines. These lines would be better regarded as transition zones of indeterminate width.
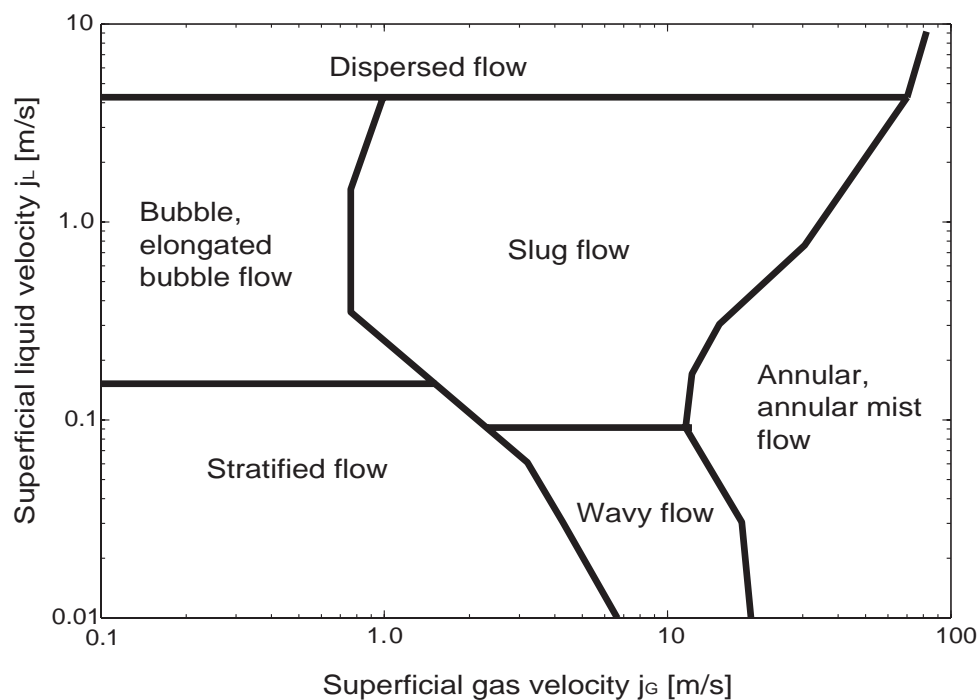
Figure 1.2: Flow pattern map proposed by Mandhane et al. [1974].

1.2.1 Models in Two-Phase Flows

Two-phase flows obey all of the basic laws of fluid mechanics. Navier-Stokes equations are valid within each region. However, the presence of a deformable gas-liquid interface leads to a limitless number of different interface configurations. Therefore, the equations are more complicated or more numerous than those of single-phase flows.

There are two main formulation methods for deriving equations that describe two-phase flows. The first is the Eulerian-Lagrangian formulation, where the dispersed phase is treated from a Lagrangian point of view in which the particles are tracked. The continuous phase is seen from an Eulerian point of view with the effect of the dispersed phase entering through source terms in the conservation equations. This method is physically intuitive but is not computationally practical for other than very dilute dispersed phases.

In the Eulerian framework, there are three main ways in which one can approach the modelling of two-phase flows: the homogeneous model, the drift flux model and the separated or two-fluid model. The simplest formulation is to consider the two-phase fluid as a homogeneous mixture, which has some pseudo properties of a single phase fluid. The most complex approach is to consider the two phases separately and to write a set of conservation equations for each phase.

1.2.1.1 Homogeneous Model

The homogeneous model considers the two-phase mixture to be a single fluid with pseudo properties. These properties are weighted by the volumetric fraction of each phase. The average properties which are normally required are the velocity, thermodynamic properties (e.g. temperature and density) and transport properties (e.g. viscosity). These models do not consider the exchange of momentum, heat and mass transfer between the phases. It is assumed that these processes proceed fast enough to reach equilibrium. This is the case when one phase is finely dispersed in the other (e.g. high pressure bubbly flow). In many other cases the use of homogeneous theory is obviously inappropriate [Wallis, 1969].

1.2.1.2 Drift Flux Model

Differences in velocity, temperature and chemical potential between the phases promote mutual momentum and heat and mass transfer. The drift-flux formulation accounts for velocity differences between the phases. It is basically a separated-flow model in which the relative motion is determined with the help of a continuity equation for each phase and a momentum equation for the mixture. The two continuity equations do not use the same velocity. The momentum equation requires an algebraic correlation or a sub-model for the calculation of the relative velocities. This theory is especially convenient for analysing flow regimes in which gravity (or some other body force) is balanced by the pressure gradient and the forces between the components [Wallis, 1969].

1.2.1.3 Separated or Two-Fluid Model

The separated flow model accounts for different velocities and properties of the phases. This approach can be made with several degrees of complexity. In the most complicated version (the six equation, two-fluid model), separate equations of continuity, momentum and energy are written for each phase and resolved simultaneously. However, these equations are not a complete description of a multiphase flow. For closure reasons, they need to be supplemented by suitable constitutive relationships, which describe how the phases interact with each other. Using this model, improved descriptions of transient behaviour can be obtained and departures from equilibrium between the phases can be captured. However, the description of a system by only six equations may be inadequate, e.g. annular flow with significant liquid entrainment, in which it may be more appropriate to write a further set of balance equations describing the entrained droplets; this would result in a nine equation model [Hewitt, 2002].

1.2.2 Simulation Tools

The simulation tools available today can be classified into four main groups. In general, they differ with respect to the turbulence modelling and the spatial resolution of the calculation region.

1.2.2.1 System Codes

Several studies on transient two-phase flows have been intensively conducted in the nuclear industry, since it has become indispensable to predict the transient flow behaviour during potential loss of coolant accidents (LOCAs) for licensing pressurized water reactors (PWRs) and boiling water reactors (BWRs). To further develop the methodology for the calculation of transients and accidents in nuclear power plants, several thermal hydraulic system codes using a six-equation, two-fluid model, such as RELAP (deriving from the Idaho National Energy Laboratory, Idaho, USA), TRAC (developed at the Los Alamos National Laboratory, New Mexico, USA), CATHARE (from the Centre d'Etudes Nucleaires, Grenoble, France) and ATHLET (developed by the Gesellschaft für Anlagen- und Reaktorsicherheit, Germany) were developed. These codes, the so-called system codes, predict the behaviour of highly complex systems with many interacting components, and many of them include the associated nuclear physics and chemistry. The system codes balance continuity, momentum and energy for both phases in the Eulerian frame of reference. In these equations, viscosity and turbulence are not taken into consideration. The additional pressure losses due to "internal friction" are modelled as "wall friction". On the basis of the 1D-treatment alone, these codes show a limited possibility for the resolution of 2D and 3D-problems, but this can be compensated by adding suitable 2D and 3D-modules. They do not usually attempt to predict the detailed flow characteristics (temperature, pressure, volume fraction or velocity fields) within a given component, but work

by involving suitable closure relationships, which are often based on empirical correlations of experimental data. Such codes are frequently used for reactor safety.

1.2.2.2 Direct Numerical Simulation

The "direct numerical simulation" (DNS) solves numerically the Navier-Stokes equations without any turbulence model. This means that the whole range of spatial and temporal scales of the turbulence must be resolved. All spatial scales of the turbulence must be resolved within the computational mesh (the resolved length scale must be in the dimension of the Kolmogorov length scale), which leads to a very fine discretisation. Therefore, such calculations are extremely time-consuming, making the practical application in reactor safety impossible.

1.2.2.3 Large Eddy Simulation

A little coarser discretisation is permitted by the "large eddy simulation" (LES), where only the big eddys are simulated directly, while the unresolved fine structure of the turbulence, the so-called subgrid-scale structure, is described by models. The practical applicability in reactor safety is out of the question using this approach, since the required resolution is very fine.

Till now, there are no commercial DNS or LES tools for two-phase flows.

1.2.2.4 Reynolds Averaged Navier-Stokes

The "Reynolds averaged Navier-Stokes" (RANS) equations do not resolve any turbulence structures. Turbulence must be decribed by models. The quantities are expressed as the sum of a mean and a fluctuating part. Generic computational fluid dynamics (CFD) codes, such as CFX, FLUENT and PHOENICS, have been used for the simulation of transient phenomena in the field of nuclear reactors. These codes were originally written for single phase flows, currently they include different two-phase models. They solve the ensemble averaged Navier-Stokes equations and incorporate detailed models for fluid turbulence. These codes are able to give much more detailed characteristics of the two-phase flow field compared with the nuclear system codes. However, several models used in these codes are empirical in nature, employing a variety of fitted constants. Empirical and mechanistic models are sometimes extrapolated to situations outside the range of data for which they were derived.

In the future, computational multifluid dynamics (CMFD) methods will be wide spread, where CFD and interface tracking (IT) methods are combined; being able to solve 3D problems while tracking the configuration of the phases.

1.3 Present Contribution

In order to gain insight into the two-phase flow phenomena and to develop numerical codes more accurately, great efforts have been made in the past four decades to establish a database, as well as to develop new instrumentation. However, further experimental work is necessary to attain a thorough physical understanding of the internal structure of the different two-phase flow patterns.

Transient phenomena are frequently encountered in pipelines. They can occur either due to changes in operating conditions, such as a change in inlet flow rates, exit pressures (imposed transients) or from induced terrain slugging (these are natural transients due to the pipe geometry). A good knowledge of the flow characteristics, such as the operating flow regime, the pressure drop, the liquid holdup or the maximum slug length is very important to properly design two-phase flow lines, fluid treating, separation facilities or for the safety of nuclear reactors. The prediction of these flow characteristics and the numerical modelling of such flows remain a difficult and challenging task for researchers, mainly due to the chaotic distribution of turbulent interfaces between the different phases.

From a practical point of view, slug flow is one of the most interesting flow regimes of two-phase flows in horizontal pipes since the rapid transport of large liquid slugs may lead to equipment vibration and the possible influence of the slugs on the overall behaviour in subsequent components. On the other hand, intermittent flows are particularly challenging for computational schemes, and resolving them accurately will not only improve our understanding of gas-liquid flows but also provide a reliable tool for future prediction. In this work, particular efforts will be devoted to the investigation of the development of stratified and wavy flow regimes to intermittent flow regimes in horizontal pipes.

The capability of a nuclear system code of predicting transient gas-liquid flows in horizontal pipes will be assessed. Particularly, a study of the feasibility and accuracy of ATHLET 2.1A simulations for an adiabatic air-water intermittent flow in horizontal pipes will be carried out. The following issues will be analysed:

   ▷ Accuracy of the prediction of stratified, wavy and intermittent flow characteristics.

   ▷ Accuracy of the prediction of the flow pattern transition.

   ▷ Influence of the node size on the predicted flow characteristics.

   ▷ Impact of steady/unsteady inlet boundary conditions on the predictions.

In experimental studies of hydrodynamic slugging, it is common practice to design the entrance of the fluids into the pipe so that a stratified flow configuration occurs. With such a configuration at the pipe entrance, slugs originate from waves at the gas-liquid interface that grow to fill the pipe cross section. The two-phase mixing section designed within this work ensures an initially stratified flow regime. Moreover, it is important to note that a careful design of the experimental facility is carried out. The regulation of the gas-liquid flow rates and the two-phase mixing section, which define initial and boundary conditions of the experiment, are designed to achieve results of clearly defined and quantified flow

patterns. This allows the boundary conditions of the different test cases to behave equally in the experiment and in the simulation.

Experiments are performed on the two-phase flow facility at the Lehrstuhl für Thermodynamik of the Technische Universität München to investigate intermittent flow characteristics in a horizontal pipe. The test section is a plexiglass conduct with an inner diameter of 54 mm. Measurements are carried out for two different pipe lengths, 223*D* and 268*D*. The experimental data is acquired at pressures and temperatures close to atmospheric conditions. The range of the superficial liquid velocity is from 0.09 m/s up to 1.0 m/s and for the superficial gas velocity from 0.15 m/s up to 5.50 m/s. These operating points include stratified, wavy, plug and slug flow regimes. Figure 1.3 shows the acquired operating points as seen in the flow pattern map according to Taitel and Dukler [1976].
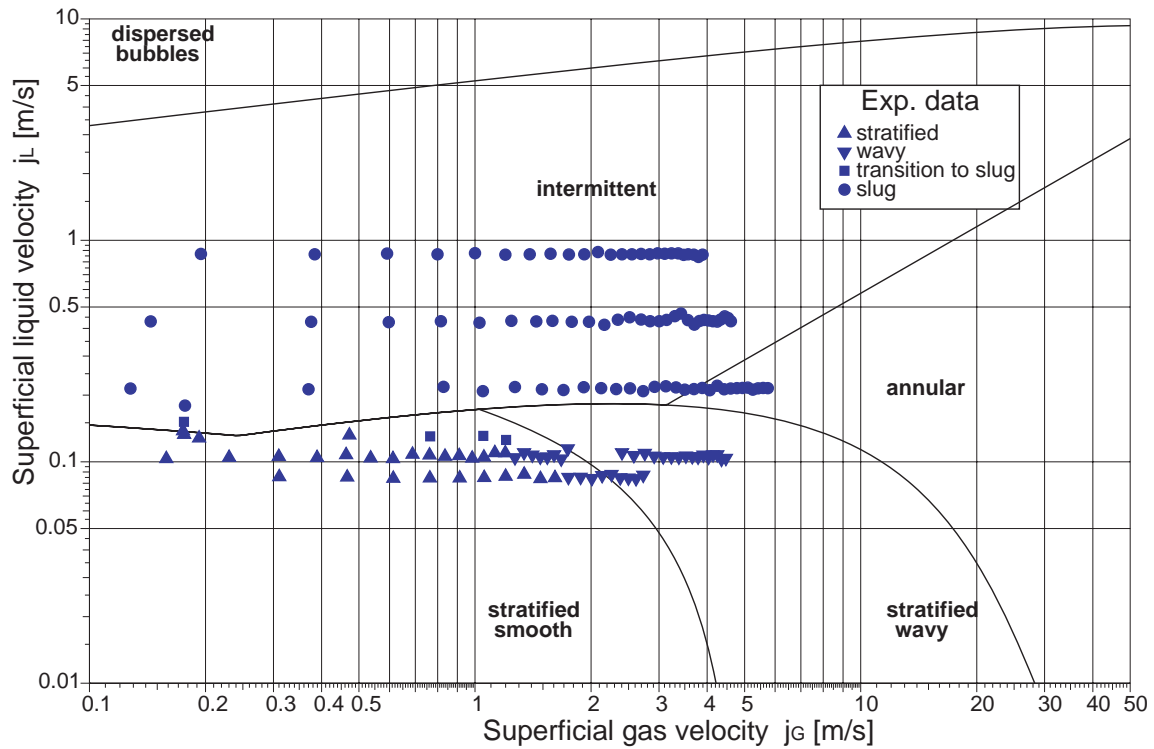
Figure 1.3: Flow pattern map with experimental data [Taitel and Dukler, 1976].

Void fraction measurements are carried out by means of wire-mesh sensors. Four sensors are placed along the measuring test section to enable the study of the evolution of the flow pattern along the horizontal pipe. In order to further develop the physical understanding of intermittent flows, experimental data is acquired with careful attention to the boundaries between plug flow (also called elongated bubble flow) and slug flow. The main differences between both regimes will be elucidated. Relevant flow characteristics will be identified, allowing a detailed analysis of the influence of the slug void fraction on the flow characteristics as well as the behaviour of the dispersed bubbles in the slug body.

The simultaneous use of Particle Image Velocimetry (PIV) technique and Pulsed Shadow-graph (PS) techniques for the acquisition of experimental data enables the calculation of the velocity field of the liquid phase. These techniques are adapted for horizontal two-phase pipe flows within this work. The technical difficulties of this task as well as the limitations of these measuring techniques for horizontal two-phase flows will be discussed. The velocity fields of stratified, wavy, plug and slug flows will be studied and statistically analysed. Turbulent quantities of these flows will be also presented.

2 Review of Intermittent Flows

Intermittent flow regimes are commonly observed in horizontal two-phase flows. They are defined as the regimes in which the flow is intermittent, with the tube periodically being filled with a liquid continuum which may or may not contain gas bubbles. At this point, it is important to note that intermittent flows are often called slug flows in the literature (this affects to the whole terminology of intermittent flows). Many authors do not make a differentiation between plug and slug flow and term both regimes as slug flows. But generally, it is accepted that plug flow (or also called elongated bubble flow) occurs at very low gas velocities and consists of elongated gas bubbles that move along the top of the pipe. The liquid slug body is almost free of gas bubbles. Slug flow is found at higher gas velocities; it is a stratified flow with the intermittent appearance of high-velocity liquid slugs, which bridge the whole pipe and which can be highly aerated.

Intermittent flows have been studied for years, both experimentally and theoretically, but a full understanding of its nature has not been reached (see for example the reviews of Fabre and Liné [1992], Hale [2000] or Ujang [2003]). This is mainly due to its complexity, irregularity and intermittency.

Slug flow, in extreme situations, can be hazardous to the structure of the pipe system or to the apparatus due to several issues as:

- ▷ Large variations in the gas and liquid flow rates (the liquid flow rate in a slug can be several times larger than the average value of the liquid phase).

- ▷ Considerable momentum of long slugs (liquid slugs travel at high velocities within the pipe, so the reactions forces at pipe bends can be quite high).

- ▷ Large pressure losses (high pressure gradients accompany the liquid slugs).

- ▷ Resonance problems (if the slug frequency approaches the resonant frequency of the multiphase pipe system).

2.1 Terminology of Intermittent Flows

The flow field is characterized by the superficial velocities as a function of the gas and liquid volumetric flow rates Q_G and Q_L, respectively. For the gas phase the superficial velocity is defined as:

$$j_G = \frac{Q_G}{A} = \alpha_G u_G, \qquad (2.1)$$

and for the liquid phase:

$$j_L = \frac{Q_L}{A} = \alpha_L u_L, \tag{2.2}$$

where A is the area of the cross section of the pipe, u is the velocity of the liquid or the gas phase and α indicates the phase volumetric concentration for gas (also called void fraction) and liquid (also called liquid hold-up or liquid fraction), respectively:

$$\alpha_G = \frac{A_G}{A}, \tag{2.3}$$

$$\alpha_L = \frac{A_L}{A}. \tag{2.4}$$

The two volumetric concentrations are linked by the fundamental relation:

$$\alpha_G + \alpha_L = 1. \tag{2.5}$$

Assuming that liquid slugs are present in the pipe, the scheme of one slug unit is shown in figure 2.1.
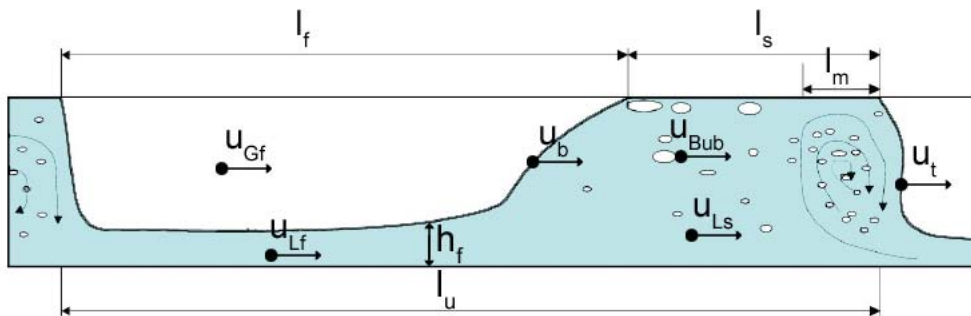
Figure 2.1: Slug unit schema [Dukler and Hubbard, 1975].

The slug unit is divided in two regions, the liquid slug region, also called slug body, of length l_s and the liquid film region of length l_f, consisting of a liquid film with height h_f and an elongated gas bubble. Gas from the film region tends to be entrained into the front part of the slug as illustrated in figure 2.1, and there is a mixing region of length l_m. The slug unit length, l_u is defined by:

$$l_u = l_s + l_f. \tag{2.6}$$

The liquid slug front velocity is termed u_t and the tail velocity u_b. The average liquid velocity in the slug body is designated as u_{Ls} and the velocity of the bubbles within the slug u_{Bub}. The average liquid velocity in the film is designated as u_{Lf}.

In steady state flow and assuming incompressible flow, continuity dictates that the overall volumetric flow rate at any cross section of the pipe must be the same [Woods and Hanratty, 1996]:

$$Q_G + Q_L = A(j_G + j_L) = constant. \tag{2.7}$$

Dividing equation 2.7 by the area, then:

$$j_G + j_L = U_M = constant. \tag{2.8}$$

where U_M is usually called the mixture velocity or no-slip velocity. Equation 2.8 has to be also satisfied in the slug and film region:

$$U_M = \alpha_{Gs} u_{Gs} + \alpha_{Ls} u_{Ls} = \alpha_{Gs} u_{Gs} + (1 - \alpha_{Gs}) u_{Ls}, \tag{2.9}$$

$$U_M = \alpha_{Gf} u_{Gf} + \alpha_{Lf} u_{Lf} = \alpha_{Gf} u_{Gf} + (1 - \alpha_{Gf}) u_{Lf}. \tag{2.10}$$

In the same manner, equation 2.5 has to be also satisfied in the slug and film region:

$$\alpha_{Gs} + \alpha_{Ls} = 1, \tag{2.11}$$

$$\alpha_{Gf} + \alpha_{Lf} = 1. \tag{2.12}$$

The slip ratio S between the mean phase velocities in the slug is defined as:

$$S = \frac{u_{Gs}}{u_{Ls}}. \tag{2.13}$$

It is commun practice to assume the average liquid velocity in the slug body u_{Ls} as the flow mixture velocity U_M. Many authors expect it to be well approximated over a wide range of flow rates [Nicholson et al., 1978]. From 2.9 and 2.13, it can be obtained:

$$u_{Ls} = \frac{U_M}{1 - (S - 1)\alpha_{Gs}}. \tag{2.14}$$

Therefore, when $S = 1$ or $\alpha_{Gs} = 0$, the mean phase velocities in the slug are equal to the superficial mixture velocity.

2.2 Initiation of Intermittent Flows

Intermittent flows can be classified into two main groups depending on its formation: hydrodynamic and terrain slugging. Hydrodynamic slugging is the normal slugging pattern encountered in straight flow lines. Terrain slugging, also called severe slugging, appears when the pipe exhibits a dip where the possibility of blockage of the free gas flow may be caused by the liquid filling the dip. Slugs can also be initiated by some operating transients, for example when the inlet gas flow rate is quickly increased.

In many experimental studies of hydrodynamic slugging, the entrance of the fluids into the pipeline is designed to assure a stratified flow configuration, in which the gas flows above the liquid in parallel streams, so that slugs originate from waves at the gas-liquid interface that grow to fill the pipe cross section. An accepted mechanism for this wave growth is the Kelvin-Helmholtz instability. First, the interface is elevated due to the friction between the pipe wall and the liquid phase, which leads to an acceleration of the gaseous phase. As the gas accelerates, the pressure in the gas phase over the wave decreases owing to the Bernoulli effect; this suction tends to further elevate the interface, increasing the wave amplitude. The wave growth is counteracted by gravity, giving rise to a criterion for instability, where the acceleration of the gas is sufficient to overcome gravity effects. Surface tension also opposes wave growth, but acts on a length-scale that is too small to directly influence the formation of slugs.

Wallis and Dobson [1973] analysed the onset of slugging in horizontal and near horizontal gas-liquid flows, but a prediction of horizontal flow regime transitions in pipes was first made by Taitel and Dukler [1976], where comparisons of the onset of intermittent flow with the classical inviscid Kelvin-Helmholtz instability showed that the instability occurs in conduits at lower velocities than predicted. So they suggested a semi-empirical equation for the onset of Kelvin-Helmholtz instability in a pipe. This correction only predicts correctly for the effects of inertia for an air-water flow.

Predictions on the onset of intermittent flow, including viscous effects were made by Lin and Hanratty [1986]. Their results in the context of viscous stability theory predicted well the initiation of slugs for gas superficial velocities lower than 3.3 m/s. The authors explained that the mechanism of slug formation is different for large and small gas velocities.

Barnea and Taitel [1994] used the linear stability analysis to derive both the inviscid and viscous limits. They concluded that the viscous Kelvin-Helmholtz limit provided a good approximation for the transition from stratified flow to intermittent flow in horizontal pipes.

Bendiksen and Espedal [1992] reported that the viscous Kelvin-Helmholtz analysis merely gives the transition between stratified and wavy flow. Once a wave has bridged the pipe, stable intermittent flow will form according to the idea from Ruder et al. [1989], where they gave a limit gas velocity below which slugs cannot exist and a minimum height of the liquid layer over which stable slugs can propagate.

Hurlburt and Hanratty [2002] combined the use of the three existing theoretical methods (the Kelvin-Helmholtz theory, viscous long wave theory and the necessary conditions for a slug to be stable) depending on the gas superficial velocity.

2.3 Characteristics of Intermittent Flows

Some of the most relevant properties of intermittent flows will be examined in the present subsection, such as the slug frequency, slug velocity, slug body length, the pressure gradient and the slug liquid hold-up. Few theoretical methods are available for the prediction of these. Instead, they are generally given by graphical or empirical relations based on limited data sets. As a result, the derived relationships are only truly applicable to a specific geometry and fluid pair.

2.3.1 Slug Frequency

The slug period is defined as the time that a slug unit needs to pass through the measuring device. The inverse of the slug period is the slug frequency ν_u at a certain position from the inlet.

Most of the empirical correlations for slug frequency relate to strictly developed slugs downstream.

Gregory and Scott [1969] measured the slug frequency in a carbon dioxide-water system with a 19.1 mm diameter pipe. They proposed the following correlation:

$$\nu_u = 0.0226\,\text{Hz} \left[\frac{j_L}{g\,D} \left(\frac{19.75\,\text{m}^2/\text{s}^2}{U_M} + U_M \right) \right]^{1.2}. \tag{2.15}$$

Greskovich and Shrier [1972] based their correlation on air-water data collected in a 1.5 and 1.25 inch pipe. By re-arranging terms of Gregory´s and Scott´s correlation, they proposed:

$$\nu_u = 0.0226\,\text{Hz} \left[\lambda_L \left(\frac{2.02\,\text{m}}{D} + Fr_M \right) \right]^{1.2}, \tag{2.16}$$

where λ_L is the no-slip hold-up:

$$\lambda_L = \frac{j_L}{U_M}, \tag{2.17}$$

and Fr_M is the mixture Froude number:

$$Fr_M = \frac{U_M^2}{g\,D}. \tag{2.18}$$

Taitel and Dukler [1977] developed a model to predict slug frequency, as they affirmed that the above correlations are not reliable for use under flow conditions different from the

ones used in their systems. They proposed a model to calculate the initiation frequency in terms of the elapsing time between successive pipe-bridging events. This elapsing time is composed of two parts; once the liquid height has built to its equilibrium level, there is a lapse of time for a wave to bridge the pipe and the liquid to drop to its lowest level. Then, there is a lapse of time for the layer to rebuild to its equilibrium level. They concluded that the problem of predicting slug frequency reduces to the determination of the elapsing time required for the liquid to rebuild from its lowest level.

Heywood and Richardson [1979] calculated the probability density function and power spectral density of the hold-up in order to estimate the average slug frequency:

$$\nu_u = 0.0434\,\mathrm{Hz} \left[\lambda_L \left(\frac{2.02\,\mathrm{m}}{D} + Fr_M \right) \right]^{1.02}. \tag{2.19}$$

Tronconi [1990] assumed that the slug frequency is one half of the frequency of the unstable waves precursors of slugs. He used linear stability analysis and the concept of a "most dangerous wave" proposed by Mishima and Ishii [1980] to identify the frequency of the unstable wave responsible for initiating a slug.

Woods and Hanratty [1999] investigated the influence of the Froude number on determining the frequency of slugging. They affirmed that the mechanism responsible for slug formation, and thus the slug frequency, depends on the liquid Froude number of the wavy stratified flow, the gas velocity and the bridging location. Their results and interpretations did not support the proposals by Taitel and Dukler [1977] and Tronconi [1990].

2.3.2 Slug Velocity

It is well established that the slug moves at a higher velocity than the total mixture velocity. This implies that liquid is picked up at the slug front and shed at its end. The rate of shedding determines the translational velocity. Several authors suggest that intermittent flow is fully developed when the rate of pick-up of liquid at the nose of the advancing slug is equal to the rate of liquid shedding at its tail. When this happens, the velocity at the front u_t of the slug equals the velocity at the slug tail u_b and the length of the slugs l_s are then constant.

The motion of slug bubbles in horizontal pipes has been studied less due to the asymmetric bubble shape. For the vertical case Nicklin et al. [1962] found that the bubble translational velocity u_b is well correlated by:

$$u_b = C_0\,u_{Ls} + u_d = C_0\,u_{Ls} + C_1\,(g\,D)^{\frac{1}{2}}. \tag{2.20}$$

In this expression, C_0 represents a weighted velocity/liquid fraction distribution parameter, while u_d represents the weighted mean drift velocity of the gas phase relative to the liquid. C_1 is a weighted mean drift velocity proportionality constant.

For the horizontal case, many researchers (Hughmark [1965], Gregory and Scott [1969], Dukler and Hubbard [1975], Nydal et al. [1992]) neglected the contribution of the drift velocity on the basis that gravity cannot act in horizontal direction and assumed that the relationship is given in the simpler form of:

$$u_b = (1+C) u_{Ls} = C_0 u_{Ls}. \tag{2.21}$$

Gregory and Scott [1969] correlated the slug velocity u_b to the mixture velocity U_M as:

$$u_b = 1.35 U_M. \tag{2.22}$$

Dukler and Hubbard [1975] assumed a turbulent velocity profile within the slug while estimating the shedding rate. They also related the translational velocity at the slug nose u_t to the mixture velocity:

$$u_t = (1+C) U_M, \tag{2.23}$$

where C was correlated by the equation:

$$C = -0.021 \, ln \, (Re_s) + 0.022, \tag{2.24}$$

and Re_s is the liquid Reynolds number in the slug:

$$Re_s = U_M D \frac{\alpha_{Gs} \rho_G + (1 - \alpha_{Gs}) \rho_L}{\alpha_{Gs} \mu_G + (1 - \alpha_{Gs}) \mu_L}. \tag{2.25}$$

Nicholson et al. [1978] noted that the drift velocity cannot be neglected, as it is expected to be particularly important in large diameter pipes and inclined pipes. The average translational velocity of slug and bubble units of intermittent flow is given by:

$$u_b = 1.196 \, u_{Ls} + 0.27 \, \text{m/s} = 1.196 \, U_M + 0.27 \, \text{m/s} \quad for \quad D = 2.58 \, cm, \tag{2.26}$$
$$u_b = 1.128 \, u_{Ls} + 0.28 \, \text{m/s} = 1.128 \, U_M + 0.28 \, \text{m/s} \quad for \quad D = 5.12 \, cm. \tag{2.27}$$

Ferré [1979] found in his experimental investigation using a 45 mm inside diameter pipe of 50 m length two different critical Froude numbers at which the values of C_0 and the drift velocity change (cited by Fabre and Liné [1992]):

$$u_b = 1.1 \, u_{Ls} + 0.45 \, u_d \quad for \quad Fr_{crit} < 2.0, \tag{2.28}$$
$$u_b = 1.3 \, u_{Ls} \quad for \quad 2 < Fr_{crit} < 8.0, \tag{2.29}$$
$$u_b = 1.02 \, u_{Ls} + 3 \, u_d \quad for \quad Fr_{crit} > 8.0, \tag{2.30}$$

where the critical Froude number is given by:

$$Fr_{crit} = \frac{U_{Ls}}{\sqrt{gD}}.$$
(2.31)

Bendiksen [1984] explained horizontal drift due to the effect of elevation differences along the bubble nose. In analysing the motion of single bubbles in a 25 mm pipe, he also noticed that there was a critical Froude number at which the values change (suggesting the secondary influence of surface tension):

$$u_b = 1.05\,u_{Ls} + 0.54\,u_d \quad for \quad Fr_{crit} < 3.5,$$
(2.32)

$$u_b = 1.2\,u_{Ls} \quad for \quad Fr_{crit} \geq 3.5.$$
(2.33)

Nydal et al. [1992] computed the coefficient C_0 according to equation 2.21, obtaining a value of $1.2 - 1.3$. They suggested that the differences between experimental C_0 and the values given by the ratio of the mean to the centreline velocity in turbulent flow could be due to:

▷ The presence of bubbles in the slug which modify the velocity profiles at the slug tail.

▷ An appreciable slip between the phase velocities in the slug.

▷ Some of the small bubbles in the slug body may coalesce at the bubble nose and modify the displacement velocity of the bubble boundary.

Cook and Behnia [1997], in their experiments in 32 mm and 50 mm pipe, suggested that the drift component does not need to be considered at the mixture velocities that they investigated (from 1.0 m/s to 8 m/s). Their data supported the linear relationship between u_b and U_M (being very close to $C_0 = 1.2$).

2.3.3 Slug Body Length

Since intermittent flow is a stochastic phenomenon, the slug body length l_s will be different for every slug moving along the pipe, being widely dispersed around its average. It is generally accepted, that the proccess of growth or decay of slugs depends on the process of shedding from the rear and the pick-up of liquid at the nose. Figure 2.2 shows the velocity profiles as they develop in two liquid slugs. The velocity profile of the first slug develops from a mixing wall jet profile to a fully developed pipe flow at the slug tail. For the second slug, the profile at the rear of the liquid slug is not yet fully developed. The maximum value of the velocity profile at the slug tail of the second slug is larger than this of the first one, being the shedding for the short slug also larger. The short slug will lose liquid at the tail at a higher rate than it will be picking it up at the front, leading eventually bubble *B* to overtake bubble *A*. This process is terminated as all the slugs are long enough

so that the velocity profile at the slug tail is fully developed (Moissis and Griffith [1962], Taitel et al. [1980], Barnea and Brauner [1985], Dukler et al. [1985]).

Table 2.1 shows the mean stable slug lengths observed by different researchers. Experimental observations suggest that the stable liquid slug length is relatively insensitive to gas and liquid flow rates.

Table 2.1: Mean slug lengths in horizontal pipes.

Mean Slug Length	Fluids	Diameter	Reference
12D-30D	air-water	1.5"	Dukler and Hubbard [1975]
$\approx 30D$	air-light oil	25.8 mm,51.2 mm	Nicholson et al. [1978]
$\approx 30D$	air-light oil	25.8 mm,51.2 mm	Gregory et al. [1978]
15D-20D	air-water	53 mm	Nydal et al. [1992]
12D-16D	air-water	90 mm	Nydal et al. [1992]

Much longer slugs were observed for long and large-diameter pipelines. Taitel [1987] suggested that gas expansion due to the decrease in pressure in long pipelines cause slug length growth in two-phase gas-liquid flow. He reported that the effects of inlet pressure, pipe diameter and angle of inclination are small.

Brill et al. [1981] investigated the slug length distribution in large diameter flow lines in Prudhoe Bay Field, suggesting for the first time that the distribution follows a log-normal pattern. Nydal et al. [1992] found also that the slug body length is lognormally distributed for air-water intermittent flow in 53 and 90 mm inner diameter horizontal pipes.

Barnea and Taitel [1993] suggested a model for the slug length distribution based on the bubble overtaking mechanism which occurs when the liquid slugs are shorter than the stable developed length. Based on this work, Cook and Behnia [2000b] proposed a slug length prediction model for near horizontal pipes. The model employs the correlation for slug collapse to simulate the evolution of the slug length distribution away from the inlet. However, the experimental data consistently shows slug lengths longer than the maximum predicted slug length.
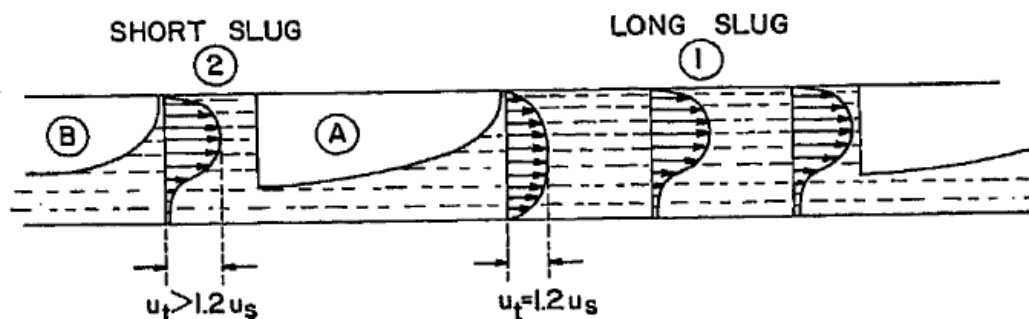
Figure 2.2: Velocity profiles in liquid slugs [Taitel and Barnea, 1990b].

2.3.4 Pressure

The pressure drop for two-phase flow is higher than in single phase flow for the same mass flow. The lower density leads to a larger fluid velocity. For the same fluid density, two-phase flow has larger turbulences than a single phase, leading to larger dissipative pressure losses than for a single phase flow. For this complex phenomenon there is not any analytical description. Most of the models, predicting the pressure gradient along the pipe in two-phase flows, are based on the Martinelli and Nelson [1948] two-phase multiplier. Using the separated flow approach, the best known correlation is perhaps that of Lockhart and Martinelli [1949]. This correlation is based on data acquired in pipes up to 25.8 mm inner diameter. They calculated the adiabatic two-phase frictional pressure drop by correcting the continuous phase using a multiplier ϕ_L^2 or ϕ_G^2 such that:

$$
\left(\frac{dp}{dx}\right)_M = \phi_L^2 \left(\frac{dp}{dx}\right)_L = \phi_G^2 \left(\frac{dp}{dx}\right)_G , \tag{2.34}
$$

where the pressure gradient for the fluid (liquid or gas, respectively), if it were flowing alone in the pipe, is given by:

$$
\left(\frac{dp}{dx}\right)_L = \frac{4 f_{w,L}}{D} \frac{\rho_L j_L^2}{2} , \tag{2.35}
$$

$$
\left(\frac{dp}{dx}\right)_G = \frac{4 f_{w,G}}{D} \frac{\rho_G j_G^2}{2} , \tag{2.36}
$$

the respective fluid-wall friction factors as:

$$
f_{w,L} = \frac{16}{Re_L} \quad for \quad Re_L = \frac{\rho_L j_L D}{\mu_L} < 2000, \tag{2.37}
$$

$$
f_{w,L} = 0.046 \, Re_L^{-0.2} \quad for \quad Re_L = \frac{\rho_L j_L D}{\mu_L} \geq 2000, \tag{2.38}
$$

$$
f_{w,G} = \frac{16}{Re_G} \quad for \quad Re_G = \frac{\rho_G j_L D}{\mu_G} < 2000, \tag{2.39}
$$

$$
f_{w,G} = 0.046 \, Re_G^{-0.2} \quad for \quad Re_G = \frac{\rho_G j_L D}{\mu_G} \geq 2000. \tag{2.40}
$$

The multipliers ϕ_L^2 and ϕ_G^2 are given by a graphical representation as a function of $X_{Lock-Mart}$, which is defined as follows:

$$
X_{Lock-Mart} = \left[\frac{\left(\frac{dp}{dx}\right)_L}{\left(\frac{dp}{dx}\right)_G} \right]^{\frac{1}{2}} . \tag{2.41}
$$

Chisholm [1967] curve-fitted these relationships with the following equations:

$$\phi_L^2 = 1 + \frac{C_{Chis}}{X_{Lock-Mart}} + \frac{1}{X_{Lock-Mart}^2}, \tag{2.42}$$

$$\phi_G^2 = 1 + C_{Chis} X_{Lock-Mart} + X_{Lock-Mart}^2, \tag{2.43}$$

where C_{Chis} has different values for laminar- and turbulent- gas and liquid flows, as shown in Table 2.2.

Table 2.2: Chisholm coefficients.

Gas	Liquid	C_{Chis}
Laminar	Laminar	5
Laminar	Turbulent	10
Turbulent	Laminar	12
Turbulent	Turbulent	20

Cook and Behnia [2000a] compared their experimental data collected in 32 and 50 mm inner diameter pipes with this widely used correlation. They reported good agreement for small diameter pipes, but less satisfactory agreement for pressure gradients obtained in the 50 mm pipe, highlighting the limitations of the use of empirically based correlations.

Since the slug is not a homogeneous structure, the local axial pressure drop is not constant along a slug unit (see figure 2.3). In fact, the flow of liquid slugs is associated with high pressure drop generated due the blockage of the pipe cross sectional area by the liquid, and many researches have used the large pressure pulsations that accompany slugs in order to detect their existence, e.g. Lin and Hanratty [1987].

Figure 2.3 shows the physical model proposed by Dukler and Hubbard [1975]. They calculated the pressure drop across the slug Δp_s as the sum of two terms:

$$\Delta p_s = \Delta p_a + \Delta p_f, \tag{2.44}$$

where Δp_a is the pressure drop that results from the acceleration of the slow moving liquid film to slug velocity and Δp_f is the pressure drop required to overcome wall shear in the back section of the slug. The pressure drop in the film region was neglected.

Taitel and Barnea [1990a] calculated the pressure drop of a slug unit by means of a global balance in which only hydrostatic and frictional pressure drop terms are considered throughout the slug and film regions.

However, Andreussi et al. [1993] reported that all these intermittent models generally underpredict the experimental data up to 30%. They proposed the calculation of the pressure gradient as the sum of the frictional, gravitational and acceleration terms. Nonetheless, their model underpredicts the experimental data up to 15-20%.
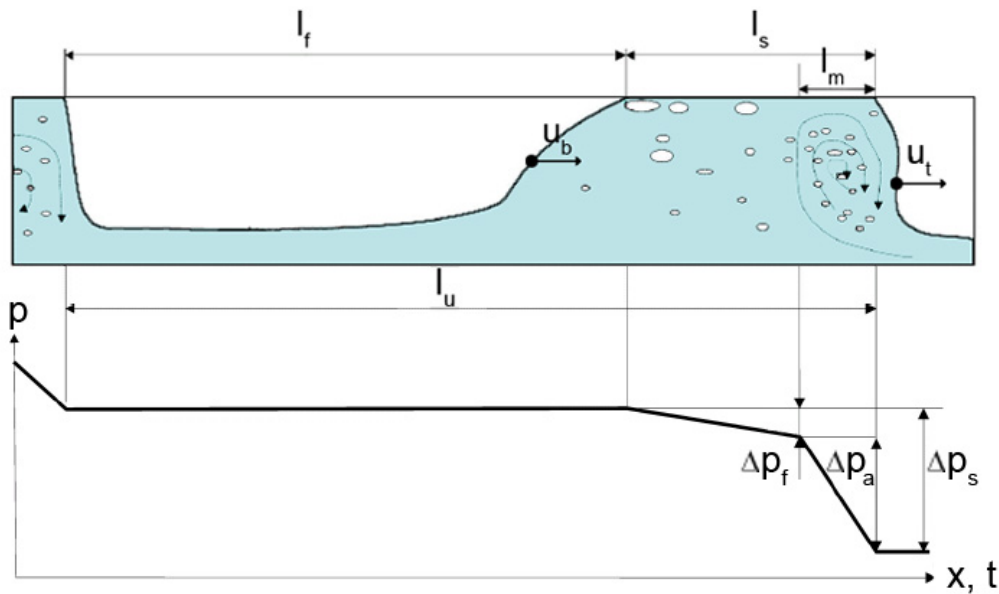
Figure 2.3: Pressure drop over a single slug unit [Dukler and Hubbard, 1975].

Cook and Behnia [2000a] associated the pressure loss with the viscous dissipation within a slug and accounted for the presence of dispersed bubbles in the slug body. In their model, the pressure gradient is given by the sum of four terms: the hydrostatic head loss in an inclined pipe, the frictional loss caused by wall shear stress, viscous losses associated with the eddy motion in the mixing vortex and the accelerational pressure loss due to gas expansion.

Over the past 40 years, many attempts have been made to derive better correlations for frictional pressure gradients. The main difficulty is that the empirical correlations are based on the assumption that the frictional pressure gradient is a function only of channel cross section geometry, mass flux and physical properties. However, in two-phase flow, the effects of flow development are considerable, and any wide-ranging database on two-phase flow contains data with a variety on inlet configurations and channel lengths, which will give a range of pressure gradients for the same nominal conditions.

2.3.5 Slug Liquid Hold-up

Different experimental investigations of intermittent flow have shown that under certain conditions small gas bubbles are entrained in the slug region, making the slug liquid hold-up α_{Ls} smaller than unity. Within the intermittent regime, some authors even distinguish between plug or elongated bubble flow and slug flow depending on the absence or presence of bubbles in the slug body. Plug flow occurs at very low gas velocities, the slug body is almost free of gas bubbles, so the liquid hold-up is unity. When the gas superficial velocity increases, bubbles are entrained, and dispersed flow occurs in the body of the slug (the so-called slug flow). For horizontal air-water slug flow, the bubbles at the slug front are fairly

homogeneously distributed over the cross section, but tend to migrate towards the upper part of the pipe along the slug region. Only at high flow rates is the bubble distribution uniform along the liquid slug length [Bendiksen et al., 1996]. These bubbles in liquid slugs result from coupled phenomena involving their production by fragmentation of the bubble tail, their entrainment coming from the bubble wake and their drift relative to the mean flow [Fabre and Liné, 1992]. Aeration increases with slug velocity, and can only be neglected, if the slug velocity is sufficiently low. Unpleasant flow instabilities, level surges and break-up of large slugs into a train of smaller ones may occur with high gas entrainment in liquid slugs Nydal and Andreussi [1991]. Therefore, the gas entrainment has an important role in determining the slug flow characteristics. As in the case of the above parameters, few empirical correlations are available for the prediction of the average liquid hold up within the slug region.

Gregory et al. [1978] measured the liquid volume fraction by means of a capacitance-type liquid volume fraction sensors in air-light oil mixtures in 25.8 mm and 51.2 mm diameter pipes. They correlated their data in terms of the mixture velocity as:

$$\alpha_{Ls} = \frac{1}{1 + \left(\frac{U_M}{8.66\,\mathrm{m/s}}\right)^{1.39}}. \tag{2.45}$$

Based on the same data, Malnes [1982] proposed the following correlation (cited by Bonizzi [2003]):

$$\alpha_{Ls} = 1 - \frac{U_M}{C_{Maln} + U_M}, \tag{2.46}$$

where C_{Maln} is a function of physical properties defined as:

$$C_{Maln} = 83 \left(\frac{g\,\sigma}{\rho_L}\right)^{\frac{1}{4}}, \tag{2.47}$$

where σ is the gas-liquid surface tension.

Andreussi and Bendiksen [1989] developed a relation for the slug hold-up, assuming that the net rate of gas bubble entrainment in the liquid slug is given by the difference between the bubble production and loss rate. The void fraction was determined for an air-water flow by a conductance probe technique. The measurements were acquired in two plexiglass tubes of inner diameter 50 mm and 90 mm and a maximum length of 17 m. Their semi-empirical correlation is given by:

$$\alpha_{Ls} = 1 - \frac{U_M - u_{mf}}{U_M + u_{m0}}, \tag{2.48}$$

where

$$u_{mf} = 2.6 \left[1 - 2\left(\frac{D_0}{D}\right)^2\right] \sqrt{g\,D}, \; D_0 = 2.5cm, \tag{2.49}$$

$$u_{m0} = 2400 \left(1 - \frac{1}{3}\sin\beta\right) Bo^{-\frac{3}{4}} \sqrt{g\,D}, \tag{2.50}$$

and the Bond number, which expresses the ratio of body forces (gravitational) to surface tension forces:

$$Bo = \frac{\rho_L g D^2}{\sigma}. \tag{2.51}$$

More recently, Abdul-Majeed [2000] suggested a new empirical equation based on 435 slug liquid hold-up points taken from seven different sources. He found that the liquid slug hold-up is affected very slightly by the pipe diameter and surface tension, therefore this correlation only depends on the fluids viscosities, μ_G and μ_L, mixture velocity U_M and inclination angle β:

$$\alpha_{Ls} = (1.009 - C_{Abd} U_M)(1 - \sin\beta), \tag{2.52}$$

where

$$C_{Abd-Mash} = 0.006 + 1.3377 \frac{\mu_G}{\mu_L}. \tag{2.53}$$

Taitel and Barnea [1990b] proposed the following relationship for the average void fraction of a slug unit as:

$$\alpha_u = \frac{j_G - u_{Bub} \alpha_{Gs} + u_b \alpha_{Gs}}{u_b}. \tag{2.54}$$

For the simple case when the liquid slug is not aerated, equation 2.54 reduces to:

$$\alpha_u = \frac{j_G}{u_b}. \tag{2.55}$$

Cook and Behnia [2000a] also expressed the overall average liquid hold-up as a weighted average of the hold-up in the slug and film regions:

$$\alpha_u = 1 - \left(\frac{j_L}{u_t} + \alpha_{Ls} \frac{U_M}{u_t} \right). \tag{2.56}$$

2.3.6 Velocity of the Dispersed Bubbles in the Liquid Slug

The bubbles with a chord length larger than the pipe diameter D are considered elongated bubbles. Smaller bubbles are usually termed as dispersed bubbles within the liquid slug.

Taitel and Barnea [1990b] estimated the velocity of the bubbles u_{Bub} in the liquid slug for the general case as a linear combination of the mixture velocity and the drift velocity:

$$u_{Bub} = B_0 u_{Ls} + u_d, \tag{2.57}$$

where B_0 is the distribution parameter which has been shown to depend on the concentration distribution of bubbles in the liquid slug Zuber and Findlay [1965]. For horizontal pipes, Taitel and Dukler assumed the drift velocity to be zero, and they recommended the use of $B_0 = 1$ in the absence of any detailed information.

Bonizzi [2003] calculates the bubble velocity from a local balance between the pressure and drag forces:

$$u_{Bub} = u_M - \sqrt{\frac{-4 D_{Bub} (dp/dx)}{3 C_D \rho_L}},$$ (2.58)

where C_D is the drag coefficient and it is given by the correlation of Tomiyama [1998] for a contaminated system as:

$$C_D = \frac{C_{DT}}{\sqrt{\alpha_{Ls}}},$$ (2.59)

where

$$C_{DT} = max \left[\frac{24}{Re_{Bub}} \left(1 + 0.15 \, Re_{Bub}^{0.687} \right), \frac{8}{3} \frac{Eo}{Eo + 4} \right].$$ (2.60)

The bubble Reynolds and Eötvös numbers are given by:

$$Re_{Bub} = \frac{\rho_L D_{Bub} |U_M - u_{Bub}|}{\mu_L},$$ (2.61)

$$Eo = \frac{g (\rho_L - \rho_G) D_{Bub}^2}{\sigma}.$$ (2.62)

2.4 Models for Intermittent Flows

The first works on the modelling of intermittent flows are considered to be those by Griffith and Wallis [1961] and Nicklin et al. [1962], who were the first to recognize the importance of the long bubble motion [Fabre and Liné, 1992]. The most distinctive feature of plug and slug flow is intermittency. The first models developed to predict intermittent flows are the steady state models. They are the easiest approach to model these flows, where intermittency is reduced to periodicity and a fully developed flow is assumed. Steady state models cannot give a detailed and dynamic representation of the flow in the pipe. They are not necessarily capable of predicting some phenomena which occur in inclined pipes, such as the dissipation of slugs in a downward inclined section [Taitel et al., 2000]. For this purpose, transient codes were developed.

2.4.1 Steady State Models

The intermittency of plug and slug regimes is "averaged out" into a quasi "steady state flow". In these models, it is assumed that all slugs have the same slug velocity, length and consequently the same slug frequency. The characteristics of the intermittent flow

do not change in time. This simplification allows an easier analysis of the pressure drop associated with the passage of slugs.

Wallis [1969] introduced the "equivalent unit-cell concept" and used in a simplified model the end of the elongated bubble and its main body to predict the pressure gradient arising from the liquid slug.

Dukler and Hubbard [1975] developed the "unit-cell model" for horizontal flow. Figure 2.1 shows the cell that they considered, consisting of a liquid slug body and a long bubble. They were the first to identify a mixing section at the front of the slug and to propose relations for the pick-up process at the front and the shedding at the tail of the slug. The balance equations for the two phases are expressed in a frame of reference moving at the slug velocity so that the flow appears to be steady. After providing closure for their model, the pressure drop, and consequently, the pressure gradient per unit slug length could be calculated.

Taitel and Barnea [1990b] reviewed the model presented by Dukler and Hubbard [1975] and proposed the "equivalent cell" description, capable of accounting for all pipe inclinations. The main outcome of this model is the calculation of the pressure drop, while closure models provide the rest of information as slug voidage, slug velocity and slug body length. The model was then extended to account for more complex slug related phenomena, such as terrain-induced slugging, severe slugging and transient slug flows.

Cook and Behnia [2000a] proposed an alternative "equivalent cell" model. The main conceptual differences from the model presented by Taitel and Barnea [1990b] are first, that the former accounts for the effects of gas bubbles on the viscosity of the liquid-gas mixture in the body of the slug, and secondly the model accounts for gas expansion along the pipe.

2.4.2 Transient Models

2.4.2.1 System Codes

In order to account for transient phenomena and to capture the flow behaviour which is generated in multiphase pipelines, different general transient flow simulation methods have been developed. Among these models, the major two-phase flow solvers are TRAC, RELAP, CATHARE and ATHLET for nuclear reactor safety; OLGA, TACITE and PLAC for the oil and gas industry. These system codes (also described in section 1.2.2) are capable of numerically solving the fluid and thermodynamics for the whole range of possible flow patterns (separated, dispersed or intermittent). Their basic approach is to use the so called "two-fluid model" described in section 1.2.1, in which continuity, momentum and energy equations are written down for the two phases and are then solved numerically in space and time. All of these codes solve the set of governing equations in a transient and one-dimensional way on a fixed grid. In order to keep the latter manageable, large mesh spacings of the computational grid are typically used, and closure models are required both to establish the local flow pattern (i.e. dispersed, stratified, annular or intermittent) and to

calculate the relevant flow parameters (such as friction factors and the velocities at which the slugs move along the pipe) pertaining to the particular regime that is determined.

Transient models that are especially developed for the prediction of intermittent flows can be classified into three main groups: empirical slug specification, slug tracking and slug capturing.

2.4.2.2 Empirical Slug Specification Models

"Empirical slug specification models" are used to describe slug formation, growth, collapse and also the shape of slug front and tail in a transient formulation. They are subdivided into "stratified-slug transition" models (among others, De Henau and Raithby [1995a] and De Henau and Raithby [1995b]), based on the classical Kelvin-Helmholz stability theory, and "slug growth" models [Fagundes Netto et al., 1999], that assume that slugs are somehow generated in the pipe. Thus, to predict intermittent flows, it is necessary to invoke detailed models of interface evolution and of the motion and growth of waves on the interface leading to bridging and the formation of slug precursors. In order to follow the history of slug precursors in the downstream region, the slug tracking model was developed.

2.4.2.3 Slug Tracking Models

"Slug tracking models" (among others, Zheng et al. [1994], Taitel and Barnea [1998] and Nydal and Banerjee [1996]) predict intermittent flows in long pipelines, including complex terrain and transients. The slug tracking technique is conceptually based on the processes that control the growth/collapse of the slugs, i.e. the pick-up process at the slug front and the shedding at the slug tail. The slug propagation model treats each wave or slug as a separate object. The computational nodes follow the translation of the waves and slugs as they proceed in the pipe. Therefore, this approach is also known as the lagrangian slug capturing scheme. These models are capable of modelling the evolution of intermittent flows from a known initial condition, if there is a known distribution of slugs through the pipe. The computation is very effective.

2.4.2.4 Slug Capturing

The technique is based on the transient one-dimensional "two-fluid model". The same set of equations is retained regardless of the local flow pattern (either stratified or intermittent flow) generated in the pipe. Slugs develop, grow, merge or collapse depending solely on the solution of the two-fluid model equations. The intermittent flow regime is predicted as a mechanistic and automatic outcome of the growth of hydrodynamic instabilities (Issa and Woodburn [1998], Issa and Kempf [2003]). In order to capture the natural growth of instabilities at the gas-liquid interface, their mesh spacings need to be sufficiently fine (at least $0.5D$). Their mesh sizes are several orders of magnitude below those commonly used

in the commercial simulators. The slug capturing approach is capable of predicting the correct flow pattern (stratified, wavy or intermittent flow) for various pipe inclinations and the complex phenomenon of severe slugging. The gas entrainment mechanism, which is not naturally included in the two-fluid model, has been modelled by means of an additional transport equation for the dispersed gas bubbles [Bonizzi, 2003].

Recently, Renault [2007] combined the slug capturing and slug tracking scheme and is able to capture directly the slug initiation process and to track the motion of every single slug in the pipe without numerical diffusion.

3 Numerical Simulation with ATHLET

The accurate prediction of transient two-phase flow is essential for nuclear reactor safety analyses under off-normal or accident conditions. In general, the ability to predict these thermohydraulic phenomena of two-phase flow depends on the availability of mathematical models and experimental correlations.

The thermal-hydraulic computer code ATHLET (Analysis of THermal-hydraulics of LEaks and Transients) is being developed by the Gesellschaft für Anlagen- und Reaktorsicherheit (GRS) in Germany, for the analysis of anticipated and abnormal plant transients, small and intermediate leaks as well as large breaks in light water reactors.

From a practical point of view, slug flow is one of the most interesting flow regimes of two-phase flows in horizontal pipes since the rapid transport of large liquid slugs may lead to equipment vibration and the possible influence of the slugs on the overall transient behaviour in subsequent components. Because of the importance of slug flow, an attempt has been made to use the ATHLET code to predict intermittent flow behaviour in a horizontal pipe. In the following, the fundamentals of ATHLET, the modelling of the implemented terms which are flow pattern related [Austregesilo et al., 2006] and a study of the feasibility and accuracy against a small scale experiment in a horizontal pipe will be presented.

3.1 ATHLET Fundamentals

ATHLET provides a modular network approach for the representation of a thermal-hydraulic system. A given system configuration can be simulated by connecting basic fluiddynamic elements called objects. These objects can be represented as a number of consecutive volumes (control volumes) connected by flow paths (junctions) as it is shown in figure 3.1. The control domain of the junctions is defined between the centers of adjacent control volumes, leading to a staggered grid.

The mass and the energy conservation equations are spatially integrated using the control volume as the integration domain, whereas the junction is the integration domain for the momentum balances. The control volume and junction related quantities are spatially averaged, leading to the so-called "lumped parameter model".

The six equation model is the most general equation system of the current ATHLET version. It solves the mass and energy balances in the control volumes separately for liquid and vapor phases, and the separate momentum balances at the junctions. The solution
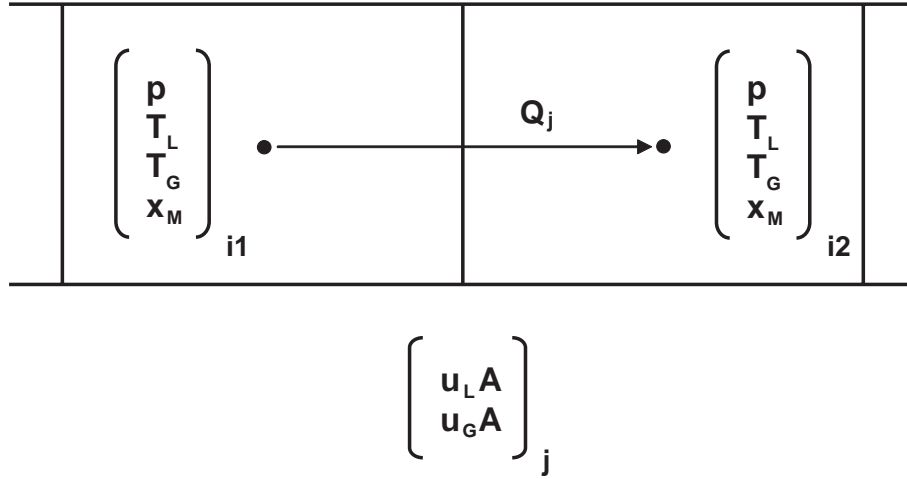
Figure 3.1: Displaced grid of control volumes and junctions [Austregesilo et al., 2006].

variables of the derived system of differential equations are the pressure p, the liquid temperature T_L, the vapor temperature T_G and the mass quality x_M within the control volumes, as well as the phase velocities multiplied by the total area ($u_L A$, $u_G A$) for the junctions.

The time integration of the thermo-fluid dynamics is performed with the general purpose ODE solver, the so-called FEBE (Forward-Euler, Backward-Euler). It provides the solution of a general nonlinear system of differential equations of first order which have been integrated implicitly (default option).

3.1.1 ATHLET Model Equations

Assuming isothermal conditions and no mass exchange between the phases, the transient one-dimensional two-fluid model equations for horizontal pipes reduce to:

Gas Continuity Equation

$$\frac{\partial(\alpha_G \rho_G)}{\partial t} + \frac{\partial(\alpha_G \rho_G \vec{u}_G)}{\partial x} = 0, \tag{3.1}$$

Liquid Continuity Equation

$$\frac{\partial((1-\alpha_G)\rho_L)}{\partial t} + \frac{\partial((1-\alpha_G)\rho_L \vec{u}_L)}{\partial x} = 0, \tag{3.2}$$

Gas Momentum Equation

$$\frac{\partial(\alpha_G \rho_G \vec{u}_G)}{\partial t} + \frac{\partial(\alpha_G \rho_G \vec{u}_G \vec{u}_G)}{\partial x} + \frac{\partial(\alpha_G p)}{\partial x} =$$
$$-\vec{\tau}_{int} + \alpha_G \vec{f}_w + \alpha_G \rho_G \vec{g} - \alpha_G(1-\alpha_G)(\rho_L - \rho_G)\vec{g}D_h\frac{\partial \alpha_G}{\partial x}, \tag{3.3}$$

Liquid Momentum Equation

$$\frac{\partial((1-\alpha_G)\rho_L\vec{u}_L)}{\partial t} + \frac{\partial((1-\alpha_G)\rho_L\vec{u}_L\vec{u}_L)}{\partial x} + \frac{\partial((1-\alpha_G)p)}{\partial x} =$$

$$+\vec{\tau}_{int} + (1-\alpha_G)\vec{f}_w + (1-\alpha_G)\rho_G\vec{g} + \alpha_G(1-\alpha_G)(\rho_L-\rho_G)\vec{g}D_h\frac{\partial\alpha_G}{\partial x}, \quad (3.4)$$

and

$$\rho_M = \alpha_G\rho_G + (1-\alpha_G)\rho_L, \quad (3.5)$$

$$\vec{u}_r = \vec{u}_G - \vec{u}_L. \quad (3.6)$$

Therefore, the two-fluid model represents a set of nonlinear first order partial differential equations. In the above equations, x and t are the spatial and temporal coordinates, respectively, α_G is the void fraction, ρ is the density, u_r is the relative velocity between the phases, p is the pressure, τ_{int} is the interfacial friction, f_w is the wall friction and g is the gravity constant. The last term on the right hand side of the momentum equations is the water level force, which considers the force resulting from different water levels in adjacent control volumes. For the derivation of this term it is assumed that gas and water flow are completely separated [Austregesilo et al., 2006].

As mentioned in section 1.2.1.3, these equations do not provide a complete description of a multiphase flow. They need to be supplemented by suitable constitutive relationships which describe how the phases interact with each other. ATHLET contains several constitutive models which account for the fluid properties, the interface mass and energy transfer, the wall friction and form losses and the modelling of interfacial shear forces among others. The flow pattern related constitutive models implemented in ATHLET are the modelling of the interfacial shear force term and the interface mass and energy transfer. For adiabatic flow only the interfacial shear force term is needed. In the following section its modelling in ATHLET will be presented. The reader may refer to the manual [Austregesilo et al., 2006] for further models implemented in ATHLET.

3.1.2 Interfacial Shear Forces

The modelling of the interfacial shear forces is flow pattern related. A simplified flow pattern model contains the essential information needed for their calculation.

For horizontal pipes, the model distinguishes between:

- ▷ stratified-nonstratified (wavy) flow
- ▷ wavy-intermittent flow
- ▷ onset of liquid entrainment (dispersed flow).

It is important to note that bubble flow is treated in the same way as intermittent flow. There is no modelling of gas entrainment into the liquid phase.

The interfacial shear forces are given by:

$$\tau_{int}\frac{P_{int}}{A} = C_{int}u_r^2, \tag{3.7}$$

where P_{int} denotes the interface perimeter, C_{int} is the interfacial shear stress coefficient which is flow pattern related and u_r is the relative velocity between the phases.

For stratified flow, the interfacial shear stress coefficient is based on the correlation of Wallis [1969]:

$$C_{int,Strat} = 0.005\frac{1}{\pi D}\left[\alpha_G\left(1-\alpha_G\right)\left(1+75\sqrt{1-\alpha_G}\right)\right]\rho_G. \tag{3.8}$$

For intermittent flow, the following correlation developed by Ishii [1979] is used:

$$C_{int,Slug} = 9.8\alpha_G\left(1-\alpha_G\right)^3\frac{\rho_L}{D}. \tag{3.9}$$

For the transition between stratified smooth and intermittent flow, the parameter E_w (fraction of nonstratified liquid) is used as a weighting factor in a simple linear transformation:

$$C_{int,Trans} = \left(1-E_w\right)C_{int,Strat} + E_wC_{int,Slug}. \tag{3.10}$$

Before E_w is defined, the simplified flow pattern model implemented in ATHLET will be described.

ATHLET uses the criteria proposed by Taitel and Dukler [1976] for the prediction of stratified smooth-stratified wavy and wavy-slug transitions. The minimum gas velocity for wave formation is defined as:

$$u_{G,Wave} = \frac{2}{\sqrt{s}}\left[g\frac{\mu_L}{u_L}\frac{(\rho_L-\rho_G)}{\rho_L\rho_G}\right]^{\frac{1}{2}}, \tag{3.11}$$

where the sheltering coefficient $s = 0.01$.

The minimum gas velocity for onset of slugging is given by:

$$u_{G,Slug} = \left(1-\frac{h_{CL}}{D}\right)\left[\frac{\pi}{4}\alpha_G g\frac{D}{\sqrt{1-\left(2\frac{h_{CL}}{D}-1\right)^2}}\frac{(\rho_L-\rho_G)}{\rho_G}\right]^{\frac{1}{2}}, \tag{3.12}$$

where h_{CL} is the height of collapsed liquid level calculated for the whole liquid in the pipe cross section.

In ATHLET, the transition between stratified and intermittent flow is described as a function of the fraction of nonstratified liquid E_w. For stratified flow:

$$E_w = 0 \quad for \quad u_{max} < u_{r,Slug}. \tag{3.13}$$

For wavy flow (considered as a transition between stratified smooth and intermittent flow):

$$E_w = \frac{u_{max} - u_{r,Slug}}{u_{r,Slug}} \quad for \quad u_{r,Slug} < u_{max} < 2.0 u_{r,Slug}. \tag{3.14}$$

And for intermittent flow:

$$E_w = 1 \quad for \quad u_{max} > 2.0 u_{r,Slug}, \tag{3.15}$$

with

$$u_{r,Slug} = u_{G,Slug} + u_{min}, \tag{3.16}$$

where u_{max} and u_{min} represent the largest and smallest absolute value of the phase velocities, respectively.

According to the classification made in section 2.4, ATHLET belongs to the transient models. At this point, it is important to note that ATHLET is not especially developed for the prediction of intermittent flow regime. It does not have any closure models for the calculation of relevant flow parameters pertaining to intermittent flow pattern. ATHLET just includes a simplified flow pattern model (the flow pattern is determined as a function of a critical phase velocity) that is only used for the calculation of the interfacial shear stress coefficient.

3.2 Simulation of Stratified, Wavy and Intermittent Flows

3.2.1 Discretisation and Inlet Boundary Conditions

Several alternative configurations were analysed to represent the experimental facility in ATHLET. It is important to note that the nozzle of the two-phase separator delivers a preconditioned flow stream into the body of the separator. Depending on the fluid velocities, the water slightly accumulates at the end of the test pipe. The liquid fraction and the height of the film at the end of the pipe are higher than when the fluids flow through a pipe into an empty reservoir. In order to account for this effect in the simulations, the pressure losses were increased at the end of the pipe. The representation of the two-phase separator was implemented by means of a TIMEDEPVOL component (Time Development Volume or pressure-enthalpy boundary component) which always maintains atmospheric conditions (the liquid at the end of the pipe falls into a big empty reservoir with constant atmospheric conditions).

Four wire-mesh sensors were placed along the measuring test section, which has a length of around 14 m with an internal diameter of 54 mm. The first sensor was placed between two flanges $94.8D$ downstream of the two-phase mixer, the second $141.5D$, the third $208.7D$ and the fourth wire-mesh sensor $253.7D$. Pressure measurements were acquired at $0D$, $79.60D$, $186.40D$ and $243.71D$. The liquid fraction and the pressure drop predicted by the code were read at these positions.

For the calculations presented in this work, the representation in ATHLET consist of an initialisation branch, two single junction pipes with a FILL (one for air and one for water), a PIPE object, a single junction pipe with a LEAK and an ordinary branch with a TIMEDEPVOL component. Figure 3.2 illustrates this representation.
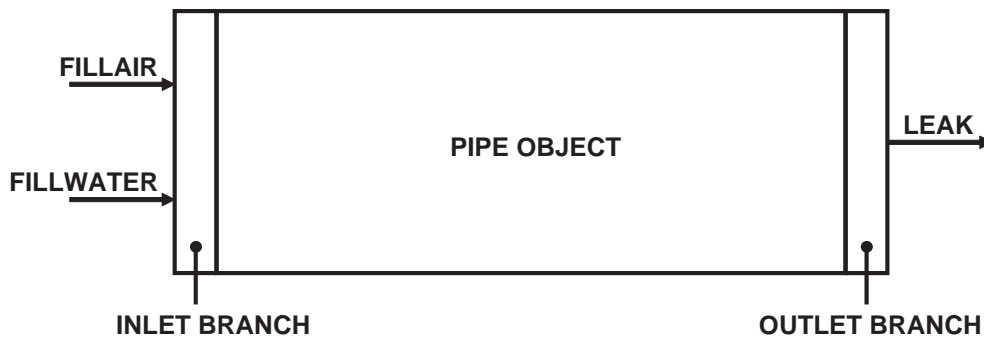
Figure 3.2: Representation of the pipe test section in ATHLET.

The wall friction and form losses for the two-fluid model are calculated separately for the two phases. In ATHLET, the additional pressure drop of two-phase flow is considered by the Martinelli-Nelson model [Martinelli and Nelson, 1948]. The Darcy-Weissbach friction factor is calculated as a function of the Reynolds number (see manual [Austregesilo et al., 2006]). The wall roughness of the plexiglass pipe has a value of $1.5 \cdot 10^{-6}$ m in the simulations. For the adjustment of the pressure drop along the pipe, measurements were carried out when only water flows into the pipe. These operating points were compared with the results of the simulations and the different pressure parameter options of the programm were adjusted. In this manner, the pressure drop introduced by the wire-mesh sensors and flanges was also taken into account.

3.2.1.1 Discretisation

It is an essential feature of numerical methods that the solution shall not be sensitive to the grid size. In order to study the influence of the mesh, a set of simulations with the same boundary conditions and geometry, but different nodalisation (number of control volumes along the pipe), have been carried out. Figure 3.3 shows the local liquid fraction α_L at $186.40D$ from the inlet for different node sizes and same fluid flow rates ($j_L = 0.75$ m/s, $j_G = 1.0$ m/s). The mean length of a slug body for such an operating point is around 0.8 m.
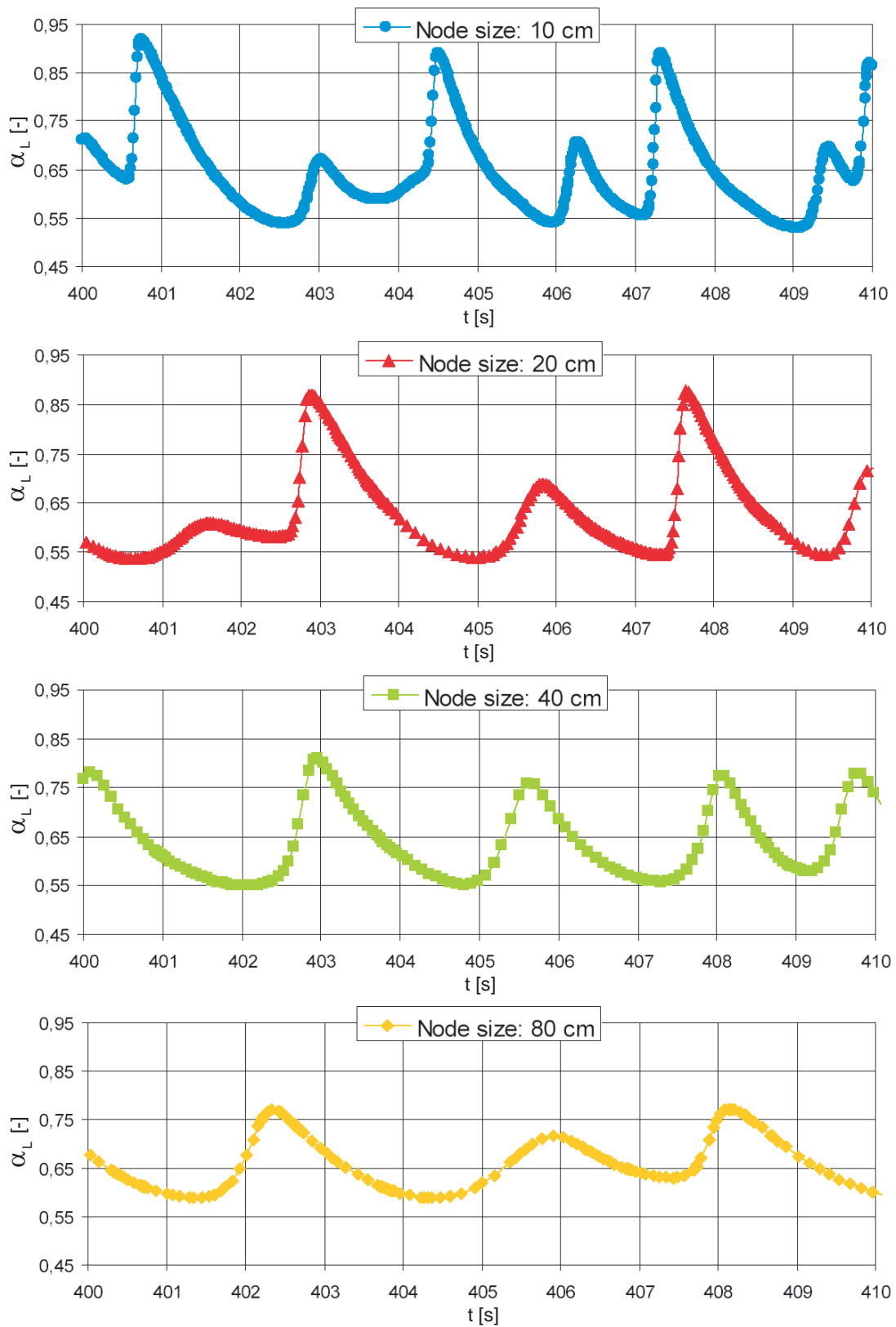
Figure 3.3: Node size study.

The smallest size of the nodes which ATHLET is able to give a stable solution for is 10 cm. For this operating point, it is not possible to reduce the size of the nodes below 10 cm and to find a numerical solution independent of the nodalisation. For smaller nodes, numerical instabilities appear and the solution oscillates strongly. As the node size is refined, ATHLET also refines the time step. The time step becomes smaller and smaller until the code stops. This may be due to the ill-possedness of the equations.

For a fine nodalisation the predicted liquid fraction in the slug body α_{Ls} is close to unity (see figure 3.3). As the node size is increased, the value of the predicted liquid fraction in the slug body decreases, becoming much smaller than unity. For node sizes of 40 cm, waves and slugs cannot be distinguished from each other, and it seems that a wavy configuration instead of intermittent flow is present in the pipe. Slug frequency decreases dramatically as the size of the nodes are increased. For coarse nodalisations, the liquid slug region is averaged with the film region. The pressure drop, the liquid velocity and the liquid fraction of the slug region is underpredicted by the code. Slug properties are not calculated correctly, such as slug frequency, slug length or slug velocity. It should also be noted that as the inlet gas velocity increases, ATHLET cannot give a solution for 10 cm nodes. In order to get a stable numerical solution of operating points with higher fluid velocities, the node size has to be enlarged.

Unfortunately, for the prediction of intermittent flow, the numerical solution given by ATHLET is always sensitive to grid size.

It is important to mention that such codes operating on complex problems such as a PWR LOCA actually use node sizes of approx. 100 cm. As it is shown in figure 3.3, with such a gross nodalisation, the code is not able to capture the slug phenomenon properly. A fine local nodalisation is strongly recommended if intermittent flow occurs in the pipe, in order to avoid that the slug and the film regions are smeared out.

3.2.1.2 Boundary Conditions

In order to study the influence of the inlet boundary conditions, different simulations with the same nodalisation (10 cm node size) and same fluid flow rates ($j_L =0.75$ m/s and $j_G =1.0$ m/s) have been carried out and compared with each other. Figure 3.4 shows the local liquid fraction α_L for three different cases at $186.40D$ from the inlet:

    ▷ Case 1: The total system is initialised with air and then water is introduced.

    ▷ Case 2: The total system is initialised with water and then air is introduced.

    ▷ Case 3: Air and water are introduced at the same time.

The liquid fraction oscillates between the same values for the three cases. The results show almost no influence of the boundary conditions on the slug characteristics (the mean slug frequency and the mean slug length values are similar for the three cases). Such a result is to be expected, since the onset of slug formation in the code depends on a critical value of the gaseous phase velocity (see 3.1.2).
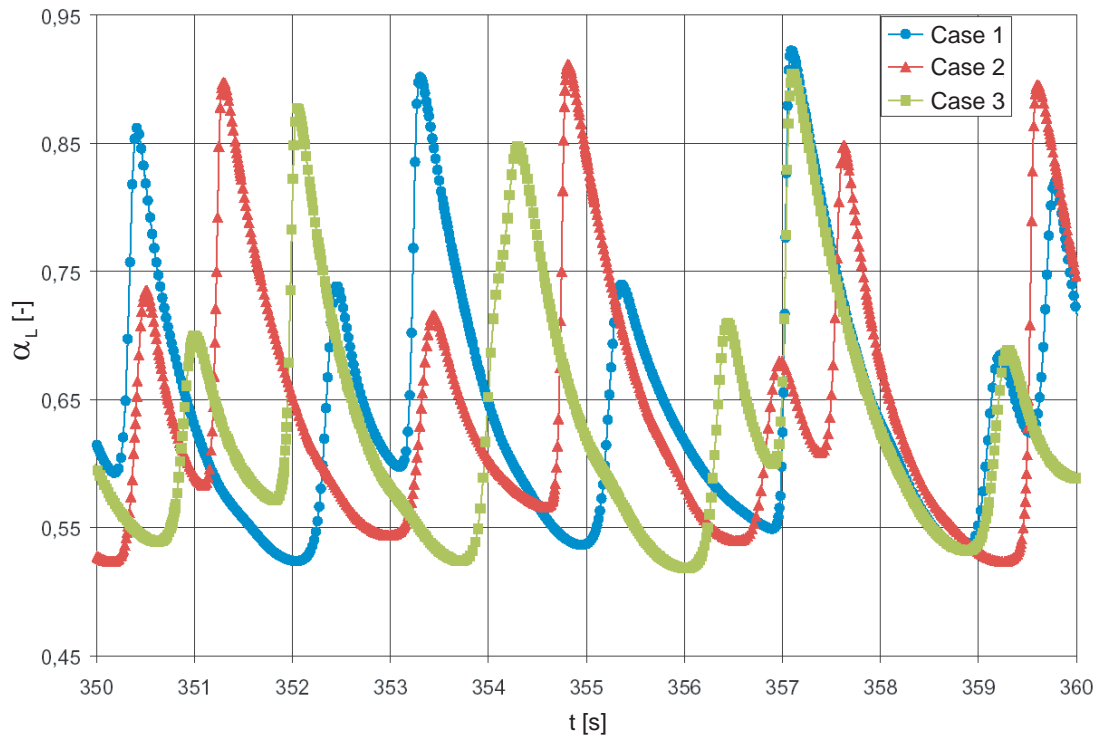
Figure 3.4: Boundary condition study.

3.2.2 Results of the Simulations

3.2.2.1 Flow Transition

Several simulations were made in order to detect the transitions between stratified-wavy flows and intermittent flows (20 cm node size). The flow pattern predicted by the code is identified by means of the parameter E_w (fraction of nonstratified liquid, see 3.1.2). Figure 3.5 shows the flow pattern map with the line transitions according to Taitel and Dukler [1976]. The line transition between stratified-wavy and intermittent flows predicted by ATHLET 2.1A (red line) and the experimental data are also presented in this figure. The experimental data and the flow pattern transitions according to Taitel and Dukler [1976] show that the code overpredicts this transition. ATHLET 2.1A predicts stratified and wavy flow for superficial velocities in which intermittent flow occurs.

Analysing the causes of the discrepancies between the experimental data and the code predictions, it was noticed that the correlation for the calculation of the interfacial shear stress coefficient was not implemented correctly in the code, leading to a higher value of the interfacial shear forces. Equation 3.8 was not divided by π in the code, so that the values of the interfacial shear forces were π times bigger than expected, leading to an overprediction between stratified-wavy flow and intermittent flow. The first constant of equation 3.8 was also modified (from 0.005 to 0.003) in order to get a better agreement with the experimental data.

Equation 3.8 is implemented in the modified code as follows:

$$C_{i,Strat} = 0.003 \frac{1}{\pi D} \left[\alpha_G (1 - \alpha_G) \left(1 + 75 \sqrt{1 - \alpha_G} \right) \right] \rho_G. \tag{3.17}$$

The new transition line between stratified-wavy and intermittent flows of the modified code is presented as a green line named modified ATHLET in figure 3.5. This new transition line is in good agreement with the experimental data.
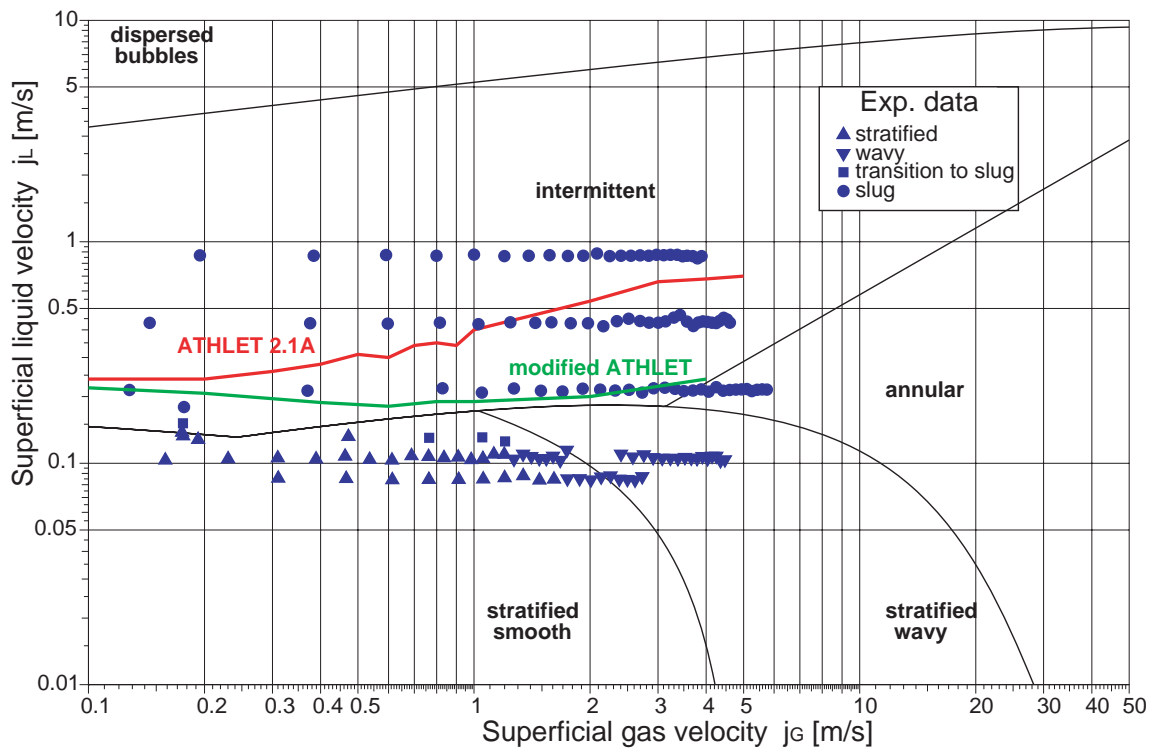
Figure 3.5: Flow regime transition [Taitel and Dukler, 1976].

The liquid fraction α_L was studied before and after the modification of equation 3.8. The upper graph of figure 3.6 shows the comparison between the predictions of the average liquid fraction by ATHLET 2.1A and the experimental data for stratified-wavy flows ($j_L = 0.09$ m/s and $j_G = 0.31 - 2.73$ m/s). It is shown that ATHLET 2.1A clearly underpredicts the average liquid fraction. The bottom graph of figure 3.6 shows the differences between between the predictions of the average liquid fraction by the modified code and the experimental data for the same operating points as the upper graph. After the modification of ATHLET 2.1A, the predictions of the average liquid fraction are in good agreement with the experimental data.
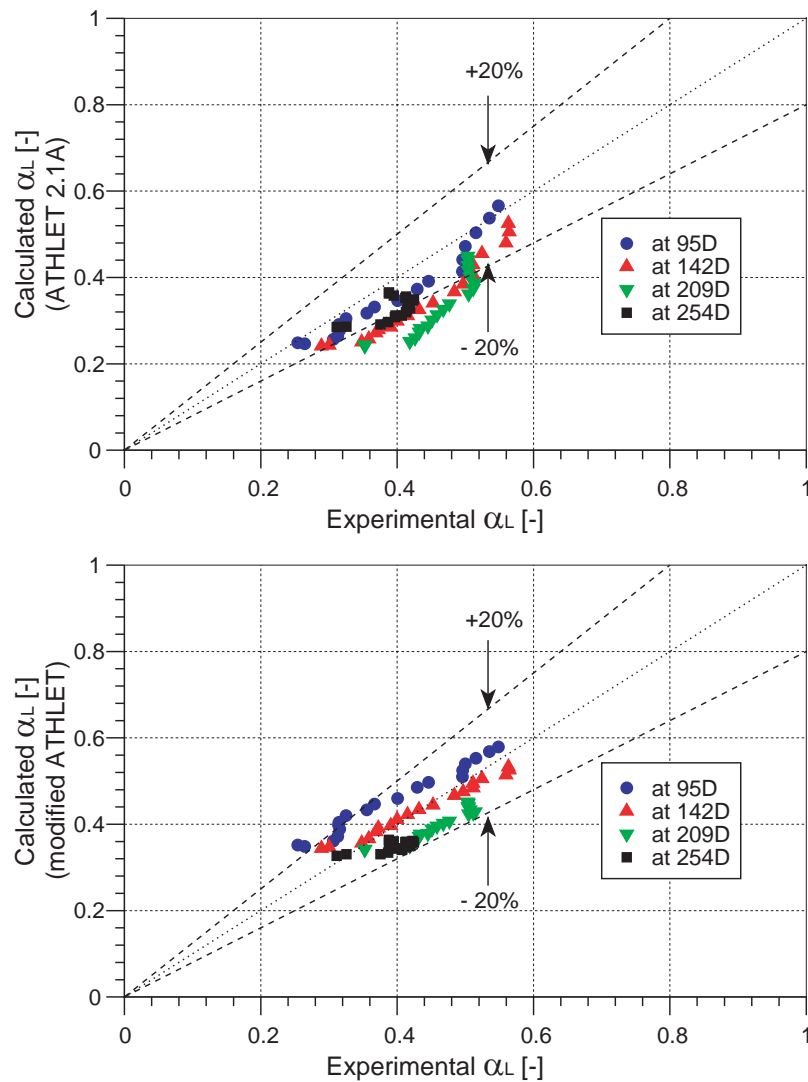
Figure 3.6: Comparison of the average liquid fraction predicted by the code and the experimental data: stratified-wavy flows.

3.2.2.2 Intermittent Flow

Figure 3.7 shows the liquid fraction α_L predicted by the modified code and the experimental data for three operating points. The numerical predictions have been obtained with a node size of 10 cm.

Table 3.1 shows an overview of the parameters for the operating points presented in figure 3.7: the liquid and gas superficial velocities, j_L and j_G, respectively, the average liquid fraction in the pipe $\overline{\alpha}_L$, the average liquid fraction in the film region $\overline{\alpha}_{Lf}$ and the average slug unit period $\overline{T}_s$. Table 3.2 shows the predictions of ATHLET of the average liquid fraction in the pipe $\overline{\alpha}_L$, the average liquid fraction in the film region $\overline{\alpha}_{Lf}$ and the average slug unit period $\overline{T}_s$.
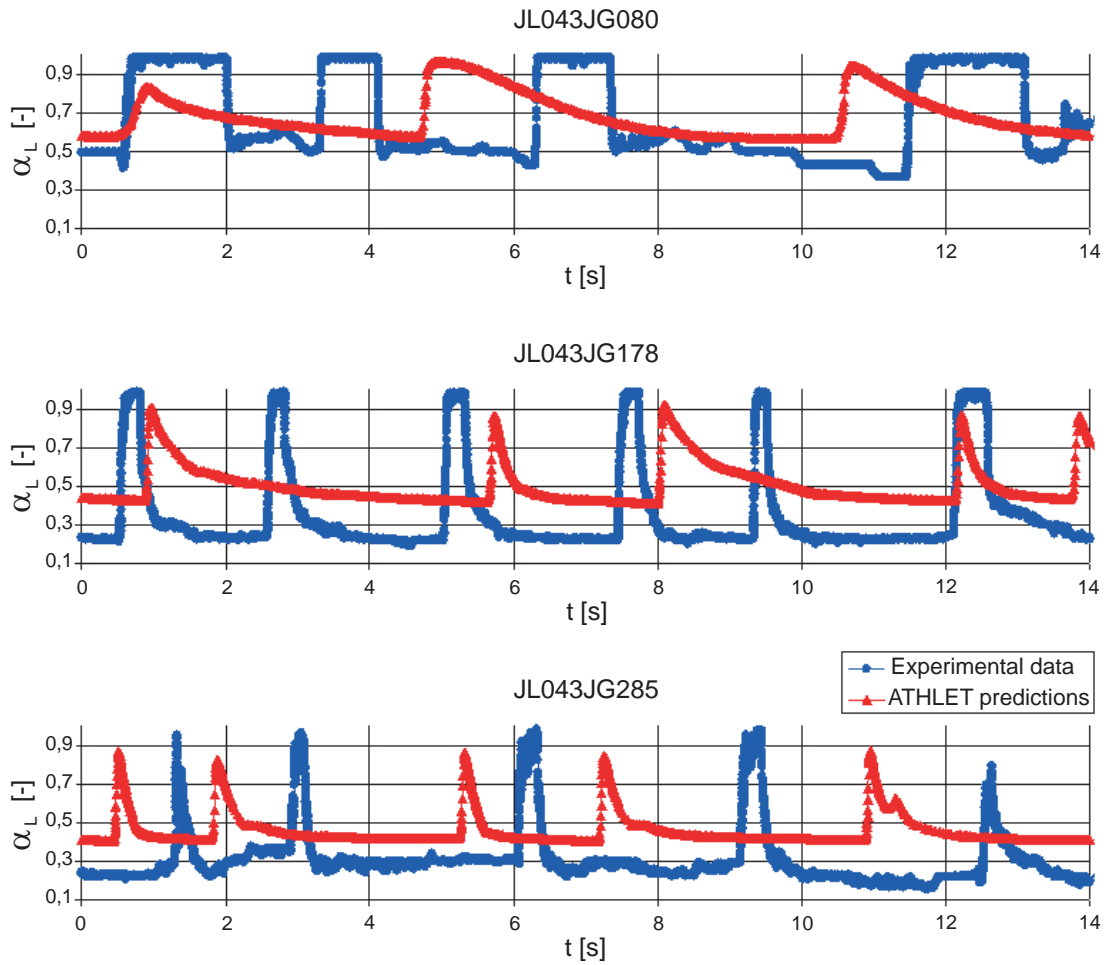
Figure 3.7: Comparison of the liquid fraction predicted by the modified ATHLET 2.1A and the experimental data: intermittent flows.

Table 3.1: Overview of the experimental data.

Name	j_L [m/s]	j_G [m/s]	$\overline{\alpha}_L$ [-]	$\overline{\alpha}_{Lf}$ [-]	$\overline{T}_s[s]$
JL043JG060	0.427	0.597	0.66	0.48	3.18
JL043JG178	0.428	1.782	0.37	0.22	2.40
JL043JG285	0.431	2.845	0.33	0.25	2.52

Table 3.2: Overview of ATHLET predictions.

Name	j_L [m/s]	j_G [m/s]	$\overline{\alpha_L}$ [-]	$\overline{\alpha_{Lf}}$ [-]	$\overline{T}_s[s]$
JL043JG060	0.427	0.597	0.67	0.55	6.04
JL043JG178	0.428	1.782	0.52	0.44	3.80
JL043JG285	0.431	2.845	0.48	0.44	2.76

The average liquid fraction in the pipe is overpredicted by ATHLET for the three cases. The prediction of the height of the film is higher than in the experiments. Slug frequency or slug length are not correctly predicted by the code.

Intermittent flow is a complex flow with inherent characterisctics, such as slug frequency, slug velocity or slug length among others. The modified code is able to predict the transition between stratified-wavy flow and intermittent flow. Under intermittent flow conditions, continuous trains of slugs are predicted by the code if a sufficiently fine nodalisation is made. Transient phenomena, such as slug growth, collapse or merging are captured by the equations, but the inherent characteristics of intermittent flow, such as slug frequency, slug body length or slug velocity are not correctly predicted by the code.

As previously mentioned, ATHLET 2.1A does not include models or closure relations to predict slug features. For adiabatic flows, the only flow pattern related constitutive model implemented in ATHLET is the interfacial shear force model. A simplified flow pattern model is used for the calculation of the interfacial shear stress coefficient. The flow pattern is determined as a function of a critical phase velocity. Bubble flow and intermittent flow in horizontal pipes are modelled in a similar manner. This modelling is suitable to adequately predict the transition between stratified-wavy flow and intermittent flow for adiabatic flows, but it is not suitable for the prediction of slug characteristics. The simplified flow pattern model implemented in ATHLET does not account for gas entrainment into the liquid phase. Better results might be achieved by means of a specific modelling of bubble entrainment into the liquid phase. A different modelling of the interfacial friction for bubble flow and for intermittent flow could lead to better agreement with the experimental data.

4 Test Rig Design and Measuring Techniques

4.1 Experimental Flow Facility

The experimental flow facility at the Lehrstuhl für Thermodynamik of the Technische Universität München includes a horizontal measuring test section, water and air delivery systems, a two-phase mixing section, a two-phase separator and instrumentation. The entire metering and controlling of the liquid and gas flow rates, the two-phase mixing section and the instrumentation of the facility were modified for this study. The regulation of the gas-liquid flow rates and the design of the two-phase mixer, which define initial and boundary conditions of the experiment, were made to achieve results of clearly defined and quantified flow patterns. This allows the boundary conditions of the different test cases to behave equally in the experiment and in the simulation. A schematic diagram of the experimental flow system is shown in figure 4.1.
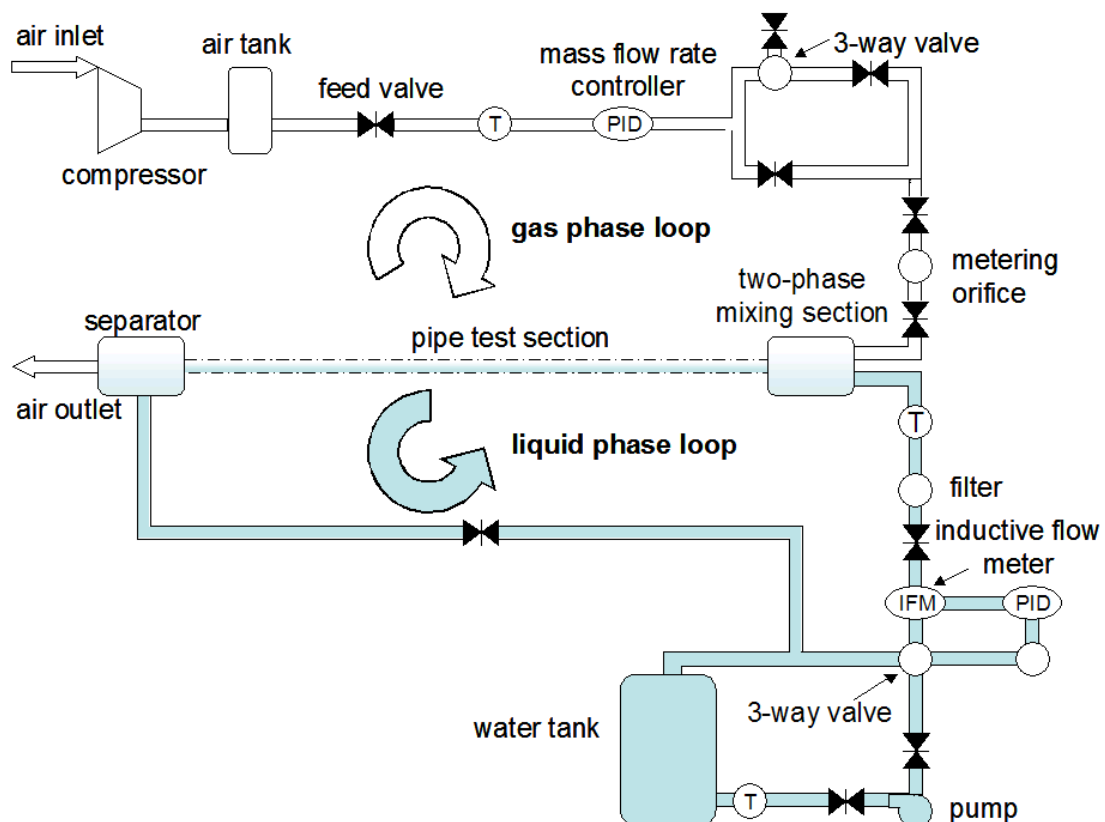
Figure 4.1: Sketch of the two-phase experimental pipe facility.

The water flows in a closed loop, whereas the air is released to the environment downstream of the horizontal test section, where both phases are separated. The two-phase loop is operated at pressures and temperatures close to atmospheric conditions. The transparent test section is a plexiglass pipe with an inner diameter of 54 mm. Measurements were carried out for two different pipe lengths, $223D$ and $268D$. The pipe consists of four or five sections (depending on its length) connected by flanges.

4.1.1 Air Flow Loop

Environmental air is compressed and stored in a reservoir at up to 16 bar. When the pressure of the tank falls under 12 bar, the compressor starts automatically and runs until 16 bar are reached. To avoid pressure oscillations in the test facility, a pressure-reducing valve maintains a constant pressure of 7 bar. The gas flow rate is accurately adjusted by a mass flow rate controller (Brooks, Type 5853S). Then a three-way magnet valve (MAC Serie 57) leads the air flow either into the plant or into the environment. In this manner, intermittent defined air volumes can be produced with a switching frequency up to 20 Hz without a negative influence on the stability of the mass flow rate controller (see figure 4.2(b)). A by-pass avoids abrupt pressure changes (backstreaming), resulting in generated flow rates as shown in figure 4.2(c). This configuration allows the production of quantified liquid slugs and elongated bubbles. The volumetric air flow rate is measured upstream of the mixing device by means of a metering orifice (Dosch Messapparate, DIN 1952). In this work the air and water flow rate were maintained constant for every operating point (see figure 4.2(a)).
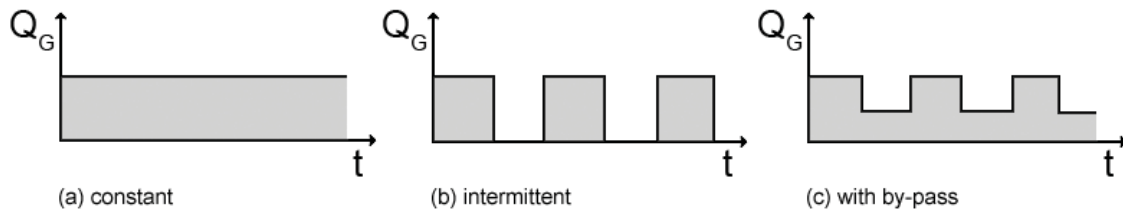
Figure 4.2: Possible air flow rate modulations at the inlet.

4.1.2 Water Flow Loop

The water is supplied by a centrifugal pump from a tank. A three-way valve moved by a motor (Honeywell Centra, Type VMM), which is controlled via a PID controller (Hengstler, Type grado 902), leads one portion of the water into the test section and the other part back into the reservoir. The water flow rate is measured before entering into the two-phase mixer by an inductive flow meter (Fischer-Porter), providing data for the PID controller.

Table 4.1: Pump and compressor data overview.

Medium	Device	Company	Type	Flow Rate
Water	Pump	KSB	ETA 40-26 K	0 - 10 m^3/h
Air	Compressor	Kaeser	AS 35/13	0 - 30 m^3/h

4.1.3 Two-Phase Mixing Section

A two-phase mixing section has been designed and manufactured for the production of stratified, plug and slug flows. As it is shown in figure 4.3, air and water are separately introduced through flexible hoses into the mixer, where a horizontal plate separates both fluids and ensures an initially stratified configuration. It is made of plexiglass in order to allow visual observation. The gas is introduced above and the liquid below. By means of a vertical perforated plate in the mixing section, fluid profiles are rectified. The void and liquid fraction at the inlet (just behind the two-phase mixer) is 50%.
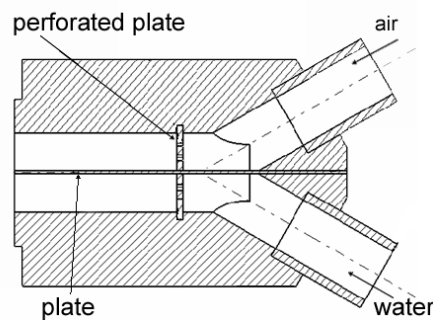
Figure 4.3: Two-phase mixing section.

4.2 Measuring Techniques and Data Acquisition

Great efforts have been made to develop new instrumentation in order to gain insight into the two-phase flow phenomena. The instrumentation can be categorized between intrusive and nonintrusive techniques. The main advantage of using nonintrusive techniques is that the data is obtained without interfering with the experiment. In this work, nonintrusive as well as intrusive measuring techniques have been used depending on which flow parameters were to be measured.

Both pressure and differential-pressure measurements were carried out by several pressure transducers at the two-phase mixer and along the test section. The pressure drop data was acquired from a total of 7 pressure taps (see table 4.2) distributed along the bottom center of the pipe in order to avoid, as much as possible, the presence of air in the lines leading to the transducer.

Table 4.2: Pressure sensors data overview.

Measuring Device	Measuring Principle	Range	Accuracy
absolute-pressure	strain gauge	0 - 10 bar	$\pm 0.5\%$
differential-pressure	inductive principle	$\pm 0.5, \pm 1.0$ bar	$\pm 0.5\%$

Table 4.3: Flow meters data overview.

Medium	Measuring Device	Range	Accuracy
water	inductive flow meter	0.4 - 42 m^3/h	$\pm 0.1\%$
air	flow rate controller	0 - 60 m^3/h	$\pm 0.5\%$
air	metering orifice	0 - 20 m^3/h	$\pm 0.5\%$

Both the liquid and gas temperatures were acquired by two PT100 thermometers before the fluids enter the two-phase mixing section. The water and air flow rate were also measured before entering into the two-phase mixer by an inductive flow meter and a metering orifice, respectively (see table 4.3). The accuracy of all devices is in the worst case of $\pm 0.5\%$.

4.2.1 Wire-Mesh Sensors

Void fraction measurements were carried out by means of wire-mesh sensors (WMS) developed and manufactured at Forschungszentrum Rossendorf [Prasser et al., 1998]. The measuring principle of this sensor is based on the different electrical conductivities of the two-phase mixture, water and air. The sensor consists of two planes of wire grids with 16 parallel electrodes each as it can be seen in figure 4.4.
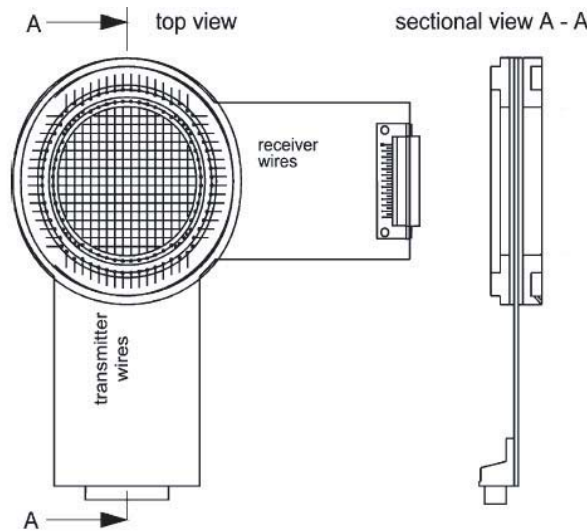

Figure 4.4: Sketch of the wire-mesh sensor [Prasser et al., 1998].

These planes are placed in a 1.5 mm distance from each other and the angle between the wires is 90°. This results in 16×16 sensitive points, which are equally distributed over the cross section. After subtracting the crossing points which are not inside the pipe cross section, a total of 232 electrode crossing points give a high spatial resolution of the void across the pipe. The wires have a thickness of 120 µm. The conductivity measurements take place between two perpendicular wires of each plane. The wires of the first plane are used as transmitter and are activated by a multiplex circuit in a successive order. The second plane (receiver plane) receives the pulses depending on the fluid, which is between both electrodes. The signal acquisition circuitry guarantees the suppression of crosstalk between selected and nonselected electrodes.

A two-dimensional matrix of the instantaneous values of the current is available, reflecting the conductivities between all crossing points of the electrodes of the two perpendicular planes. Volumetric gas fractions are obtained by relating the measuring result in the two-phase flow to a calibration measurement taken when the pipe is completely filled with liquid. The result is a matrix of local instantaneous volumetric gas fractions $\alpha_{G,i,j,k}$, where i, j are the indices representing the location in the sensor plane and k is the number of the current measurement:

$$x = i \cdot \Delta x; \quad y = j \cdot \Delta y; \quad t = k \cdot \Delta t_{sample} = k / v_{sample}.$$

Four sensors were placed along the measuring test section in order to enable the study of the evolution of the flow pattern along the horizontal test pipe. Each sensor were placed between two flanges and centered at the pipe cross section. These four sensors were managed by an electronic unit, which controles the whole system and acquires the data. Prasser et al. [2001] documented the influence of the wire-mesh sensor on a bubbly flow which is one of the flow patterns that could be more distorted by this invasive measurement technique. They concluded that even when the sensor causes a significant fragmentation of the bubbles, the measured signals still represent the structure of the two-phase flow before it is disturbed.

4.2.1.1 Extraction of the Slug Parameters

In the present work, several algorithms have been developed in order to extract the slug parameters from the data acquired by means of wire-mesh sensors. The void fraction data is spatially averaged in the pipe cross section and these averaged values are low pass filtered. Then the different slug parameters are extracted. First, the slugs identified at sensor 4, are cross correlated with the slugs identified at sensor 3. Then the slugs from sensor 3 are cross correlated with the data from sensor 2. At the position of sensor 1 the flow is not fully developed, so the slugs identified at sensor 2 are not always found at sensor 1 (this data could not be correlated automatically). Figure 4.5 shows the dimensionless liquid height h/D at three different positions along the pipe (sensor 2 at $141.5D$, sensor 3 at $208.7D$ and sensor 4 at $253.7D$ from inlet) and the cross correlated slugs between
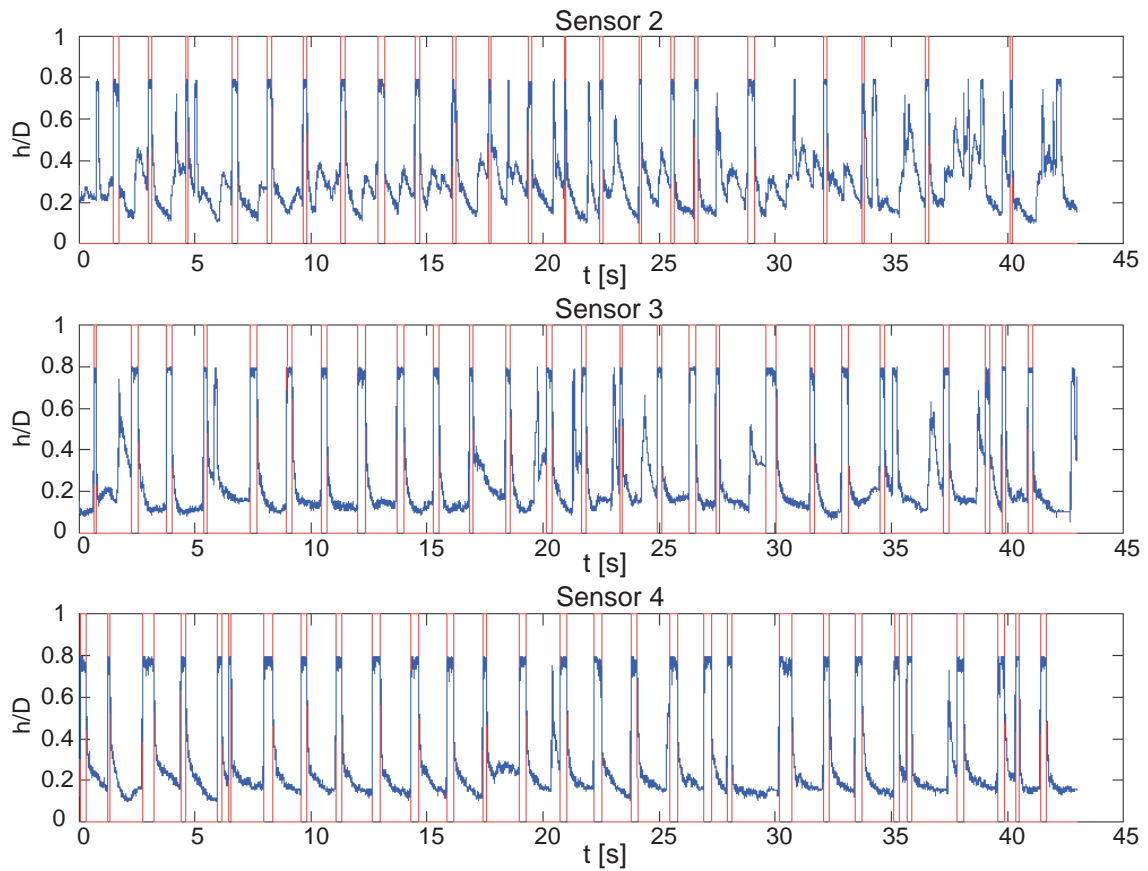
Figure 4.5: Correlated slugs between wire-mesh sensors.

sensor 2, 3 and 4 ($j_L = 0.86$ m/s, $j_G = 2.25$ m/s). The waves and slugs which are not detected by sensor 4 are not correlated.

The slug period T_u is defined as the time that one slug unit takes to go through the position of the measuring technique. The inverse of the slug period T_u is the slug frequency v_u at a certain position from the inlet:

$$v_u = \frac{1}{T_u}. \tag{4.1}$$

The average slug frequency is calculated as:

$$\overline{v}_u = \frac{\sum_{n=1}^{N} v_{u,n}}{N}. \tag{4.2}$$

The average of other parameters are calculated in an analogous way. The slug front and tail velocity, u_t and u_b, respectively, are calculated by the identification of the arrival times of the slug front and tail at two adjacent sensors, and then dividing the distance Δx between

them by the respective time differences Δt. The slug front and tail velocity between sensor 1 and sensor 2 e.g. is then given by:

$$\overline{u}_{p,s1-s2} = \frac{x_{s2} - x_{s1}}{t_{p,s2} - t_{p,s1}}; \; p = [t,b], \tag{4.3}$$

where p is the generic index representing either the slug front t or the slug tail b.

The slug body length l_s is calculated by multiplying the slug body period T_s and the liquid slug velocity u_{Ls}:

$$l_s = T_s\, u_{Ls}, \tag{4.4}$$

where the slug velocity is calculated as $u_{Ls} = \frac{1}{2}\left(u_t + u_b\right)$.

4.2.1.2 Bubble Identification, Bubble Size and Bubble Velocity

For the investigation of bubble size distributions by means of wire-mesh sensors, Prasser et al. [2001] developed a pattern recognition method based on the identification of bubbles from the data supplied by a single sensor. They defined a bubble as a region of connected gas-containing elements in the gas fraction data array $\alpha_{G,i,j,k}$ that is completely surrounded by elements containing liquid phase. During the bubble recognition process, each element of such a region receives a common number n that is unique for the detected bubble. These numbers are stored in the elements $b_{i,j,k}$ of a second array with the same dimensions as the gas fraction array. The volume of the bubble with the number n is calculated by integrating the local gas fraction over elements owning the given bubble number. The sum of gas fraction is multiplied by the axial bubble velocity $u_{Bub,n}$ and the extension of the control volume, which is the product of the lateral electrode pitch in x and in y directions and the sampling frequency:

$$V_{Bub,n} = \Delta x \Delta y \Delta t \cdot u_{Bub,n} \sum_{i,j,k} \alpha_{G,i,j,k}. \tag{4.5}$$

In this case the pitch equals 3 mm and the sampling rate is 5000 Hz:

$$\Delta x = \Delta y = 3\ \text{mm} \quad \text{and} \quad \Delta t = 1/\nu_{sample} = 0.2\ \text{ms}.$$

The axial bubble velocity is acquired by means of two wire-mesh sensors placed very close to each other. With a high time resolution and a very short distance between them, it is possible to measure the time of flight of individual bubbles. The distance between the sensors is of 20.25 mm.

The equivalent diameter of the bubble is defined as the diameter of a sphere:

$$D_{Bub} = \sqrt[3]{\frac{6V_{Bub}}{\pi}}. \tag{4.6}$$

4.2.2 Simultaneous PIV and PS Technique

In this work, the Particle Image Velocimetry (PIV) technique and the Pulsed Shadowgraph (PS) technique are used simultaneously to measure the velocity and turbulence fields in different two-phase flow patterns. The main problem applying PIV in two-phase flows is an accurate detection and separation of the phases. If the separation of the phases is not realized, the standard PIV image evaluation would generate incorrect velocity vectors in the gas phase and near the gas-liquid interface. The simultaneous use of a shadow technique, based on a uniform background illumination of the flow, enables a clear separation of the phases in the PIV images. With this, it is possible to determine more accurately the velocities, especially near the interface.

Tokuhiro et al. [1998], Hassan [2003], Fujiwara et al. [2004], Kitagawa et al. [2005] among others, used one or more digital cameras for PIV and an extra one for the shadow technique. These approaches cause accuracy problems arising from overlying the images. Therefore, Lindken and Merzkirch [2002], as well as Nogueira et al. [2003] used only a single camera for PIV and PS technique. With this procedure the information from the bubbles and tracers are recorded simultaneously in the same frame of the CCD chip, which eliminates this source of error.

For phase-separation by image processing the following techniques have been reported:

Hassan et al. [1998] took PIV measurements of individual ascending bubbles in a vertical pipe. Applying a predetermined threshold value on the gray-scale digital image, a binary image was obtained and a reconstruction of the bubbles was made. While fast and easily applicable, with this procedure, the recognition of the bubble contour cannot be accurately done without the use of a shadow technique.

Broeder and Sommerfeld [2002] accomplished PIV measurements in vertical bubbly flow using a pulsed panel of light emitting diodes (LEDs) located in the background of the test section opposite the camera. The shadow of the bubbles and the shadow of the tracer particles were recorded in the same image. For post processing, first, a median filter was applied to the images to eliminate the particles and further disturbances. Then the contour of the bubbles was accentuated with a sobel filter and finally the contour was extracted using the gradients of the gray values. But by first using the median filter some distortion of the gray values occurs, which may lead to subsequent shifts of the bubble contours.

Lindken and Merzkirch [2002] performed PIV/PS measurements of bubbles rising in a vertical column of stagnant liquid. Again a median filter was applied to the images to extract the tracer particles. In this work, the following separation of the image information was performed with a dynamic gray value threshold.

Nogueira et al. [2003] conducted PIV/PS measurements of a single Taylor bubble rising in a vertical column of stagnant liquid. They also first applied a median filter to eliminate the tracer particles in the images. Then, a background image is subtracted from the filtered image in order to determine the shape of the bubble after binarisation with a selected threshold.

Carpintero-Rogero et al. [2006] report a new algorithm based on the work by Lindken and Merzkirch [2002] as well as Nogueira et al. [2003] to process the images obtained from a simultaneous PIV/PS experiment. Contrary to the previous works, Carpintero-Rogero et al. [2006] avoids the use of a median filter in order not to falsify the gray values of the PIV/PS images.

4.2.2.1 PIV/PS Set Up

Figure 4.6 shows the optical set up of the experiment. The horizontal plexiglass pipe test section is surrounded by a plexiglass box filled with the same liquid as in the pipe in order to minimize the optical distortion. The light sheet projected from the bottom by the 527 nm laser illuminates the vertical symmetry plane of the flow, which is seeded with fluorescent particles. The flow is illuminated from the back by a monochrome 643 nm LED panel. A digital camera, focused on the vertical symmetry plane, records the information of the fluorescent particles of the PIV measurement and the back light shadow of the air phase. An optical filter blocking the laser wavelength eliminates the effect of light scattered and reflected at the interface regions and pipe walls.
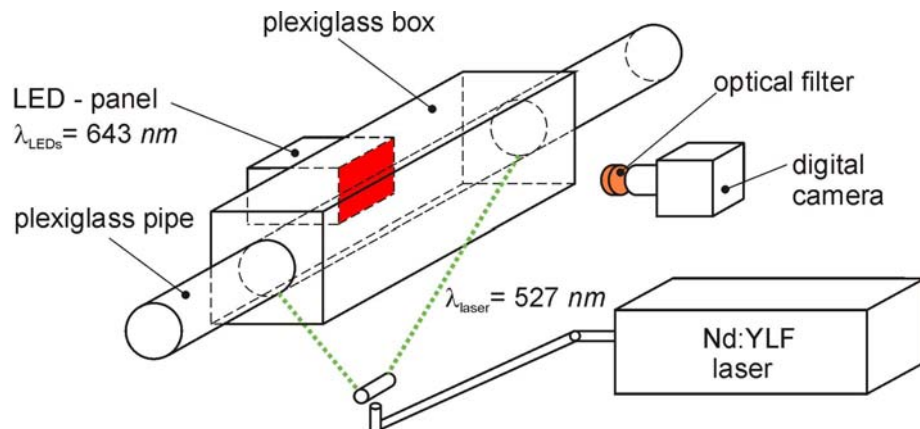
Figure 4.6: Set up of the simultaneous HS-PIV and PS technique.

Figure 4.7 explains the principle of the recording by the camera. In the upper part, the recording of the particle images (PIV) is sketched while in the lower part the acquisition of the shadow images (PS) is shown. The light of the laser at 527 nm and the LED panel at 643 nm enters the flow. The laser sheet excites fluorescence of the particles with a peak at 573 nm, but also scattering and reflections at the phase interfaces and the pipe walls are created. The optical filter located in front of the digital camera blocks wavelengths smaller than 570 nm. Therefore, only the background illumination of the LED panel, with wavelength of 643 nm, and the emitted light of the particles pass towards the camera. As a result, only the undisturbed signals from the gaseous phase and the tracers are recorded.
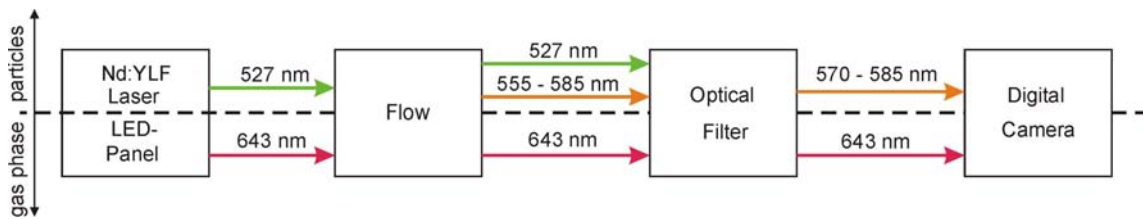
Figure 4.7: Principle of the combined PIV/PS system (modified scheme of Lindken and Merzkirch [2002]).

4.2.2.2 Particle Image Velocimetry

For a description of the PIV-technique in general, the reader may refer to Raffel et al. [1998]. In this place, only the characteristics of this technique applied to two-phase flows will be summarised. The PIV technique uses fluorescent tracer particles as markers in the water flow, which are illuminated with a New Wave Pegasus double cavity Nd:YLF laser with a wavelength of 527 nm and an energy up to 10 mJ per pulse. The fluorescent particles are made of polystyrene with Rhodamine B as fluorescence dye which is excited by the laser light sheet at wavelengths of $555 - 585$ nm with an emission peak at 573 nm. These particles have a mean diameter of 10.5 µm and a density of 1.06 g/cm^3. The concentration of tracer particles in the flow show a nominal volume content of about 10^{-5} [-], following the recommendations of Lindken [2002].

The laser beam was focused into a light sheet of about $1,5$ mm thickness in the *xy* symmetry plane of the horizontal pipe test section as it is shown in figure 4.6.

A Photron APX CMOS camera with a resolution of 1024 pixel × 1024 pixel and 8 bit was positioned orthogonally to the laser sheet. A 85 mm focal length and a 12 mm extension ring were used. The camera frequency was set to 1000 frames/s.

The whole commercial PIV System (Intelligent Laser Application, ILA) was controlled by a hardware timing unit. The distance between pulses of cavity 1 and 2 was adapted to the respective parameters of the operating point in order to get an optimal particle displacement.

4.2.2.3 Pulsed Shadowgraph

To obtain the shadow images of the gas phase, the flow was illuminated with a monochrome panel of light emitting diodes placed in the background of the test section. Due to this background illumination, the zones close to the interface of the gaseous phase produce a shadow, which was recorded by the digital camera of the PIV system. For the LED panel 144 high-power diodes with wavelength of 643 nm were used. Between the diodes and the test section a diffuser screen was located.

The LED panel was operated in a pulse mode in order to avoid a blurred image of the moving gas phase due to the long exposure time of the camera. An electronic system was

developed to synchronize the LED panel with the PIV system. These diodes feature a dead time, which results from the fact that the LEDs only emit beyond a threshold current. Since the response time and duration of the pulses have to be very short, a permanent current must be applied. Also, the wavelength of the diodes depends on their temperature, so the LED panel must be operated before taking measurements to bring them up to operating temperature.

The distinction between the light emitted by the tracer particles and the background lightning is optimized by adjusting the intensity of the LED panel. The electronic system of the LED panel is timed over the Q-switch out signals of the laser cavities (see figure 4.8).
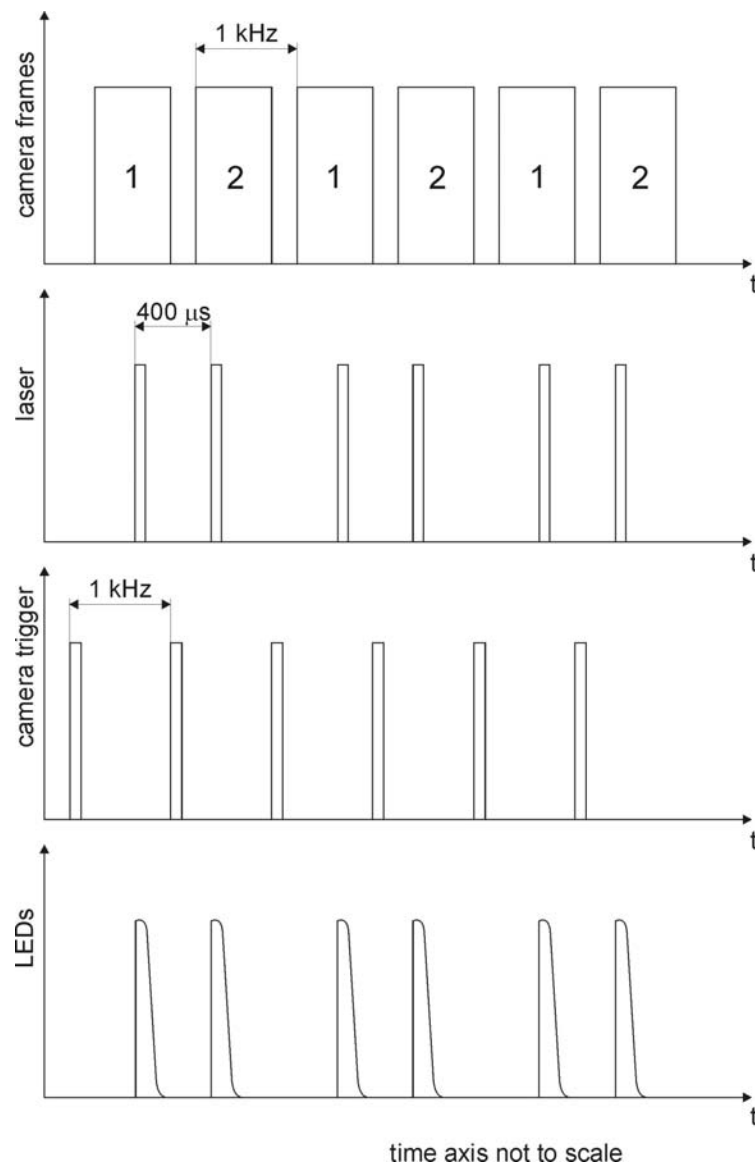
Figure 4.8: Timing diagram of the synchronization of the camera, laser and LED panel.

4.2.2.4 Image Processing

The principle of the air detection is based on the characteristic differences of gray levels recorded in the PIV/PS images relative to background image values. Three different ranges of gray levels can be observed: a high level range corresponding to the light emitted from the tracer particles, a medium gray level range containing the light coming directly from the LEDs and the lowest gray levels that correspond to the shadow zones near the interface of the gaseous phase.

Figure 4.9 shows a typical PIV/PS image of a slug front with a horizontal and a vertical white line drawn in. The gray value distribution along these white lines is shown on the bottom and on the right side of the image. The fluorescent tracer particles appear as bright points in the image and as pikes on the curve in the gray level distribution. The low levels of the gray distribution represent the gas phase. Due to the small depth of focus on the laser light sheet, the contour of the gas phase appears slightly blurred. However, it can be quite well distinguished from the background lightning by its gray tone distribution.

Therefore, given the gray values of the image pixels relative to their background image values they can be assigned to the different phases. Pixels which are brighter than the
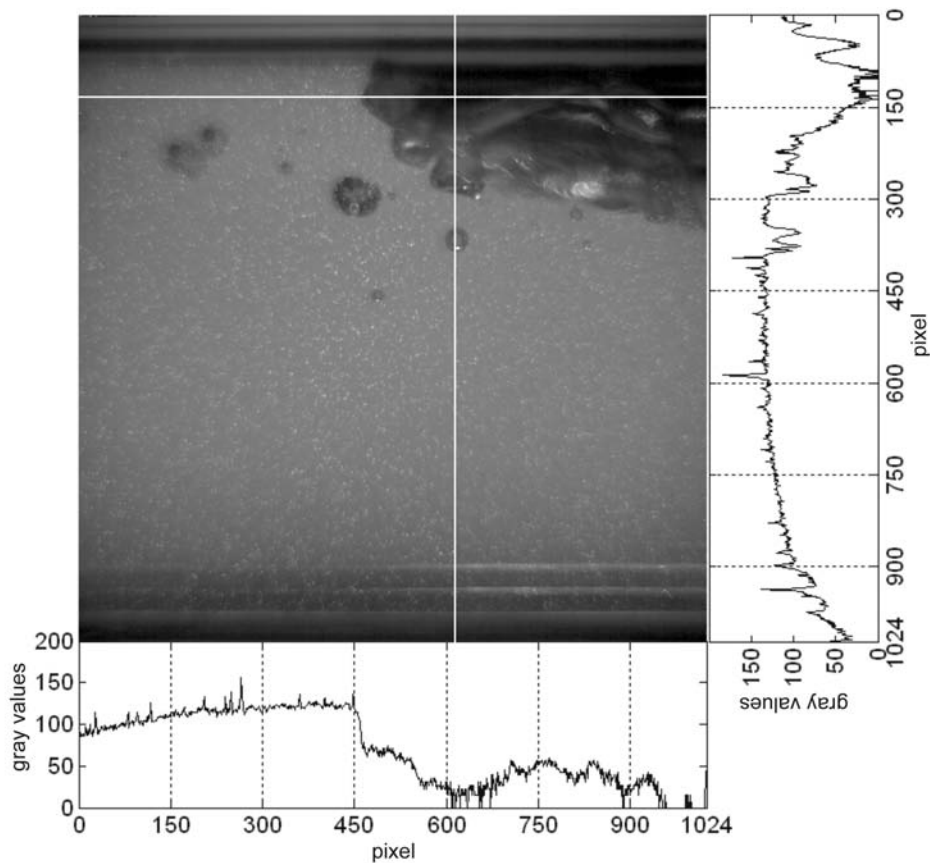
Figure 4.9: Distribution of gray values along the two white lines of a PIV/PS image.

background lightning correspond to the tracer particles. Those pixels which are darker than the background lightning represent the gas-liquid interface. Thus the image contains all information necessary to separate the phases.

Based on the principle outlined above, the images are processed with a software developed within this work.

Prior to the actual experiments, a set of background pictures of the pipe-test section filled only with water and without laser lightning must be acquired. This should be done for every pulse frequency used in the experiment in order to avoid intensity differences between PIV/PS and background images that are caused by the frequency response of the LED array. The background images for a particular pulse frequency are median filtered and then averaged individually.

Then the particular PIV/PS image, e.g. in figure 4.10(a), is read in. For optimal effect, the brightness of the PIV/PS image is calculated using a dynamic gray value threshold. This procedure removes the brightness values of the tracer particles without influencing the brightness value of the background in the PIV/PS images. After this step, an optimal background image can be assigned to each PIV image, which is slightly brighter than the background of the PIV/PS image. In order to remove the reflections at the air-water interface, which cannot be avoided despite the optical filter, a static threshold is applied. Reflections and tracer particles which both have high gray levels are now assigned to the low gray levels of the air regions.

The resulting image is binarised by subtracting the assigned background image. The gray tone values of the gas phase and tracer particles which become negative in this step are set to zero, e.g. figure 4.10(b). Then, the pipe walls are removed from the image, leaving only the flow region. Additionally, the image is inverted, i.e. the gas phase becomes white. At this point, a search is done in order to capture zones within the gaseous phase which were not set to zero by the binarisation. Every region which is enclosed by a white frame is asummed to be a zone of the gas phase and is subsequently filled with white. For the recognition of the gas phase in intermittent flows, a white border is added to the top and both sides of the image. This step gives e.g. figure 4.10(c). Following this, a size threshold is applied in order to find and remove remaining tracer particles and remaining disturbances, allowing the reconstruction of the interface.
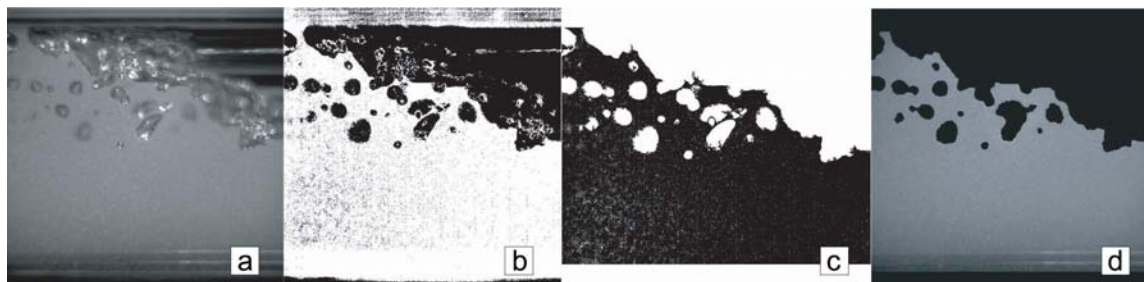

Figure 4.10: Steps of the detection of the air phase.

In the last step, the resulting binary image is subtracted from the original PIV/PS image. Now the air phase is filled with black while the liquid phase remains unchanged, as seen e.g. figure 4.10(d). Additionally, the pipe walls in the images are covered by a black bar.

The velocity field is calculated from the displacement of the particles between a pair of PIV images. Not only do these particles move, but also the gaseous phase experiences a displacement. In order to avoid erroneous vectors due to the displacement of the mask, the masking area for a pair of PIV images is the same. The mask of a pair is the sum of the areas of the gaseous phase of each PIV image of a pair. These resulting images are now ready for the PIV evaluation algorithm.

The evaluation of the vector fields from the masked PIV images is performed with the commercial software package VidPIV4.6XP from ILA. The typical displacement of the particles between a pair of images is around 4 pixel. The pulse distance between the cavities of the laser has to be adjusted for every operating point in order to obtain the mentioned displacement. The interrogation area is 16 pixel $\times$ 16 pixel with an overlap of 50% resulting in 127×127 vectors with a spatial resolution of $\Delta x = 0.49$ mm.

Afterwards, the local liquid velocity information of each image is exported and multiplied by the binarised image of its mask, setting to zero the erroneous velocity vectors in the gaseous phase calculated by the successive cross correlations of the software.

4.2.2.5 Limitations of the Measuring Technique

One of the problems with the PIV technique in two-phase flows can be clearly observed in figure 4.11(a), where the particles above the bubble are not illuminated because the laser light sheet is blocked by the bubble. The velocity vectors are calculated by the software, but they may not be correct. Another problem is showed in figure 4.11(b). The flow cannot be correctly illuminated when there is a high amount of bubbles in the liquid phase. Many bubbles overlap the flow or do not lie in the focus of the camera. A determination of the velocity vectors of the flow is not possible.
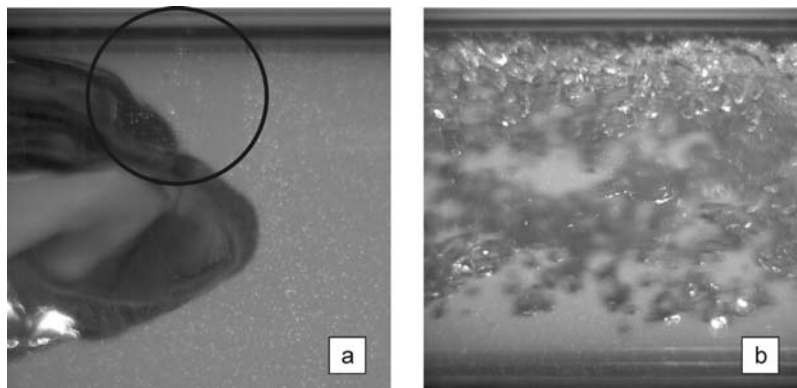

Figure 4.11: Limitations of the measuring technique.

Simultaneous PIV/PS is well suitable for the investigation of stratified, wavy and elongated bubble flow. The results show that the combined measuring technique is able to measure the velocities of the liquid phase and the interface with high resolution in two-phase flows. The measurements may also serve to investigate the turbulence structure in different flow patterns. For the investigation of bubbly, slug and plug flow this measuring technique is only conditionally applicable. If the gaseous phase is highly mixed with the liquid phase, only a part of the tracer particles can be seen and an accurate determination of the velocity vectors is not possible.

4.2.2.6 Extraction of the Velocity and Turbulence Quantities

Because turbulence consists of random fluctuations of the various flow properties, a statistical approach is used. The procedure introduced by Reynolds in which all quantities are expressed as the sum of mean and fluctuating parts is applied.

First, the local instantaneous velocity data calculated by VidPIV $u_i(x,y,t)$ is submitted to a time averaging procedure as expressed by the following relationship:

$$\overline{u}_i(x,y) = \frac{\sum_{n=1}^{N(x,y)} u_{i,n}(x,y,t)}{N(x,y)}; \ i = [x,y,z], \tag{4.7}$$

where the conditional averaging coefficient $N(x,y)$ represents how many times in a series of data there is liquid velocity information in a generic position (x,y). The average value corresponds to an arithmetic averaging:

$$\overline{u}(x,y) = \sqrt{\overline{u}_x(x,y)^2 + \overline{u}_y(x,y)^2 + \overline{u}_z(x,y)^2}. \tag{4.8}$$

Once the mean velocity field $\overline{u}_i(x,y)$ is obtained, through the Reynolds decomposition

$$u_i(x,y,t) = \overline{u}_i(x,y) + u_i'(x,y,t), \tag{4.9}$$

the instantaneous values of the fluctuating component of the velocity $u_i'(x,y,t)$ can be derived.

The principal parameters related to turbulence are based on the value of the fluctuating component of the velocity. It is common practice to describe the intensity of the turbulent fluctuations in terms of root-mean-square (rms) quantities. The local average fluctuating component of the velocity $u_{i,rms}'(x,y)$ is the rms value of the time serie, the so-called standard deviation σ_i:

$$u_{i,rms}'(x,y) = \sigma_i(x,y) = \sqrt{\overline{u_i'(x,y,t)^2}} = \sqrt{\frac{1}{N(x,y)} \sum_{n=1}^{N(x,y)} u_{i,n}'^2(x,y,t)}. \tag{4.10}$$

The relationship of a rms quantity and the mean value of the same quantity gives the relative intensity I:

$$I = \frac{u'_{rms}}{\overline{u}}. \qquad (4.11)$$

The turbulence kinetic energy k is defined as:

$$k = \frac{3}{2}u'^2_{rms}. \qquad (4.12)$$

The mean turbulence Reynolds number Re_{tur}, calculated on the basis of the integral length scale, is expressed by the following equation:

$$Re_{tur} = \frac{u'_{rms} \cdot l_{tur}}{\nu}, \qquad (4.13)$$

where ν is the kinetic viscosity and l_{tur} the turbulent integral length scale. The integral length scale has been statistically calculated as the mean distance at which the fluctuation velocity of each point is correlated with the fluctuation velocity of the other points around it. On the generic i coordinate, it is defined as:

$$l_{i,tur} = \int_0^\infty R_{i,corr}(r)dr, \qquad (4.14)$$

where r is a generic position and the correlation coefficient $R_{corr}(r)$ is obtained as a function of the distance between two points. On the generic i coordinate, $R_{i,corr}(r)$ is:

$$R_{i,corr}(r) = \frac{\overline{u'_i(0)\,u'_i(r)}}{u'_{i,rms}(0)\,u'_{i,rms}(r)}. \qquad (4.15)$$

l_{tur} is composed using an arithmetic mean procedure.

4.2.2.7 Data Analysis

Two different approaches have been used for the statistical calculations in plug and slug flow. Both of them use the averaging method above explained, but in the first case, the PIV/PS images are analysed in their whole, and in the second case the images are classified in specific parts of the slug zones and studied separately. The first method has been called "fixed window analysis" and the second one "moving window analysis". The point of view in both cases is that of an external viewer, but in the second approach the camera moves with the same velocity as the elongated bubble. The PIV/PS images are cut in a way that the gaseous phase is approximately in the same position (slug nose or the slug tail are centered in the image), leading to the creation of image series at specific zones of

the liquid slug. Figure 4.12 shows two images of the same advancing bubble nose. The lighter zones are cut and are further processed. In order to study the flow field in different zones of the slug unit, the velocity of the slug nose and the slug tail is calculated, and the images are cut as the camera would move with this velocity. In this manner, specific parts of the whole slug unit can be analysed separately. It must be noted that it is not a moving reference frame, because the values of the velocity that are used are calculated with the information recorded by the camera from its fixed position, but it allows a statistic study of the flow field in different zones of the slug unit.

Figure 4.12: Moving window analysis procedure.

4.2.3 LED System

In the course of the investigation of intermittent flows, an optical measuring technique was developed. Without disturbing the flow, the designed Light Emitting Diode (LED) system allows the acquisition of the main characteristic parameters of the intermittent flow regimes, such as frequency, front and tail velocities and length. They are easy to set up and to move along the pipe test section in order to study the flow at different positions from the inlet of the fluids. The LED system can be also used to trigger an additional measuring system when a particular zone of the flow is studied. Problems with regard to the start of the PIV-images recording can be easily solved with this device. A similar triggering device is used by Grotjahn [2001] and Nogueira et al. [2003].

The measuring principle of the LED system is based on the refraction of light at the transition from one medium, with the speed of light c, to a medium with a different speed of light c^*. The speed of light in the media behave inversely to the refractive indexes n_{RI} and n_{RI}^* (constant properties of the materials). The law of refraction is given by:

$$\frac{\sin(\theta)}{\sin(\theta^*)} = \frac{c}{c^*} = \frac{n_{RI}^*}{n_{RI}}, \qquad (4.16)$$

where θ is the angle of incidence and θ^* is the angle of refraction.

In the measuring test section appear three different media: water, air and plexiglass (poly-methyl methacrylate, PMMA). When a slug moves through the LED system, there is water in the upper part of the pipe. As soon as the film region arrives at the measuring system, there is air in the upper part of the pipe, which has a different refractive index than water. Table 4.4 shows the different refractive indexes of the used materials.

Table 4.4: Refractive index of the used materials.

Media	Refractive Index
Air	1.0003
Water	1.333
PMMA	1.492

As it can be seen in figure 4.13, the pipe test section is placed between the light source and the photosensitive device. The light beam is deflected as a result of the different refractive indexes of the media. If the pipe has air in the upper part of the pipe test section, the light beam will meet the photosensitive medium. When a liquid slug passes through the system, then the light beam is deflected and does not meet the photosensitive device.
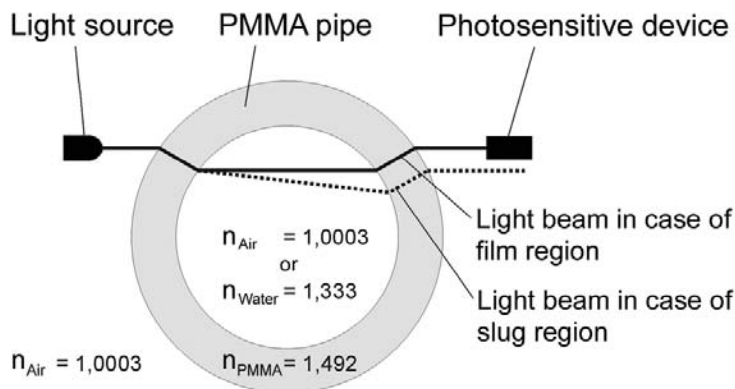
Figure 4.13: LED system.

Figure 4.14 shows the set up of the LED system. There are two LEDs and two photosensitive devices at a distance of 50 mm from each other, and they both are located at the upper part of the pipe test section (1/3 of the inner diameter of the pipe). The voltage signals delivered by the photosensitive device are transferred to the Data Acquisition Unit.

Both voltage signals are then binarised and cross correlated with each other. The extraction of the slug properties, such as front/tail slug velocity or slug body length, are calculated in an analogous way as for the wire-mesh sensors (already reported in section 4.2.1).

4.2.4 Data Acquisition and Triggering

Temperatures, pressures and fluid flow rates were acquired by means of a Hewlett Packard Data Acquisition Unit HP3852A with an integrated high speed voltmeter. The signals
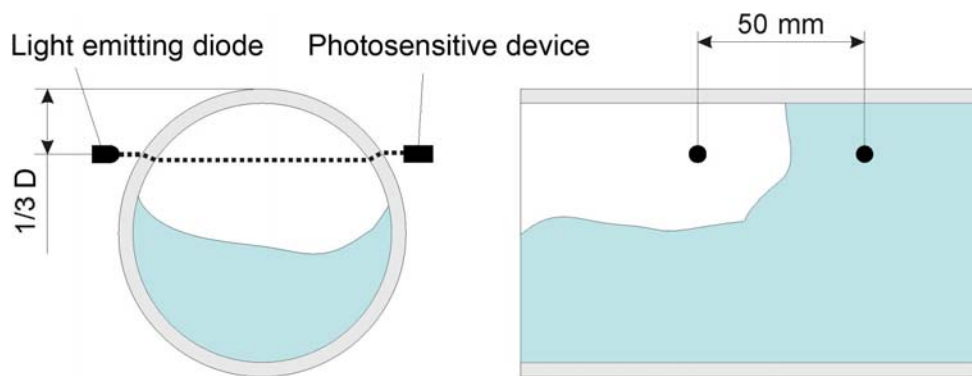
Figure 4.14: Set up of the LED system.

delivered from measuring devices which did not have an integrated amplifier, were first amplified and then transferred to the Data Acquisition Unit. The conversion of the analog voltage signals to digital data is carried out by the Data Acquisition Unit by means of an integrated fast AD-Converter. This digitized data is finally transferred to the computer by the HP-IB Bus.

For the control of all devices and measuring techniques used in the experimental facility, for the triggering and to give a format for the data recording, a program in HP-VEE was written. All measuring techniques (Hewlett Packard Data Acquisition Unit, Electronic Unit of the wire-mesh sensors and Hardware Timing Unit of the PIV system) were triggered in order to acquire all the data starting at the same time.

4.3 Experimental Procedure

In the following chapters, the flow characteristics of stratified, wavy, plug and slug flow extracted from the acquired measurements are presented and the influencing parameters are analysed. All experiments were carried out at atmospheric pressures and temperatures. The three-way magnet valve was not used for the acquisition of the experimental data presented in this work. The air and water flow rate were maintained constant for every operating point. A change in flow rate can lead to a change of flow pattern between the old and new steady states, leading to a temporary flow pattern between the respective steady states. In oder to avoid the effect of rapid flow rate changes, the measurements were acquired after a period of 3 to 5 minutes once the flow rate was changed.

Experiments have been carried out in a wide range of superficial gas and liquid velocities. The range of the superficial liquid velocity is from 0.09 m/s up to 0.87 m/s and for the superficial gas velocity from 0.15 m/s up to 4.52 m/s. Figure 1.3 shows the acquired operating points as seen in the flow pattern map according to Taitel and Dukler [1976].

The minimum measuring frequency of the instrumentation was set to 250 Hz for the pressure transducers, the air and water flow meters. The wire-mesh sensors measuring frequency was set to 2000 frames per second for the parameter evaluation of intermittent

flows and to 5000 frames per second for the investigation of bubble gas entrainment in the slug body. The measuring frequency of the simultaneous PIV/PS technique was adapted for each operating point in order to get an optimal particle displacement. Table 4.5 shows the pulse distance between the cavities of the laser for the PIV/PS data presented in this work (chapter 6.

Table 4.5: Pulse distance for the operating points of the PIV/PS experimental data.

Name	j_L [m/s]	j_G [m/s]	U_M [m/s]	Pulse distance [µs]
JL015JG010	0.15	0.10	0.25	1000
JL016JG160	0.16	1.60	1.76	390
JL051JG010	0.51	0.10	0.61	450
JL051JG060	0.51	0.60	1.11	330
JL051JG110	0.51	1.10	1.61	210
JL075JG010	0.75	0.10	0.85	280
JL075JG060	0.75	0.60	1.35	150
JL076JG110	0.76	1.10	1.85	120

5 Intermittent Flows: Plug and Slug Flow Behaviour

In the following chapter, the different characteristics between plug and slug flow will be analysed. Plug flow (or also called elongated bubble flow) occurs at very low gas velocities and the slug body is almost free of gas bubbles. When the gas superficial velocity increases, bubbles are entrained and dispersed flow occurs in the body of the liquid slug (the so-called slug flow). Not only the absence or presence of bubbles in the slug body, but also the shape of the elongated bubble (the nose and tail morphology), are a sign for this transition.

First, the observations of the initiation of intermittent flows made at the facility of the Lehrstuhl für Thermodynamik will be summarised. Then, the flow morphology of different patterns is discussed in order to elucidate the main differences between plug flow (or also called elongated bubble flow) and slug flow. Following this, in order to gain insight into the gas entrainment phenomenon, the influence of the dispersed bubbles in the liquid slug on some slug parameters is presented. Finally, the behaviour of the dispersed bubbles in the liquid slug is studied in detail.

5.1 Initiation of Intermittent Flows

In the experiment, the fluids enter into the pipe by means of a two-phase mixing section. The two-phase mixer provides a stratified flow configuration at the beginning of the pipe test section (see section 4.1.3), giving a distribution of the fluids at the inlet of 50% for each phase. For most operating points, this given distribution is not the equilibrium state: depending on the mass flow rates, the equilibrium height of the stratified flow is reached at different positions from the inlet, and thus strongly influences the initiation of slugs.

It was observed that first the water level increases in the pipe and then waves are formed. At some point along the pipe, a wave reaches the top of the pipe. This can persist as a slug along the pipe, leaving a lower liquid level behind it, or decay and carry liquid down the pipe as large amplitude roll waves. The height of the liquid flow is then recovered and the process starts again.

Figure 5.1 shows a schema of the initiation of intermittent flow in the pipe test section. At the transition from stratified-wavy flow to slug flow, which happens at very low superficial liquid velocities (around $j_L =0.1$ m/s) and relatively high gas velocities ($j_G >2.0$ m/s), slugs appear rarely and only at long distances from the inlet, e.g. not before $120D$. As the superficial liquid velocity increases, slugs form closer to the inlet. At still low liquid velocities ($j_L =0.22$ m/s, $j_G =0.15 -4.52$ m/s), slugs initiate between $17D$ and $52D$ from

the inlet. At these low liquid velocities (j_L <0.22 m/s), slugs tend to initiate farther away from the inlet when the gas velocity increases.

At higher superficial liquid velocities (j_L >0.22 m/s), the slugs tend to initiate closer to the inlet as the gas velocity increases. For a fixed gas velocity with increasing liquid velocity, slugs tend to form farther from the inlet. For j_L =0.44 m/s and j_G =0.15 −4.52 m/s, slugs are formed between 30D for low gas velocities, and 10D for higher gas velocities. For j_L =0.65 m/s and the same range of gas velocities, slugs are formed between 44D and 13D. For j_L =0.86 m/s and the same range of gas velocities, slugs are formed between 59D and 21D. In general, most of the slugs are formed before 50D downstream from the inlet.
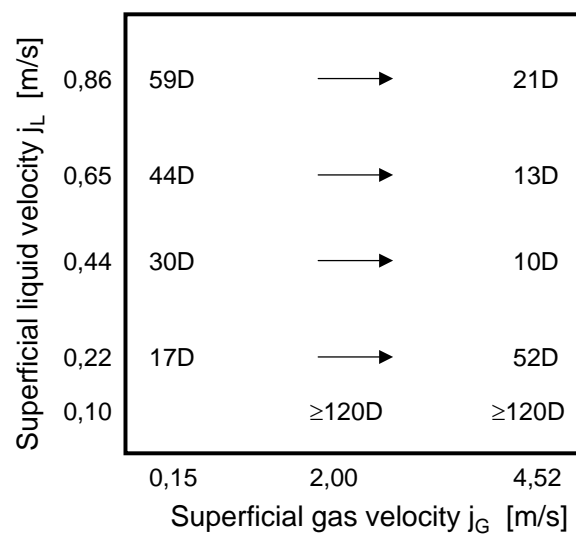
Figure 5.1: Influence of the inlet fluid velocities on the initiation of intermittent flow.

These observations are consistent with the experiments made by Woods and Hanratty [1999] in a 76.3 mm inner diameter and 20 m long pipe. They reported that for low liquid velocities (j_L =0.1 −0.2 m/s) and moderate air velocities (j_G =1.0 −4.0 m/s), slugs are not formed before 40D. As the liquid velocity increases for a fixed gas velocity, slugs are observed to form closer to the inlet. For higher liquid velocities (j_L >1.0 m/s) slugs are formed around 40D from the inlet.

5.2 Flow Morphology

Figure 5.2 illustrates the different successive time sequences of the phase distribution at the pipe cross section for different flow patterns. The blue colour denotes the liquid phase and the red colour the gas phase. Wavy, elongated bubble and slug flow are presented from the top to the bottom of the figure. The void fraction is acquired by means of a wire-mesh sensor (see section 4.2.1).

(a) Wavy flow

(b) Plug flow

(c) Slug flow

Figure 5.2: Time sequences of the phase distribution at the pipe cross section.

The images of the phase distribution at the pipe cross section reveal the important role of surface tension, gravity forces and wall friction for all of these regimes. The surface tension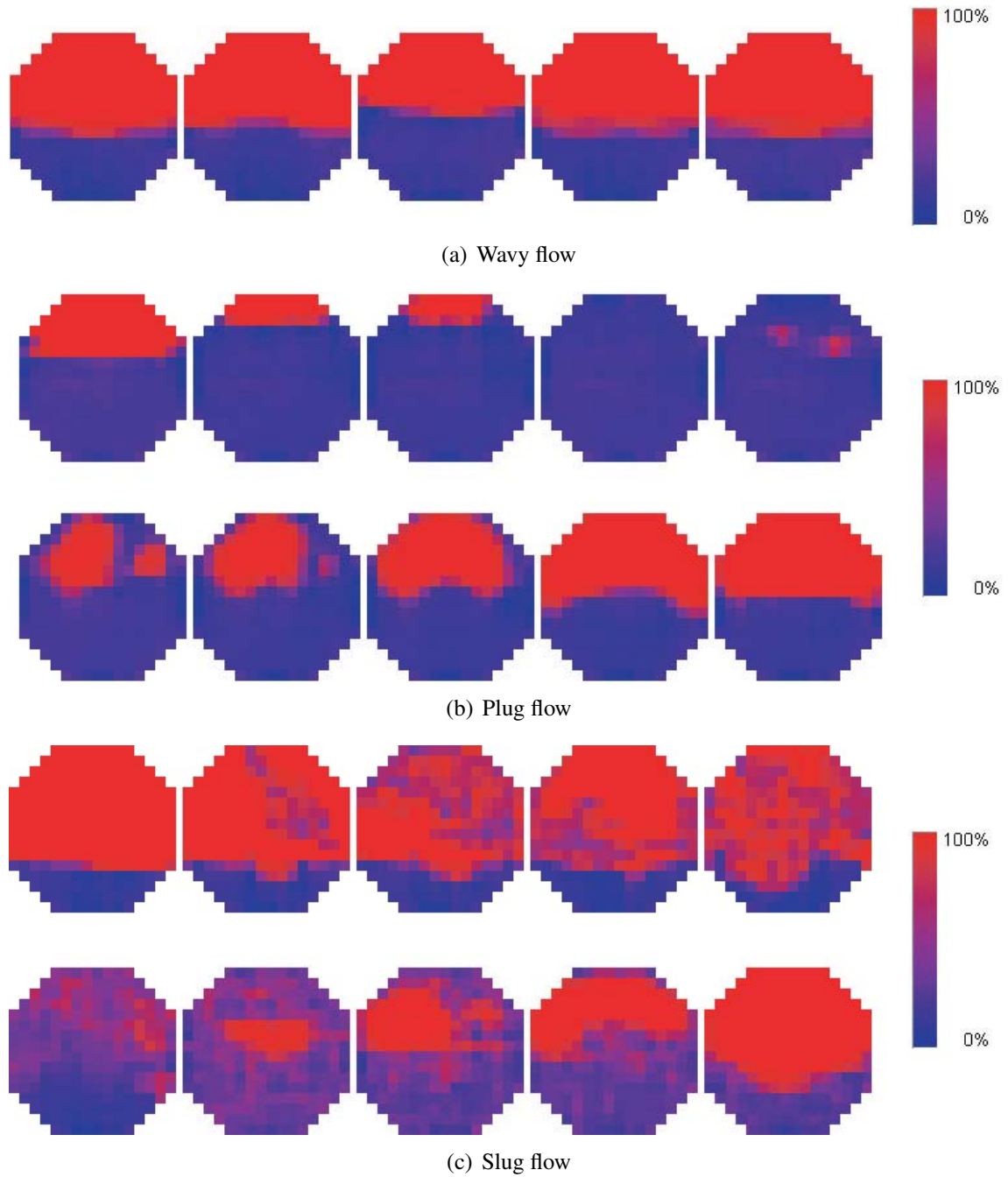 not only determines the contact angle with the pipe walls (PMMA is a hydrophilic material with a water contact angle of approx. 70°), but also the shape of the surface and the number of ripples or waves which are formed. When the water level increases in the cross section of the pipe, it is the level near the pipe walls that increases first due to the cylindrical form of the pipe. Only then, the liquid in the central part also increases. When the water level decreases, the liquid in the central part of the pipe starts to decrease. Then, the water near the pipe walls also decreases. Due to wall friction, the water near the walls takes longer to drop than the liquid in the central part of the pipe. Then, the liquid in the central part increases and sometimes even more than the level of the liquid next to the pipe walls. The water level stabilizes and the process starts again. This process can be observed in all images.

For plug flow, the liquid slug is still free of bubbles. For slug flow, with air mass flow rates higher than for elongated bubble flow, the liquid slug starts to be aerated. At very high flow rates, the liquid slug is chaoticly aerated and even the beginning of the liquid film region is strongly aerated.

Moreover, the shape of the elongated bubble changes from one flow regime to another. Ruder and Hanratty [1990] defined the transition between plug flow and slug flow regimes based on the shape characteristic of the bubble. Based on their experiments carried out in a 95.3 mm inner diameter and 24.6 m pipe, they suggested that the transition is independent of the superficial liquid velocity and occurs at a fixed superficial gas velocity of around 0.6 m/s. Fagundes Netto et al. [1999] reported from their experiments in a 53 mm inner diameter and 90 m pipe and for a wider range of superficial velocities, that this transition is mainly a function of the liquid velocity ahead the bubble. In their experiments, they introduced a single elongated bubble into the pipe and reported that for $Fr_M < 1$, the bubble presents a short nose followed by a stationary wave and a tail with a staircase shape. For $Fr_M > 2$, the tail and the stationary wave attached to the nose disappear. The nose of the bubble moves toward the center of the pipe (this is also observed by Bendiksen [1984]). The model of Fagundes Netto et al. [1999] suggests that for $1 < Fr_M < 3$, there is a transition zone in which the existence of the tail depends on the bubble length (short bubbles have a tail and longer bubbles do not). For $Fr_M < 1$, staircase bubbles are always observed and for $Fr_M > 3$ they are never observed. Moreover, they analysed Ruder and Hanratty [1990] data and showed that there is no contradiction between the transition they determined in their work and Ruder´s and Hanratty´s observations.

Similar observations were also made at the two-phase test facility of Lehrstuhl für Thermodynamik, although the transition between the two different bubble shapes was observed to be at aprox. $Fr_M = 1.5$.

For $Fr_M \leq 1.5$ (plug flows) the elongated bubble always presents a long tail. The nose of the elongated bubble is followed by a wavy interface and ends with a hydraulic jump which does not reach the top of the pipe, creating a thin long tail behind the bubble (staircase aspect). Figure 5.3 shows the typical shape of elongated bubbles for low mixture

velocities. Some times the tail breaks and these elongated bubbles present the same shape for the nose and the tail (see figures 5.3(a) and 5.3(d)). For higher mixture velocities the morphology of the elongated bubble is shown in figure 5.4.

(a) Bubble tail   (b) Hydraulic jump   (c) Bubble nose   (d) Bubble nose
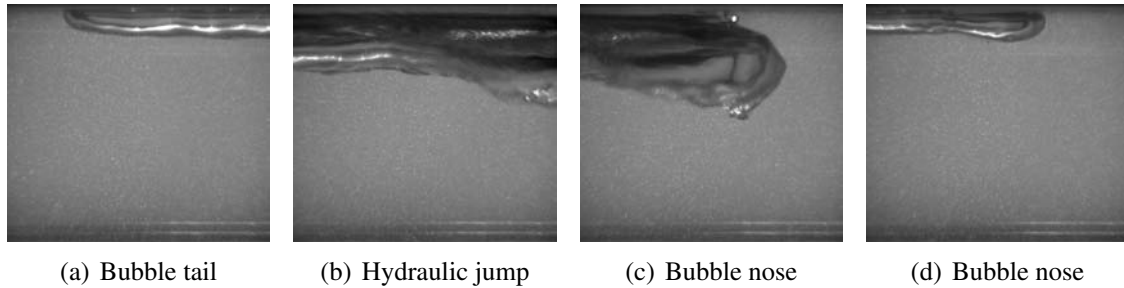
Figure 5.3: Elongated bubble shape for j_L =0.75 m/s and j_G =0.10 m/s ($Fr_M = 1.17$).

(a) Bubble tail   (b) Hydraulic jump   (c) Bubble nose
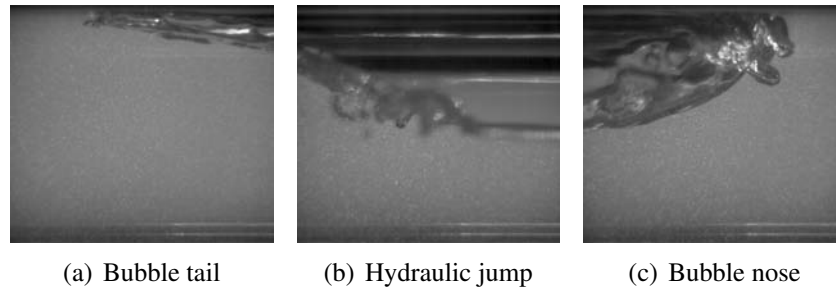
Figure 5.4: Elongated bubble shape for j_L =0.51 m/s and j_G =0.60 m/s ($Fr_M = 1.53$).

For $1.5 < Fr_M < 3$ small bubbles are entrained into the slug body and the long thin tail of the elongated bubble dissapears. Nonetheless, the tail still presents a staircase aspect (see figures 5.5, 5.6 and 5.7). The nose of the bubble moves toward the center of the pipe with increasing gas velocities. The aeration in the liquid slug increases with increasing superficial gas velocities. For $Fr_M > 3$ the slug body starts to be strongly aerated and the tail of the elongated bubble does not present a staircase aspect any more.

(a) Dispersed bubbles   (b) Hydraulic jump   (c) Bubble nose

Figure 5.5: Elongated bubble shape for j_L =0.75 m/s and j_G =0.60 m/s ($Fr_M = 1.85$).

(a) Dispersed bubbles   (b) Hydraulic jump   (c) Bubble nose
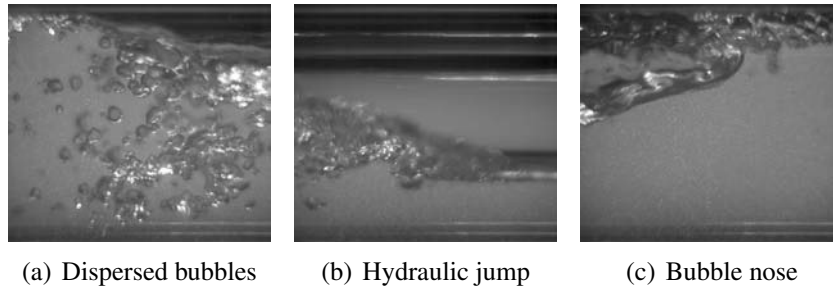
Figure 5.6: Elongated bubble shape for j_L =0.51 m/s and j_G =1.10 m/s ($Fr_M = 2.21$).

(a) Dispersed bubbles   (b) Dispersed bubbles   (c) Hydraulic jump   (d) Bubble nose

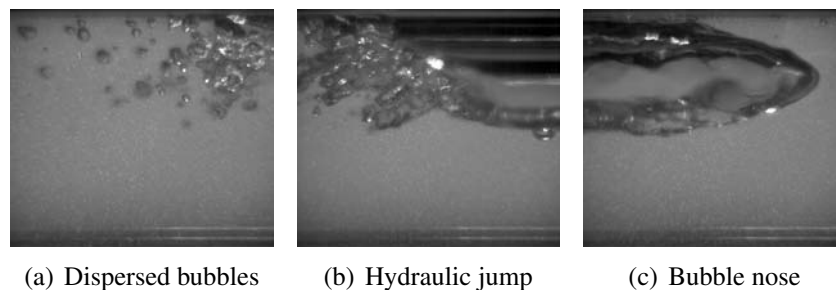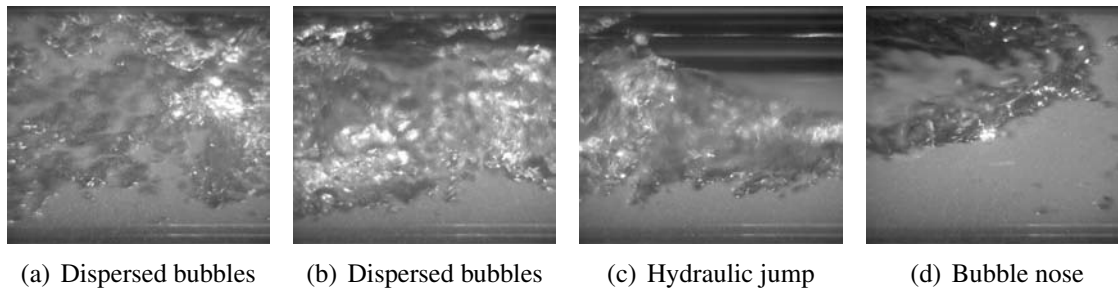**Figure 5.7:** Elongated bubble shape for j_L =0.76 m/s and j_G =1.10 m/s ($Fr_M = 2.54$).

5.3 Slug Void Fraction

It has already been mentioned that one of the main differences between plug and slug flow is the absence or presence of bubbles in the slug body. Gas entrainment has an important role in determining the flow characteristics. In order to study the void fraction in the liquid slug and its influence on the slug characteristics, several series of experimental data have been analysed. The experimental data was acquired by means of four wire-mesh sensors placed along the pipe test section (at $95D$, $142D$, $209D$ and $254D$ from the inlet). The length of the pipe was of $268D$. The range of the superficial liquid velocity was from 0.09 m/s up to 0.87 m/s and for the superficial gas velocity from 0.15 m/s up to 4.52 m/s.

The most common approach for incorporating slug characteristics, such as slug void fraction, in slug flow calculations is the use of empirical correlations. In the following sections the experimental data acquired in the test facility is analysed and compared with the most frequently used correlations.

Figure 5.8 shows the void fraction in the slug body α_{Gs} versus the mixture velocity U_M at four different positions from the inlet. In every graph of figure 5.8, the experimental data is compared to the correlations of Gregory et al. [1978], Malnes [1982], Andreussi and Bendiksen [1989] and Abdul-Majeed [2000] (section 2.3.5).

Literature and experimental data show that the void in the slug body increases with increasing mixture velocities. Moreover, the void in the slug body seems to be more influenced by the inlet gas velocities than by the inlet water velocities. The slug voidage clearly
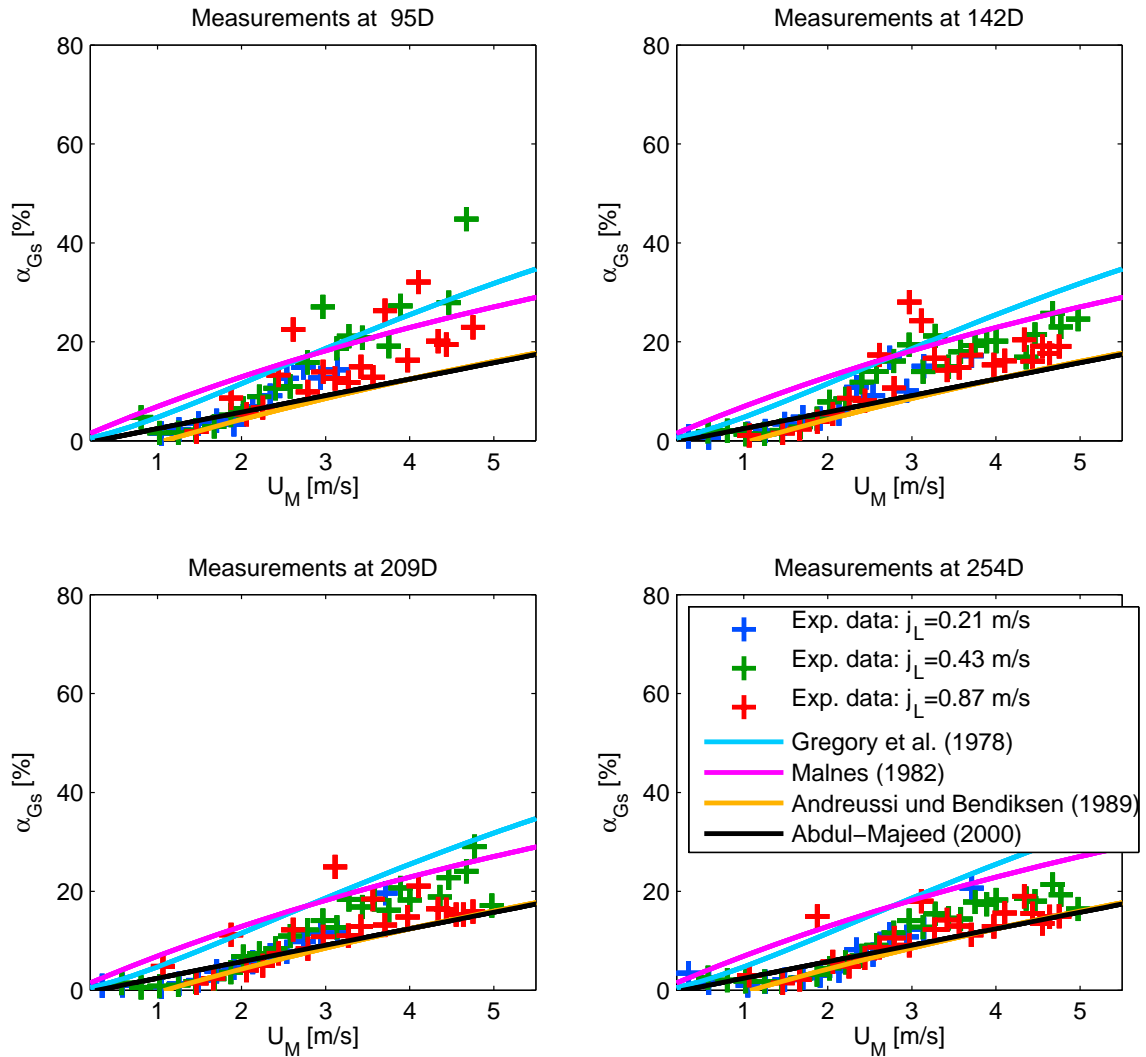
Figure 5.8: Slug void fraction α_{Gs}.

increases with increasing superficial gas velocities. These behaviours are explained in detail in section 5.6, where the properties of the dispersed bubbles in the slug body are analysed.

Comparisons between the data acquired at different positions along the pipe test section reveal that the slug voidage slightly decreases as the slug advances along the pipe.

The experimental data shows that the slug void fraction changes at three critical Froude numbers (the critical Froude number is calculated by equation 2.31 and is a ratio of inertial and gravitational forces). For $Fr_{crit} < 1.5$ ($U_M < 1.1$ m/s), the slug body is almost free of bubbles and plug flow occurs in the pipe. The experimental data shows that there is a transition between plug and slug flow for $1.5 < Fr_{crit} < 3.0$ (1.1 m/s$< U_M <$2.2 m/s). In this range, the slug voidage follows the theoretical predictions of Andreussi and Bendiksen [1989], but for $Fr_{crit} > 3.0$ ($U_M >$2.2 m/s), where the slug body starts to be strongly

aerated, the correlation of Andreussi and Bendiksen [1989] underpredicts the slug voidage. For $3.0 < Fr_{crit} < 4.1$ (2.2 m/s< U_M <3.0 m/s) the slug voidage increases with a higher slope than it did before. For $Fr_{crit} > 4.1$, the slug voidage tends to increase with increasing mixture velocity, presenting the same slope as for $1.5 < Fr_{crit} < 3.0$, i.e. parallel to the correlation of Andreussi and Bendiksen [1989].

The correlations based on air-light oil data (Gregory et al. [1978] and Malnes [1982]) overestimate the void in the slug for air-water data, especially for low mixture velocities.

5.4 Slug Front/Tail Velocity

The effect of the mixture velocity on the evolution of the mean slug front velocity u_t and the mean tail velocity u_b at different positions from the inlet is illustrated in figure 5.9. Both velocities have been extracted from the voltage signals of the wire-mesh sensors, and they have been calculated according to equation 4.3.

The slug front and slug tail velocity increase with increasing mixture velocity. The velocity at the front u_t is larger than the velocity at the slug tail u_b, especially for larger mixture velocities. This means that the rate of pick-up of liquid at the nose of the advancing slug is larger than the rate of liquid shedding at its tail.

Comparisons between the data acquired at different positions from the inlet reveal that the front and the tail velocity decrease as the slug advances along the pipe test section. This suggests that the aeration in the slug body also influences the slug velocity. As the voidage in the liquid slug decreases, the slug front and tail velocity also decreases.

Figures 5.10 and 5.11 show the slug front and tail velocity divided by the mixture velocity u_t/U_M and u_b/U_M, respectively (giving the coefficient C_0, see section 2.3.2). In both figures, the experimental data is compared to the theoretical values obtained by the correlations of Gregory and Scott [1969], Nicholson et al. [1978], Ferré [1979] and Bendiksen [1984]. The predicted values for u_t/U_M are in better agreement with the experimental data when the flow is fully developed. The theoretical values of u_b/U_M are overpredicted when the flow is fully developed. In general, the experimental data is better predicted by the correlations which take the drift velocity into account.

In section 5.3 it is observed that there are three critical Froude numbers at which the slug voidage changes. These values agree with the two critical Froude numbers at which the values of C_0 and the weighted mean drift velocity change (equation 2.20). For low mixture velocities, $Fr_{crit} < 1.5$, the slug drift velocity cannot be neglected. The experimental data is better predicted by Bendiksen's correlation. For $1.5 < Fr_{crit} < 3.0$ the values of C_0 remain approximately constant with increasing mixture velocity. In this work, the recommended value is of $C_0 = 1.25$ for $1.5 < Fr_{crit} < 3.0$. For $Fr_{crit} > 3.0$, C_0 starts to increase slowly with increasing mixture velocity. This suggests that the slug drift velocity should not be neglected for $Fr_{crit} > 3.0$ (which all correlations do).
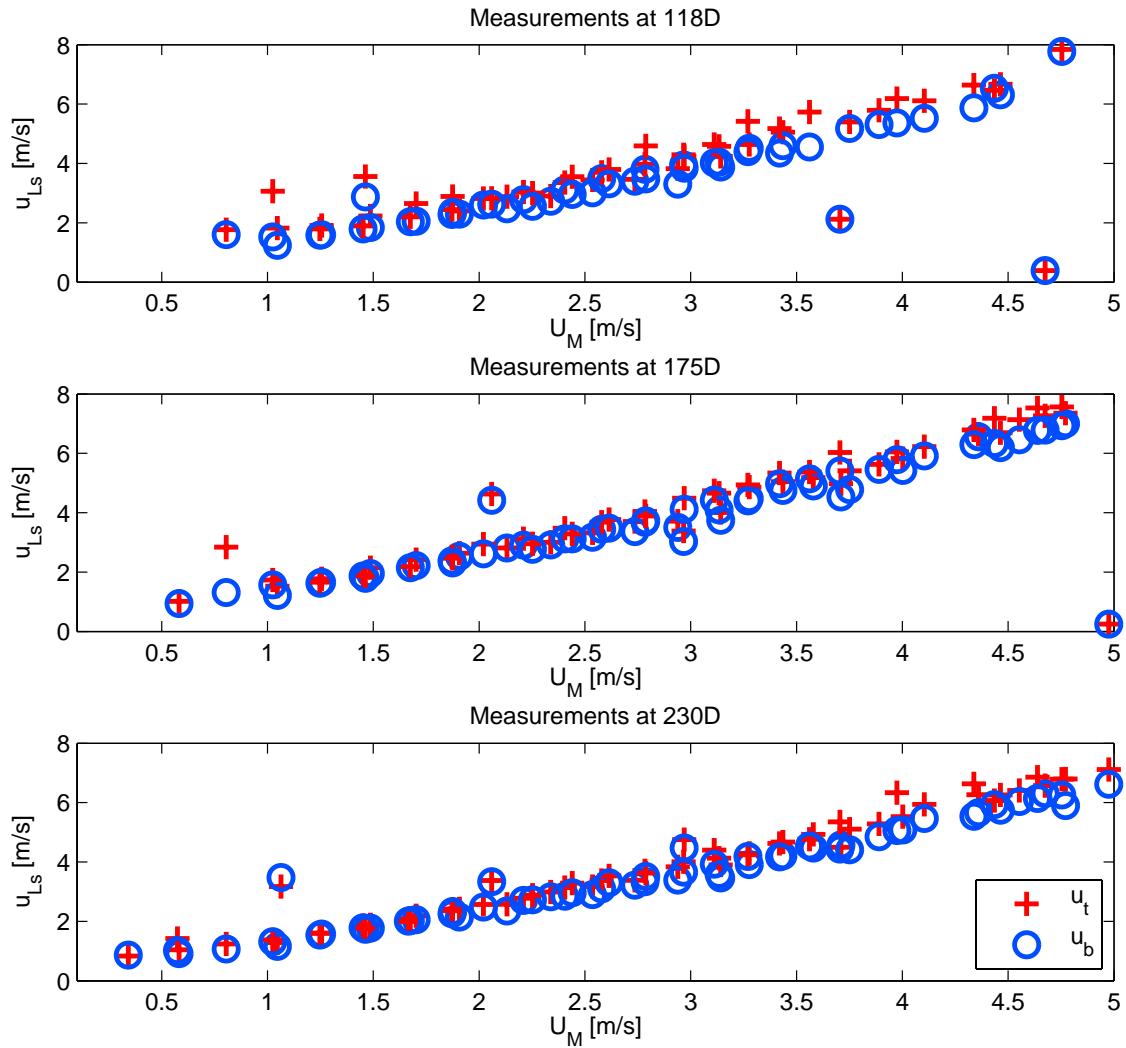
Figure 5.9: Slug front velocity u_t and slug tail velocity u_b.

5.5 Slug Body Length

Figure 5.12 shows the mean length of the slug body l_s versus the mixture velocity U_M at different positions along the pipe. The slug body length was calculated by multiplying the time of passage of the slug body T_s at a certain position by the mean slug velocity u_{Ls} (see equation 4.4). Here the slug velocity u_{Ls} was calculated by the average value between the slug front velocity u_t and the slug tail velocity u_b.

Comparisons between the slug length at different positions from the inlet show that the slug body gets larger along the pipe. This means that the rate of pick-up of liquid at the nose of the advancing slug is larger than the rate of liquid shedding at its tail, leading to an increase in its length as the slug moves downstream ($u_t > u_b$, see section 5.4).
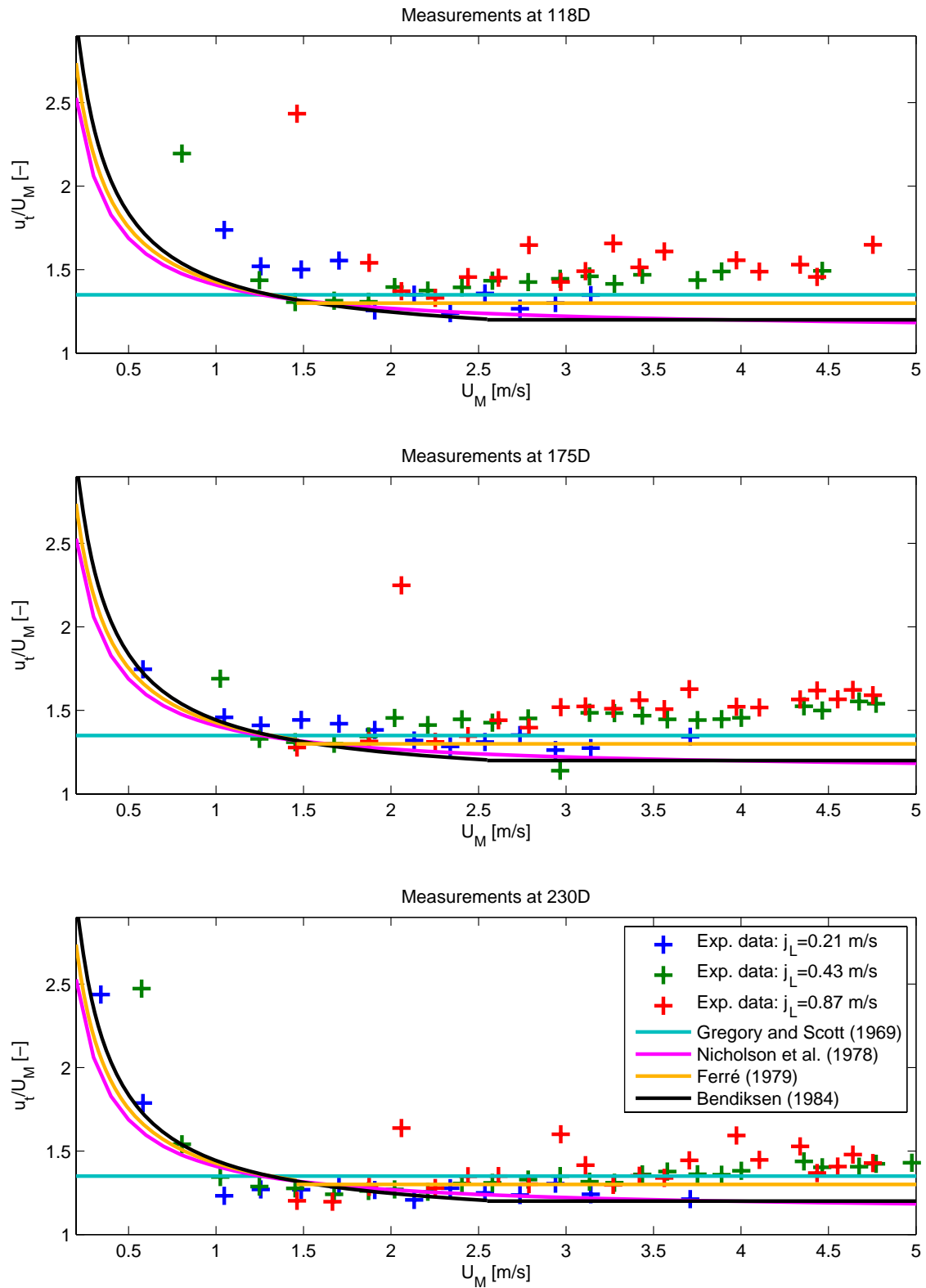
Figure 5.10: Front velocity coefficient u_t/U_M.
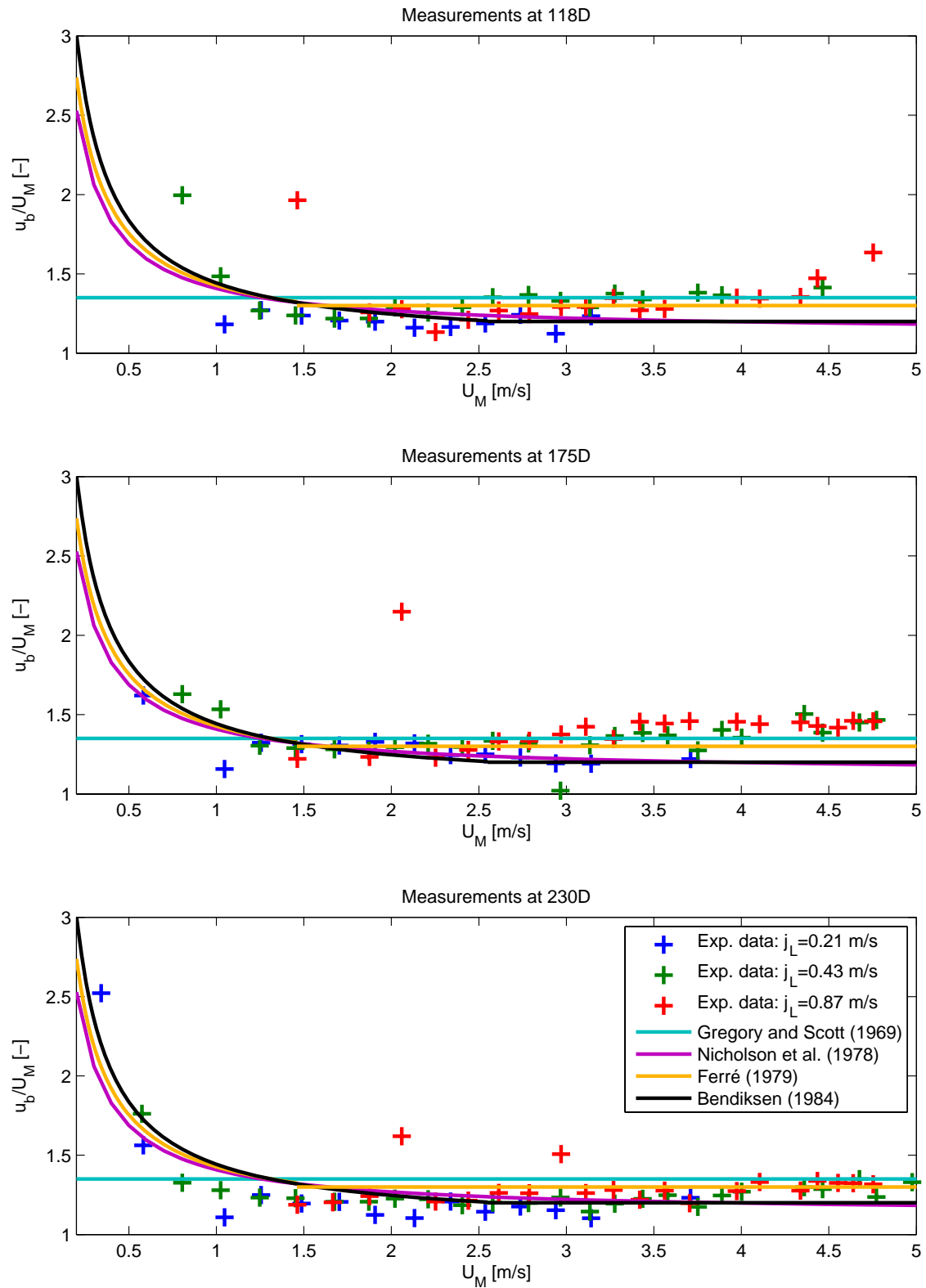
Figure 5.11: Tail velocity coefficient u_b/U_M.
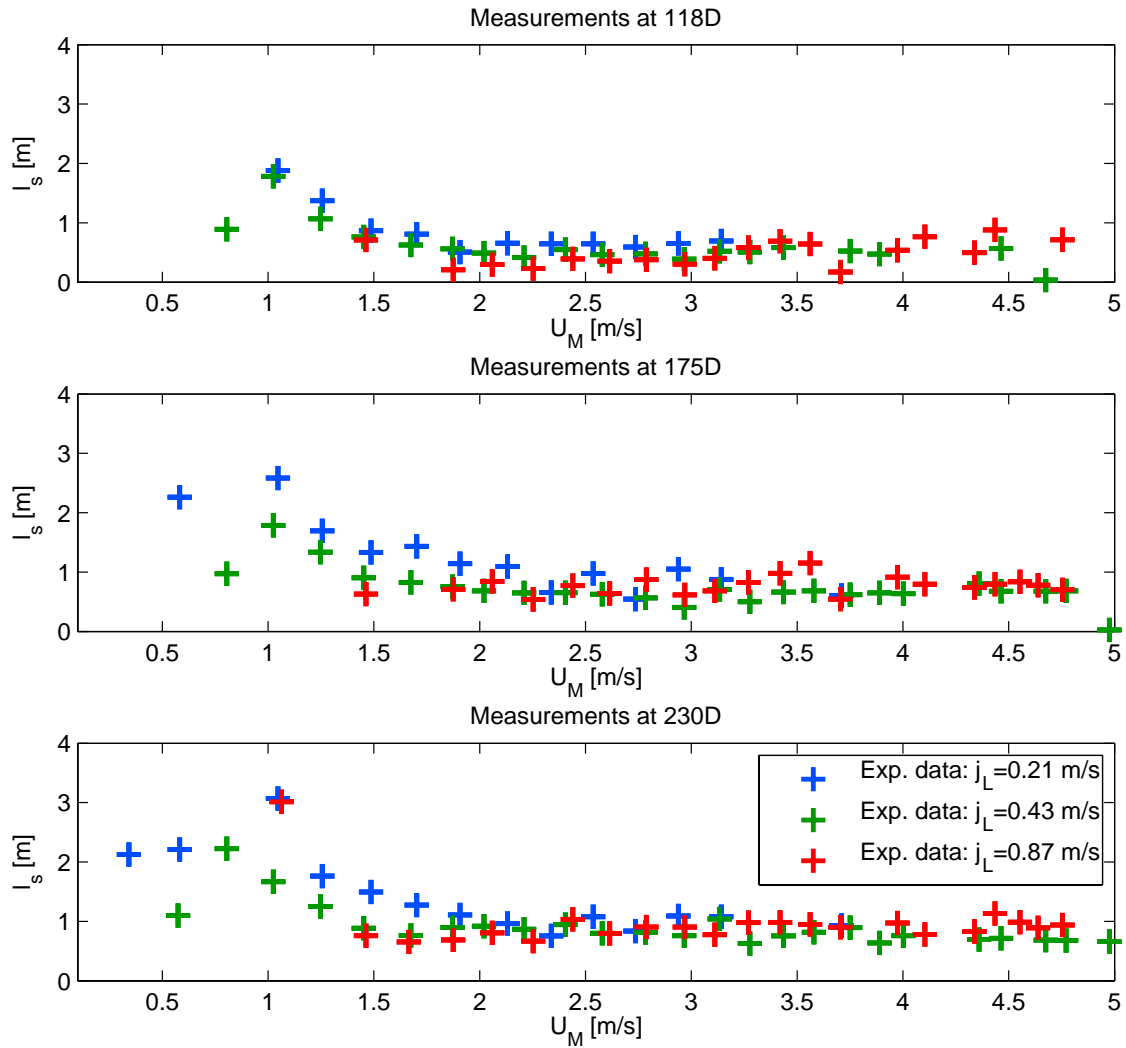
Figure 5.12: Slug body length l_s.

The experimental data suggests that here also the aeration of the slug body has a notable influence on the slug body length. There are two critical Froude numbers at which the tendency of the slug length changes. For very low mixture velocities ($Fr_{crit} < 1.5$) where there is almost no aeration in the slug, the slug body is longer. For $1.5 < Fr_{crit} < 3.0$ the length of the slug tends to decrease with increasing superficial liquid velocities. A higher superficial gas velocity also tends to produce shorter slugs. These observations are consistent with the experiments made by Ujang et al. [2006] in a 78 mm inner diameter and 37 m long pipeline. For $Fr_{crit} > 3.0$, the slug length tends to a constant value with increasing mixture velocities. Here, an increase in superficial liquid velocity slightly tends to produce larger slugs.

At the position of $230D$, the slug body has a mean length of about $17D$, which is in good agreement with the literature (see table 2.1).

5.6 Properties of the Dispersed Bubbles in the Slug Body

In order to study the dispersed bubbles properties in the liquid slug as a function of the flow velocities, six series of experimental data have been analysed in detail. The experimental data was acquired by four wire-mesh sensors. Two pairs of sensors were placed at $165D$ and at $211D$ from the inlet. The distance between the sensors of each pair was of 20.25 mm. The length of the pipe was of $223D$. For the analysis of the data, the algorithms from Prasser et al. [2001] for bubble identification, bubble size and bubble velocity have been used.

Table 5.1 shows an overview of the operating points: the liquid and gas superficial velocities, j_L and j_G, respectively, the mixture velocity U_M, the mixture Froude number Fr_M (given by equation 2.31) and the number of slugs N_{slug} used to calculate the bubble parameters for each operating point.

Table 5.1: Overview of the operating points of the WMS experimental data.

Name	$j_L\ [m/s]$	$j_G\ [m/s]$	$U_M\ [m/s]$	Fr_M	N_{slug}
JL026JG102	0.26	1.02	1.28	1.76	85
JL026JG167	0.26	1.66	1.92	2.64	122
JL026JG227	0.26	2.27	2.53	3.48	93
JL043JG102	0.44	1.01	1.45	1.99	69
JL043JG167	0.43	1.68	2.11	2.90	97
JL043JG227	0.44	2.28	2.72	13.90	41

Table 5.2 shows the number of bubbles used to calculate the bubble parameters N_{Bub} and the average time of passage of the slug body $\overline{T}_s$ (time that a liquid slug needs to pass the measuring device) at $L = 165D$ and $L = 211D$.

Table 5.2: Overview of the acquired number of bubbles.

	$L = 165D$		$L = 211D$	
Name	N_{Bub}	$\overline{T}_s\ [ms]$	N_{Bub}	$\overline{T}_s\ [ms]$
JL026JG102	59113	977	50932	1098
JL026JG167	113720	326	129928	422
JL026JG227	120083	163	157752	263
JL043JG102	15014	363	19582	474
JL043JG167	113711	264	124655	386
JL043JG227	67496	182	89358	246

In general, the average time of passage of the slug body $\overline{T}_s$ decreases with increasing mixture velocity, and it increases along the pipe (as shown in figure 5.12, where the slug increases its length as it moves downstream). It must be noted that the test rig geometry considerably influences the data acquired at $211D$. The two-phase separator is placed at $223D$ where the water flows in by means of a spiral. Due to the spiral, the water

accumulates slightly at the end of the test pipe. The liquid fraction and the height of the film at the end of the pipe are higher than without the spiral. The time of passage of the slug body T_s is also longer at this position and the tail velocity much lower. The influence of the two sensors placed upstream (at 165D) is negligible at 211D. The distance between the sensor pairs (46D) is long enough to allow the flow and its characteristics to recover.

5.6.1 Void Fraction in the Slug Body

In section 5.3, the void in the slug body α_{Gs} was already analysed for a wide range of gas and liquid velocities in order to find the critical Froude numbers at which the gas aeration in the slug body has a substantial influence on the slug characteristics. The experimental data shows that there is a transition between plug and slug flow for $1.5 < Fr_{crit} < 3.0$. Figure 5.13 shows the void fraction in the slug body versus the mixture velocity for the operating points mentioned above. The operating points are in the range of $1.8 < Fr_{crit} < 3.8$. The experimental data is compared to the correlations of Gregory et al. [1978], Malnes [1982], Andreussi and Bendiksen [1989] and Abdul-Majeed [2000] (section 2.3.5). The experimental data is best correlated with the correlation of Andreussi and Bendiksen [1989]. For $1.5 < Fr_{crit} < 3.0$, the slug voidage follows the theoretical predictions of Andreussi and Bendiksen [1989], but for $Fr_{crit} > 3.0$, where the slug body starts to be strongly aerated, the correlation of Andreussi and Bendiksen [1989] underpredicts the slug voidage.
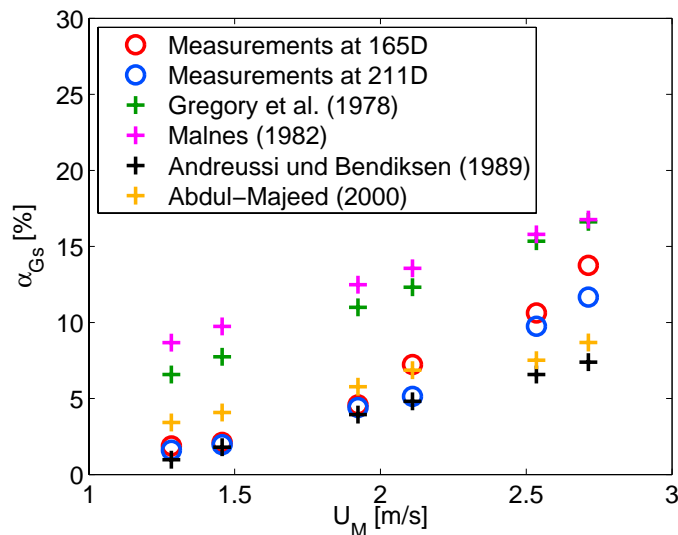

Figure 5.13: Void fraction in the slug body α_{Gs}.

5.6.2 Number of Bubbles

Figure 5.14 shows the average number of bubbles per slug $N_{Bub\ slug}$ versus the mixture velocity U_M. The number of bubbles in the slug body generally increases with increasing mixture velocities.
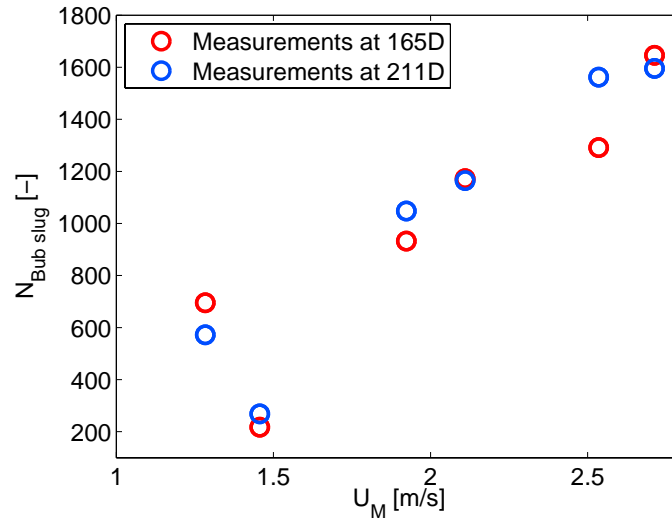

Figure 5.14: Average number of bubbles in the slug body $N_{Bub\ slug}$.

The local number of bubbles along the slug body detected by the wire-mesh sensors is illustrated in figure 5.15. The graphs on the left side show the absolute number of bubbles N_{Bub} (number of bubbles detected in a 10 ms time interval) versus the time of passage t. The graphs on the right side of figure 5.15 show the relative number of bubbles per slug $N_{Bub}/N_{Bub\ slug}$. The graphs at the top and at the bottom show the data acquired at $165D$ and $211D$ from the inlet, respectively. For all operating points, $t = 0$ indicates the passage of the liquid slug front.

The absolute number of bubbles seems to be influenced more by the inlet gas velocities than by the inlet water velocities: a similar development of the absolute number of bubbles can be observed for the operating points with the same inlet gas velocities. For these operating points, the larger number of bubbles can be found at the front of the slug (in the mixing region), and then, it decreases with similar slope and at similar times. The operating points with higher gas velocities show a higher number of bubbles in the slug body.

The graphs on the right of figure 5.15, which show the relative number of bubbles per slug, reveal that the majority of bubbles are concentrated at the beginning of the slug body for all the operating points. At all operating points the percentage of bubbles decreases with similar slope and at the same time rate. The experimental data shows that the percentage of bubbles is close to cero after 200 ms for all the operating points.

Figure 5.16 also shows the relative and absolute number of bubbles in a slug, but this time the average time which a slug takes to pass through the measuring device T_s is divided
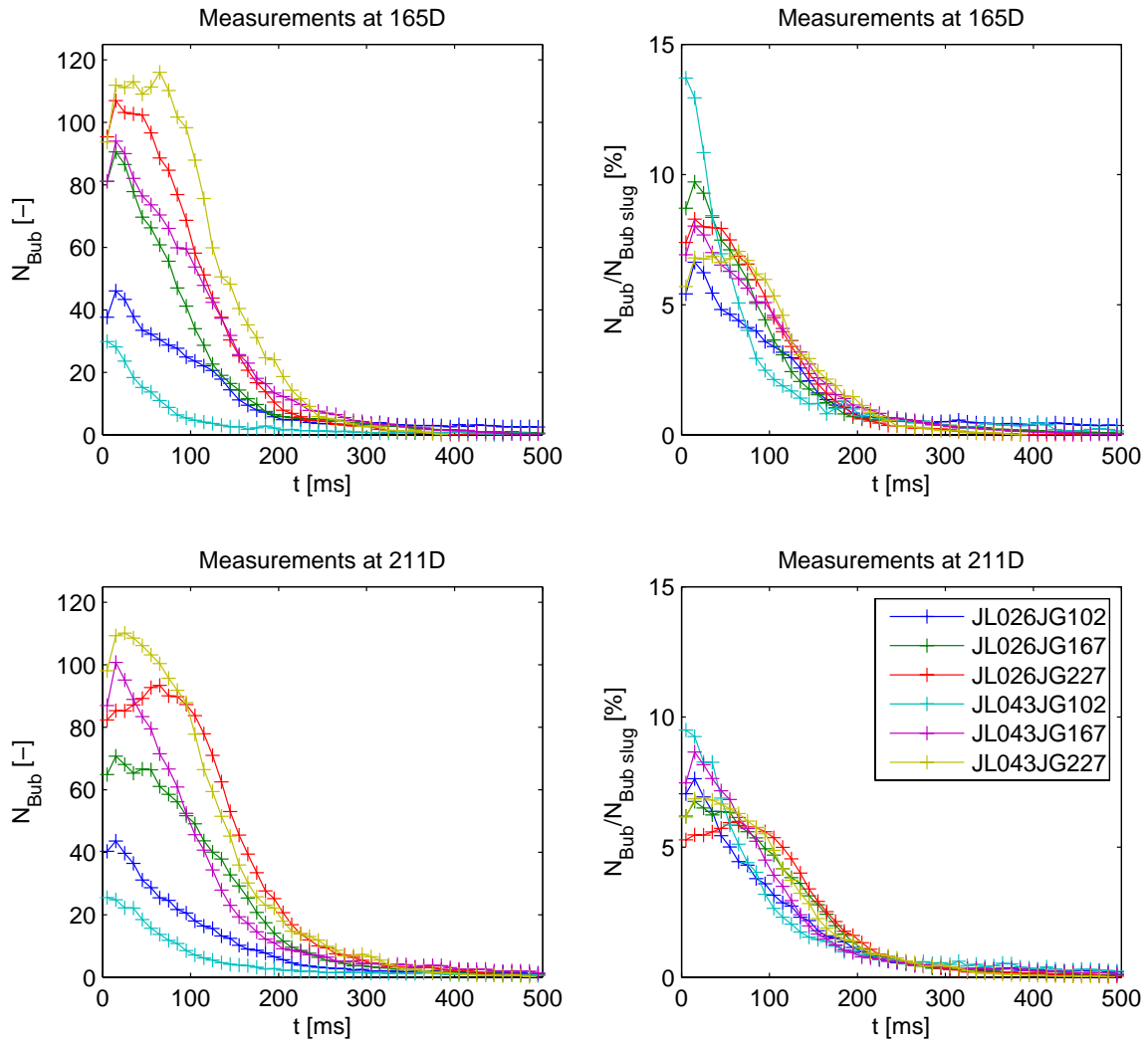
Figure 5.15: Relative and absolute number of bubbles in the slug body along the time.

in equal parts of $T_s/50$, and the number of bubbles counted in the 50 time intervals are plotted against the relative time t/T_s. In this graphs $t = 0$ represents the liquid slug front and $t = T_s$ the liquid slug end. Figure 5.16 helps to elucidate the influence of the slug length on the absolute and relative number of bubbles per slug.

The plots of figure 5.16 show that the experimental data with higher gas velocities have a larger number of bubbles N_{Bub} in the entire slug body. With increasing gas velocities, the slug becomes more aerated and the bubbles are better distributed along the slug body.

For lower gas velocities, the relative number of bubbles $N_{Bub}/N_{Bub\ slug}$ is generally bigger at the slug front, while at the slug end almost no bubbles are to be found. For higher gas velocities, the bubbles are more distributed along the slug body, nonetheless, a decrease of the number of bubbles takes place towards the slug tail.
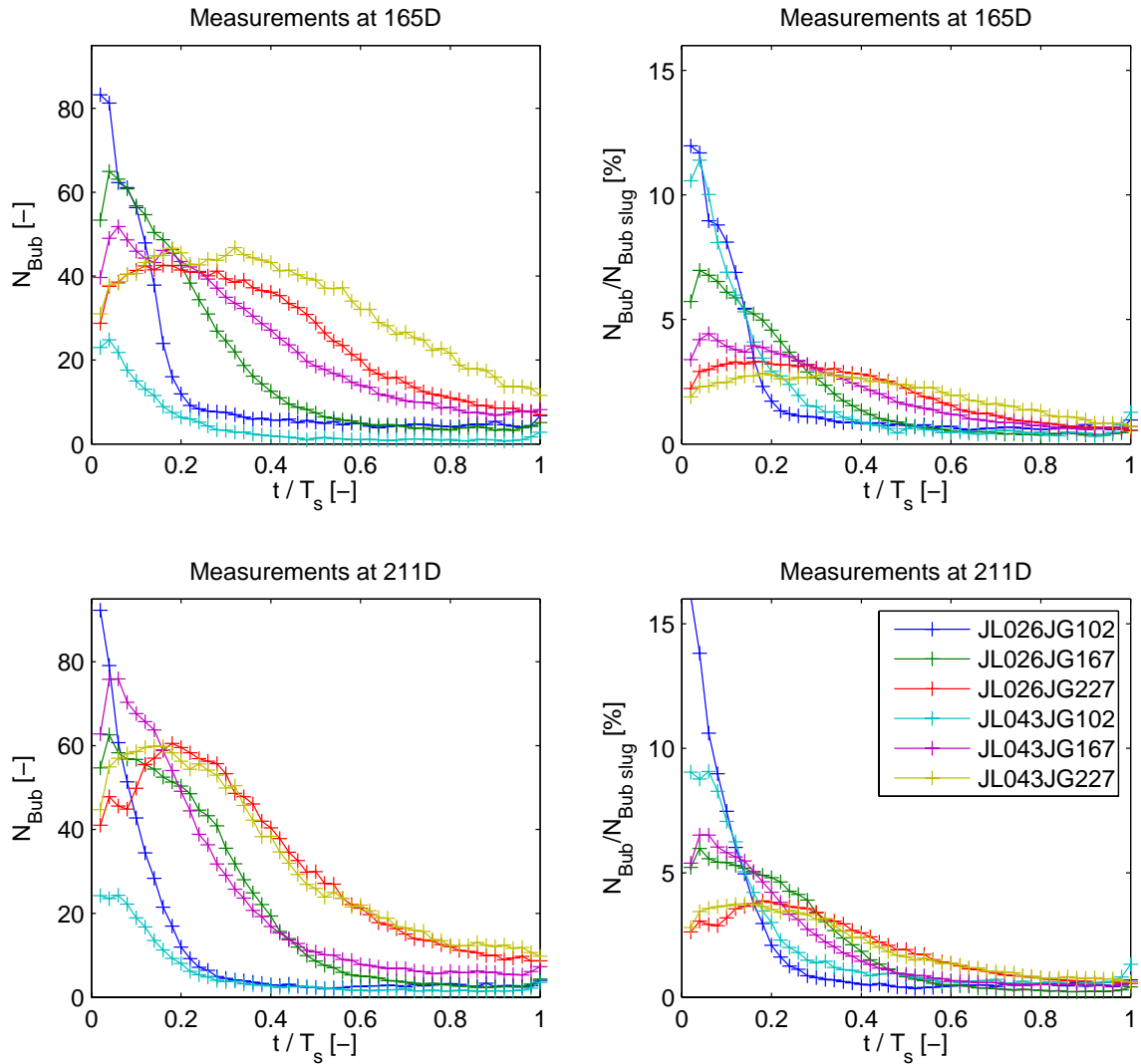
Figure 5.16: Relative and absolute number of bubbles in the slug body relative to the slug time of passage.

5.6.3 Velocity of the Bubbles

In figure 5.17, the average velocity of the slug front u_t, the slug tail u_b and the bubbles in the slug body u_{Bub} are plotted against the mixture velocity U_M. The data acquired at $165D$ is shown on the left graph and the data acquired at $211D$ on the right graph. The experimental data acquired at $165D$ shows that the average velocity of the bubbles in the slug body increases with increasing mixture velocities. The average velocity of the bubbles is sligthly lower than the slug tail velocity. This is consistent with the observations made by Nydal and Andreussi [1993], who reported that small bubbles move slower than the liquid in a water slug. As a consequence, the bubbles will at some point be caught up by the next elongated bubble. The experimental data acquired at $211D$ shows a considerable influence

of the test rig. As previously mentioned, the two-phase separator is placed at $223D$. It is important to note that the nozzle of the two-phase separator delivers a preconditioned flow stream into the body of the separator. The water slightly accumulates at the end of the test pipe depending on the local velocity of the fluids. The slug tail velocity at $211D$ is much lower than when the fluids flow through a pipe into an empty reservoir.
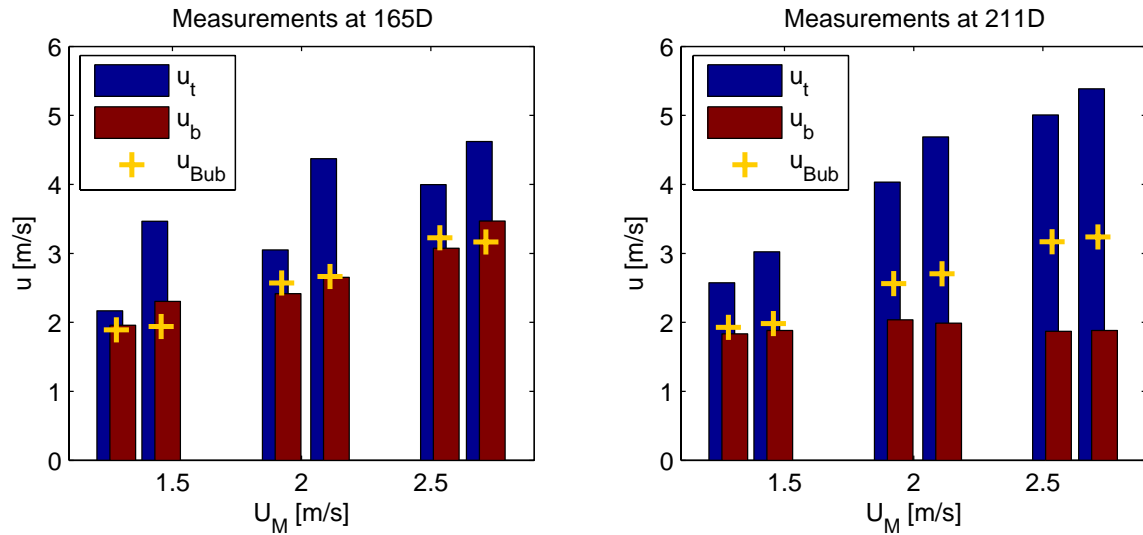
Figure 5.17: Average velocity of the slug front, slug tail and the bubbles in the slug body.

Figure 5.18 shows the average bubble velocity u_{Bub}. Again, $t = 0$ denotes the slug front. It is observed that the average bubble velocity remains fairly constant along the slug body. Operating points with the same inlet gas velocities show similar bubble velocities. The velocity of the bubbles increases with increasing inlet air velocities.
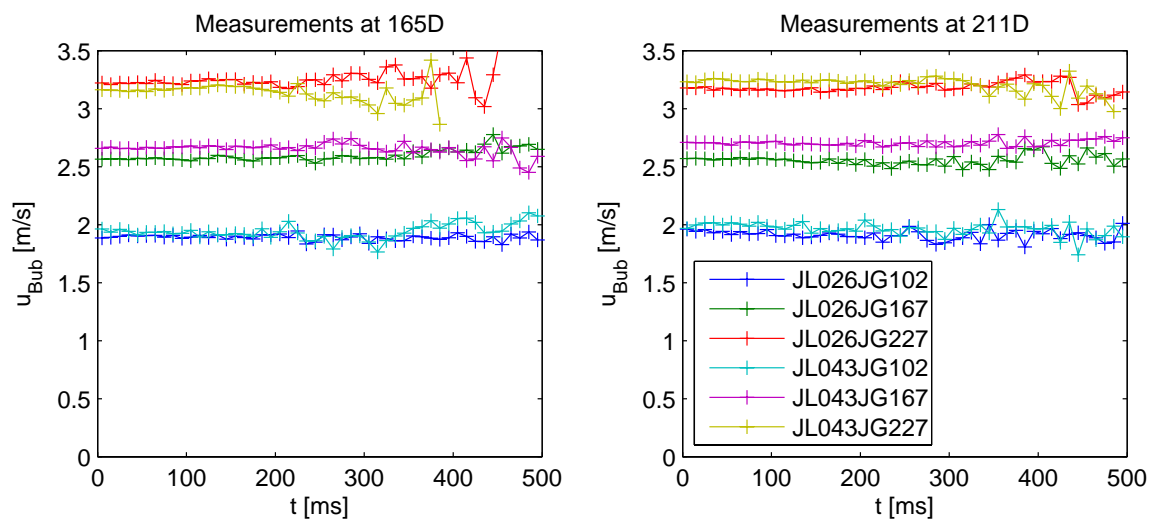
Figure 5.18: Axial bubble velocity in the slug body.

80

The mixture velocity U_M is always smaller than the average bubble velocity. This observation is not consistent with the recommendation of Taitel and Barnea [1990b] for the distribution parameter given in equation 2.57 used for the calculation of the average velocity of the dispersed bubbles in the liquid slug. A value of $B_0 = 1.2$ is required to calculate the average bubble velocity measured in this study.

5.6.4 Vertical Position of the Bubbles

The vertical position of the bubbles in the pipe has been also studied. Figure 5.19 shows the vertical average position of the bubbles at the pipe cross section.
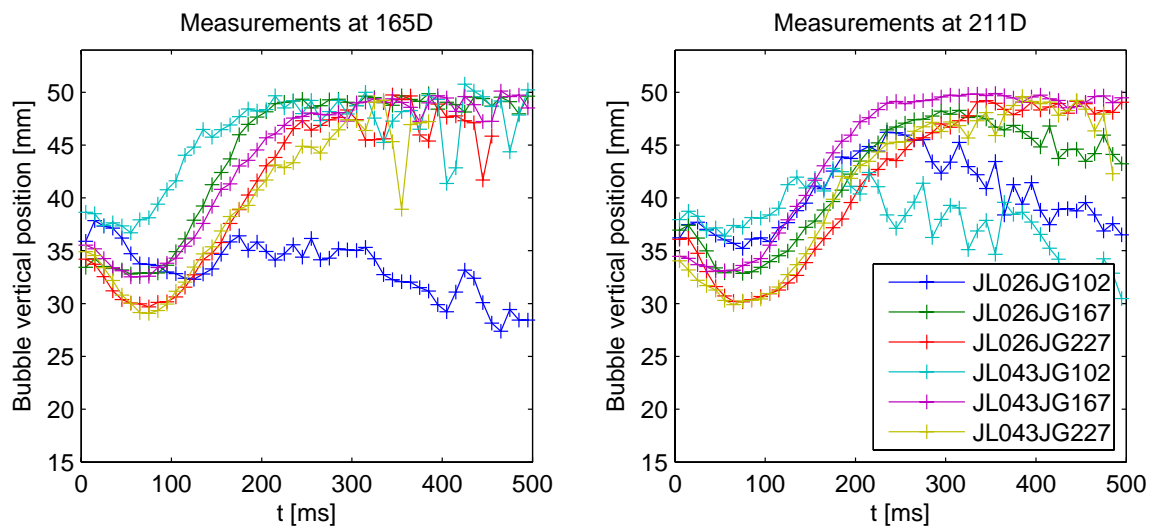
Figure 5.19: Vertical average position of the bubbles at the pipe cross section.

In general, buoyancy causes bubbles to migrate to the upper part of the pipe. However, the bubbles in the experiment show a different behaviour: they move towards the bottom due to the pick-up process in the mixing region, and then rise until a certain vertical position is reached. This position remains constant towards the end of the slug body. The position of the minimum levels and the constant level afterwards have lower values when the inlet gas velocity increases. Operating points with the same inlet gas velocities present bubbles at similar positions along the slug body. It can also be observed that the bubbles ascend with similar velocities (represented by approx. parallel slopes). This means that the bubble sizes have to be similar for all operating points.

5.6.5 Bubble Size

Another relevant parameter is the bubble size. Figure 5.20 shows the average volume of the bubbles V_{Bub} with increasing mixture velocity U_M. The average volume of the bubbles drops until a certain minimum value is achieved. Then, the average volume of the bubbles

increases slightly. It is interesting to see that also here a critical Froude number exists at which the bubble size changes. For $1.5 < Fr_{crit} < 3.0$ (1.1 m/s$< U_M <$2.2 m/s), the average volume of the dispersed bubbles drops with increasing mixture velocities. The experimental data shows that there is a transition between plug and slug flow in this range. For $Fr_{crit} > 3.0$ ($U_M >$2.2 m/s) the average volume of the bubbles increases slightly with increasing mixture velocities.
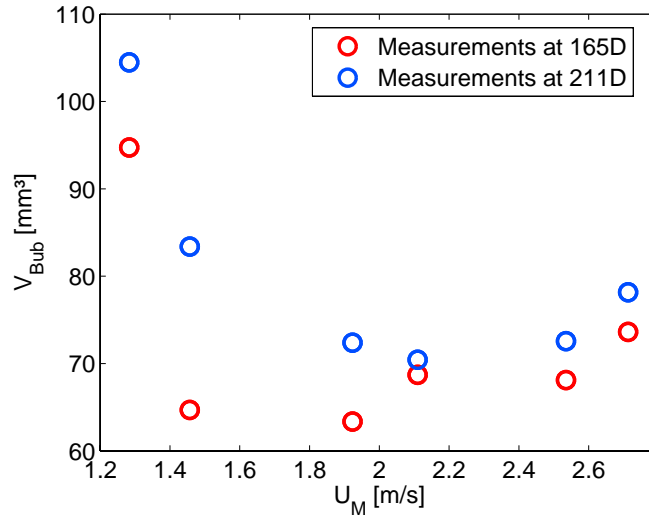

Figure 5.20: Average bubble size in the slug body.

Figure 5.21 presents the volume of the bubbles V_{Bub}. The graph on the left show the experimental data acquired at 165D and on the right, the data acquired at 211D.
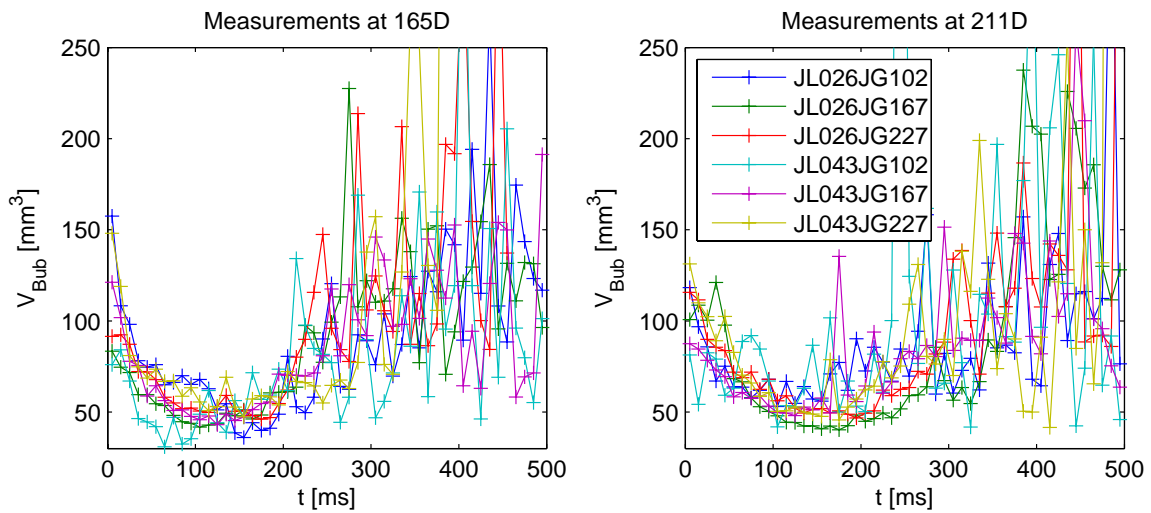

Figure 5.21: Average bubble size in the slug body.

All operating points show a decreasing size of the bubbles towards a minimum near the beginning of the slug body (mixing region). Then, the bubbles grow along the slug tail. Comparisons between figures 5.21 and 5.15 show that the bubbles have bigger sizes in the zones of the slug body where the number of bubbles is lower. This suggests that the number of bubbles decreases due to coalescence, leading to bigger but fewer bubbles. The size fluctuations at the end of the slug body can be explained by the presence of few, individual, large bubbles which lead to scatter the average value.

Comparisons between figures 5.21 and 5.19 show that the zones where the size of the bubbles are larger correspond to greater ascending slopes. This means that bubbles with larger sizes ascend slightly faster (buoyancy has a bigger influence on larger bubbles).

The development of the number of bubbles, their vertical average position and the bubble size, show an influence by the mixture length. Near the beginning of the slug body (mixing region), the behaviour of these parameters is different than in the rest of the slug body. The number of bubbles (shown in figure 5.15) is larger and their vertical average position (figure 5.19) and the bubble size (see figure 5.21) drop in this region. It is observed that the length of the mixing region is independent of the length of the slug body. The mixture region increases its length with increasing inlet gas velocities, which cause stronger turbulence.

In order to make a statement about the behaviour of the bubbles with respect to their sizes, the bubble parameters (average number, vertical average position and average velocity of the dispersed bubbles in the liquid slug) are plotted for different groups of bubble sizes from figure 5.22 to figure 5.24.

Figure 5.22 shows the number of bubbles N_{Bub} with respect to their volumes V_{Bub} at two different positions from the inlet. It is interesting to note that independent of the fluid velocities a maximum for the number of bubbles exists. The highest number of bubbles for all operating points is found for bubble volumes between $6.52 \, \text{mm}^3$ and $11.07 \, \text{mm}^3$, which corresponds to a diameter of 2.32 mm and 2.76 mm, respectively. The number of bubbles in the liquid slug drops with increasing bubble sizes. This is consistent with the idea of bubble coalescence along the liquid slug.

The axial average velocity of the dispersed bubbles for different groups of bubble sizes is presented in figure 5.23. The axial velocity of the bubble increases moderately with their size.

Figure 5.24 shows the vertical average position of the bubbles at the pipe cross section for different groups of bubble sizes. It can be observed that larger bubbles tend to be at higher vertical positions at the pipe cross section. This is to be expected, as buoyancy has a smaller influence on smaller bubbles.
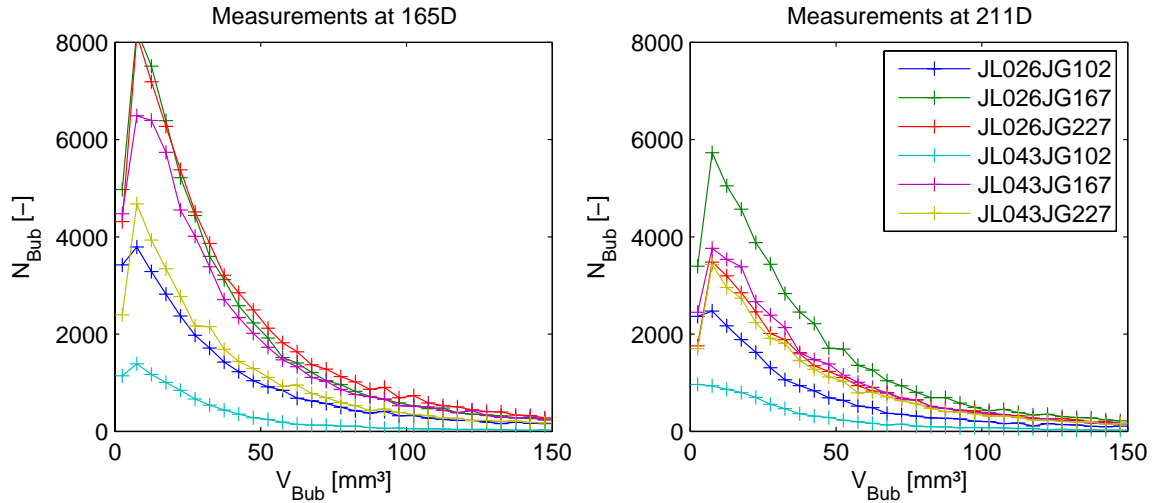
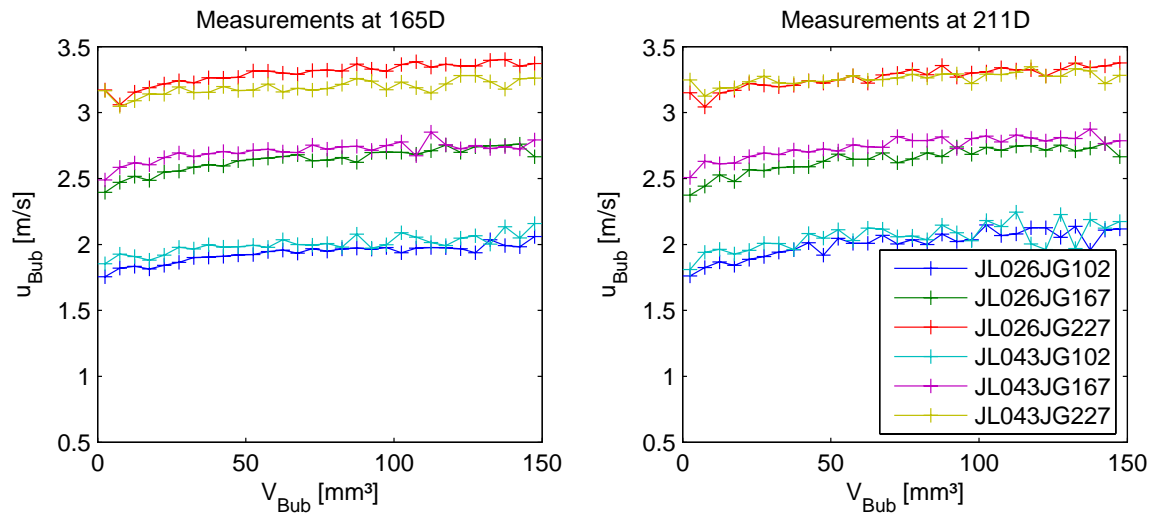**Figure 5.22:** Number of bubbles for bubble size groups.

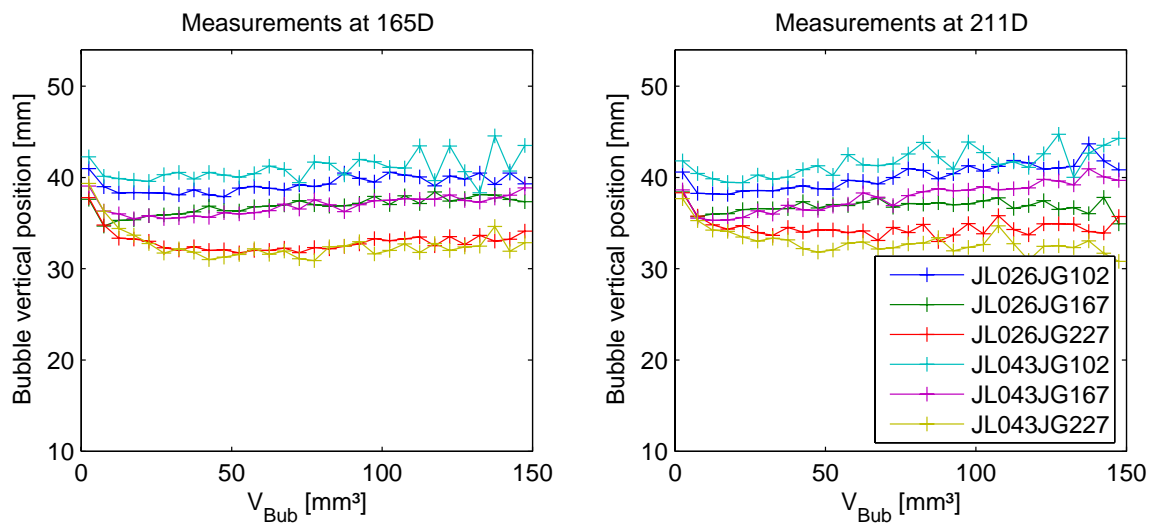**Figure 5.23:** Axial bubble velocity for bubble size groups.

Figure 5.24: Vertical average position of the bubbles relative to their sizes.

6 Velocity Field and Turbulence Field

In this chapter the velocity and turbulence fields of stratified, wavy and intermittent flows are presented. The experimental data has been acquired by means of the simultaneous PIV and PS techniques at $89D$ downstream of the two-phase mixer. Both techniques, as well as the set up and the image processing, are explained in detail in chapter 4.2.2.

Table 6.1 shows an overview of the operating points presented in this chapter: the liquid and gas superficial velocities j_L and j_G, respectively, the mixture velocity U_M, the mixture Froude number Fr_M (given by equation 2.31) and the Reynolds number for the liquid phase Re_L (calculated with the superficial liquid velocity). For the calculation of the Fr_M and Re_L, the maximal height of the film $h_{f,max}$ has been defined as characteristical length.

Table 6.1: Overview of the operating points of the PIV/PS experimental data.

Name	j_L [m/s]	j_G [m/s]	U_M [m/s]	Fr_M [-]	Re_L [-]
JL015JG010	0.15	0.10	0.25	0.46	4687.5
JL016JG160	0.16	1.60	1.76	3.97	3333.3
JL051JG010	0.51	0.10	0.61	0.84	28687.5
JL051JG060	0.51	0.60	1.11	1.53	28687.5
JL051JG110	0.51	1.10	1.61	2.21	28687.5
JL075JG010	0.75	0.10	0.85	1.17	42187.5
JL075JG060	0.75	0.60	1.35	1.85	42187.5
JL076JG110	0.76	1.10	1.85	2.54	42187.5

The operating points include stratified flow (*JL*015*JG*010), wavy flow (*JL*016*JG*160) as well as plug and slug flow (from *JL*051*JG*010 to *JL*075*JG*110). The operating points with low gas flow rates and no gas entrainment in the slug body ($Fr_M \leq 1.5$) cause plug or elongated bubble flow (*JL*051*JG*010, *JL*051*JG*060 and *JL*075*JG*010).

It is important to note that water and air are introduced into the pipe by means of a two-phase mixing section (see section 4.1.3), which assures a distribution of the fluids at the inlet of 50% for each phase, leading to a value of the local inlet velocity around twice as high as the superficial velocity. All the operating points presented in this chapter are turbulent flows.

The experimental data has been analysed with two different approaches, the "fixed window analysis" and the "moving window analysis". Both of them use the same averaging method (conditional averaging), but in the first method, the PIV/PS images containing different parts of a slug unit are analysed as a whole, and in the second method, the images are classified in specific parts of the slug zones (e.g. nose and tail) and are separately studied. Differences have already been explained in section 4.2.2.6.

6.1 Conditional Averaging Coefficient

In order to obtain mean quantities of the liquid phase in a two-phase flow, the velocity data has to be conditionally averaged. The conditional averaging coefficient $N(x,y)$ indicates how many times liquid velocity data is present in a specific position of the measuring zone along a measurement series for the same operating point. A total of 2046 PIV/PS images have been analysed for the operating point of stratified flow (*JL*015*JG*010), 4092 PIV/PS images for wavy flow operating point (*JL*016*JG*160) and for elongated bubble and slug flow 6144 PIV/PS images have been studied for each operating point (from *JL*051*JG*010 to *JL*075*JG*110). Figure 6.1 shows the conditional averaging coefficient for two different data series (wavy flow on the left graph and elongated bubble flow on the right graph).

(a) Wavy flow (*JL*016*JG*160)   (b) Plug flow (*JL*051*JG*110)
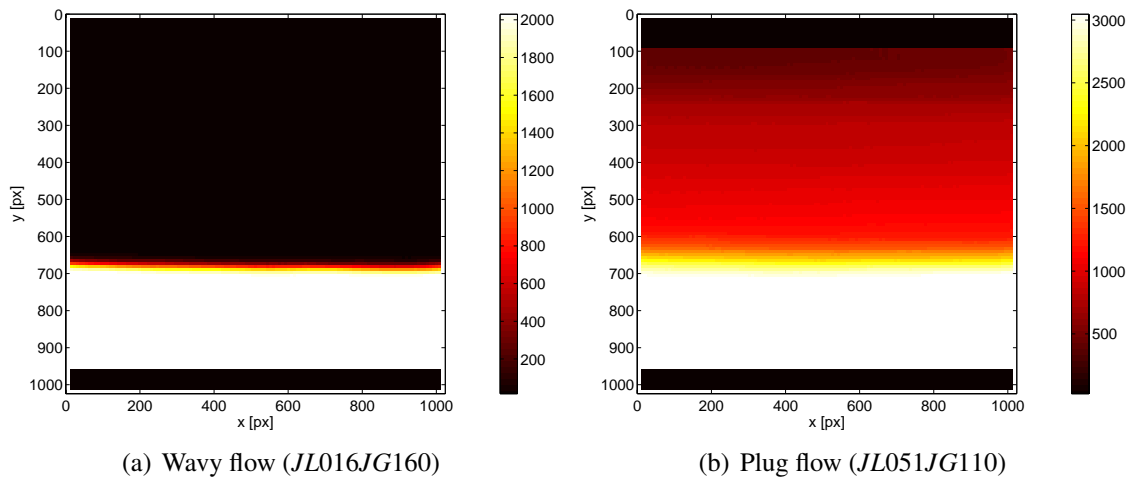
Figure 6.1: Conditional averaging coefficient $N(x,y)$.

In stratified and wavy flow, there is always water flowing in the bottom part of the pipe (liquid zone in white) and air in the upper part of the pipe (gas zone in black; there is no available velocity data in the upper part of the image, $N(x,y) = 0$). In stratified flow, the water level in the pipe remains almost constant during the entire measurement. A nearly plane interface is observed and oscillations of the water level are not significant. In fact, for the operating point *JL*015*JG*010, this zone measures around 8 pixel, a value that corresponds to approx. 0.5 mm. The conditional averaging coefficient for a wavy flow operating point is shown in figure 6.1(a). This image allows to estimate the lowest liquid height in the pipe and the range in which the water level varies (gas-liquid zone in yelow-red tonalities). The amplitude of the waves for this operating point has a maximal value of around 60 pixel (approx. 3.5 mm). The height of the water level ranges from 16 mm to a maximal value of 20 mm.

In plug and slug flow, two zones can be distinguished. The liquid zone (in white) in the bottom part of the pipe, where only water flows, and the gas-liquid zone (in yellow-red tonalities) in the upper part of the pipe, where there is water velocity information only when a liquid slug passes through the PIV/PS measuring section. This leads to lower

values of the conditional averaging coefficient in the upper part of the image than in the bottom part. For these regimes, a higher number of data series has been acquired and processed in order to get better statistical quantities in the gas-liquid zone. According to figure 6.1(b), the value of the lowest level of the liquid film is of 720 pixel (approx. 16 mm).

Table 6.2 gives an overview of the lowest level of the liquid film $h_{f,min}$ for every operating point presented in this section. When intermittent flow occurs in the conduct the minimum liquid height is given by the water level between two slug bodies. For constant inlet liquid velocities, an increase of the gas superficial velocity causes a decrease in the liquid height. An increase in the liquid flow rate leads to higher values of the film height.

Table 6.2: Minimum and maximum liquid height of the operating points of the PIV/PS experimental data.

Name	$h_{f,min}$ [mm]	$h_{f,max}$ [mm]
JL015JG010	30	30
JL016JG160	16	20
JL051JG010	36	54
JL051JG060	16	54
JL051JG110	9	54
JL075JG010	40	54
JL075JG060	25	54
JL076JG110	22	54

6.2 Fixed Window Analysis

6.2.1 Velocity Quantities

Figure 6.2 shows the relation between the instantaneous axial velocity of the liquid phase u_x (on the left vertical axis) and the instantaneous level of the liquid phase at the vertical symmetry plane of the pipe h_f (on the right vertical axis). From the top to the bottom of the figure, stratified, wavy and plug flow are presented in three different graphs. In these graphs, the instantaneous axial velocity is spatially averaged over the liquid area for every PIV/PS image.

For these regimes, it is observed that the spatially averaged value of the local velocity increases along with the water level (even with small waves, the instantaneous axial velocity increases its value slightly). This means that the waves that are formed travel with a higher velocity than the rest of the liquid film, increasing the averaged value of the local velocity.

When the air phase has a higher velocity than the water phase, pressure and friction forces perturb the equilibrium of the surface. These forces transfer energy from the air to the
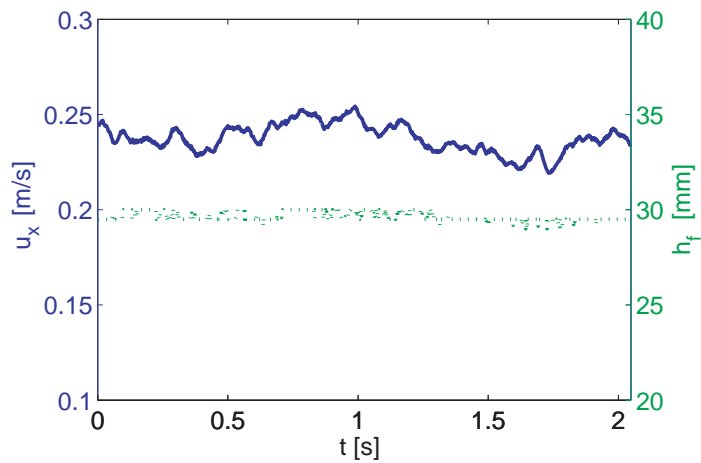
(a) Stratified flow (*JL*015*JG*010)
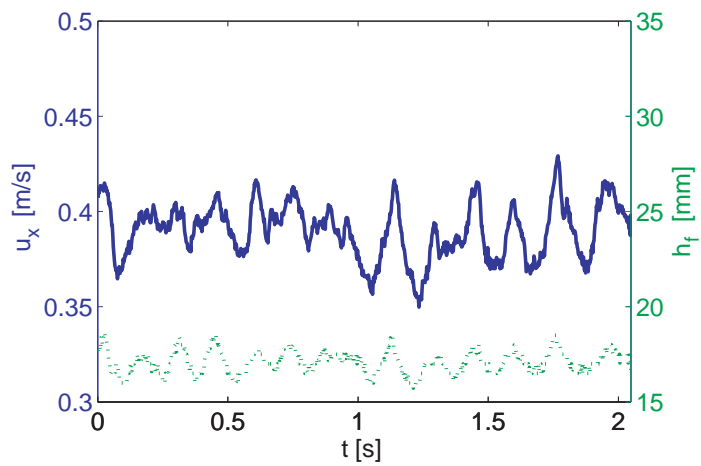
(b) Wavy flow (*JL*016*JG*160)

(c) Slug flow (*JL*051*JG*060)

Figure 6.2: Instantaneous axial velocity u_x and water level in the pipe h_f.

water, forming waves and increasing the water velocity. The operating points for stratified (*JL*015*JG*010) and wavy flow (*JL*016*JG*160) shown in figure 6.2 have nearly the same inlet liquid velocities; the air velocity for wavy flow however, is much higher than for stratified flow, leading to significant differences between both regimes. The mean height of the liquid film for stratified flow after 89*D* is approx. 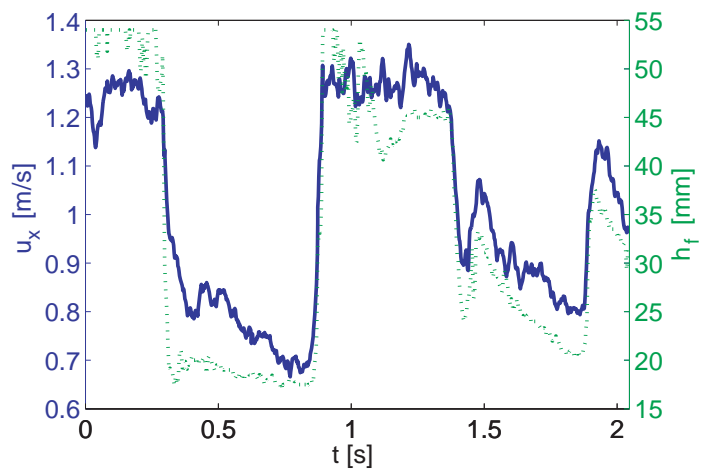30 mm and for wavy flow around 17 mm (see figures 6.2(a) and 6.2(b), respectively). According to the mass conservation law, this leads to higher liquid velocities for wavy flow (the mean value of the instantaneous velocity after 89*D* increases by one third of its inlet velocity) and lower liquid velocities for stratified flow (the mean value of the instantaneous velocity after 89*D* diminishes by one third of its inlet water velocity).

In plug flow (*JL*051*JG*060), the liquid phase intermittently blocks the cross section of the pipe; the minimum height of the liquid film $h_{f,min}$ is approx. 18 mm (see figure 6.2(c)). In the film region, the instantaneous liquid velocity after 89*D* is lower than the inlet velocity (approx. 27%), in the slug region it is higher (approx. 28%). The instantaneous velocity of the slug region is around two times higher than the mean local velocity of the film region. The instantaneous velocity at the beginning of the slug region is slighly higher than at the tail. In the film region, the instantaneous velocity is also higher at the beginning of this region than at the end.

Figure 6.3 shows the mean velocity profiles of the *x* component $\bar{u}_x$ (graph at the top) and the *y* component $\bar{u}_y$ (graph at the bottom) for different operating points. The local instantaneous velocity data is averaged according to equation 4.7.

As previously mentioned, in stratified and wavy flow, there is always air flowing in the upper part of the pipe (gas zone). Therefore, there are no water velocity vectors in this zone. In wavy flow there is a gas-liquid zone bearing water or air depending on the local amplitude of the wave. The data in this zone is conditionally averaged. For plug and slug flow, elongated bubbles travel intermittently in the upper part of the pipe. The data in the gas-liquid zone is also conditional averaged.

In general, the mean value of the axial velocity increases with increasing mixture velocities. For all the operating points, the axial velocity decreases near the pipe walls due to friction. In general, the *y* component increases its negative tendency with increasing mixture velocities. For all the operating points, the *y* component is zero at the pipe walls or at the interface.

The *y* component of the mean velocity $\bar{u}_y$ can be expected to be zero; this would imply that the *y* component profiles shown in figure 6.3(b) merely reproduce the error of the measuring technique (the *y* component of the mean velocity is approx. 2% of the *x* component magnitude). However, the analysis of the experimental data leads to believe that the *y* component profiles illustrate the mean motion of the secondary flow at the pipe cross section. The cylindrical form of the pipe, the liquid velocity and pressure differences between the vertical positions at the liquid film promote secondary flows at the pipe cross section. Figure 6.4 shows the mean velocity of the *y* component $\bar{u}_y$ divided by the average value of the mean axial velocity $\bar{u}_{x,m}$. Stratified (*JL*015*JG*010), wavy (*JL*016*JG*160) and plug flow (*JL*051*JG*010, *JL*075*JG*010 and *JL*051*JG*060) show a similar trend (see figure

6.4(a)). The experimental data shows also here that there is a transition between plug and slug flow at $Fr_{crit} = 1.5$. For the operating points with $Fr_{crit} \leq 1.5$, the y component of the mean velocity show a different secondary flow than for the operating points with $Fr_{crit} > 1.5$ (see figure 6.4(b)).

In stratified flow ($JL015JG010$), the mean axial velocity increases near the interface, where the gas zone starts and where there is no liquid velocity data (figure 6.3). This means that at $89D$, the gas phase is faster than the water. The y component of the mean velocity remains nearly zero at the bottom part of the pipe. Then, the value of the y component drops slowly. Near the interface it tends to zero, being zero at the highest position

(a) $\overline{u}_x$ [m/s]

(b) $\overline{u}_y$ [m/s]
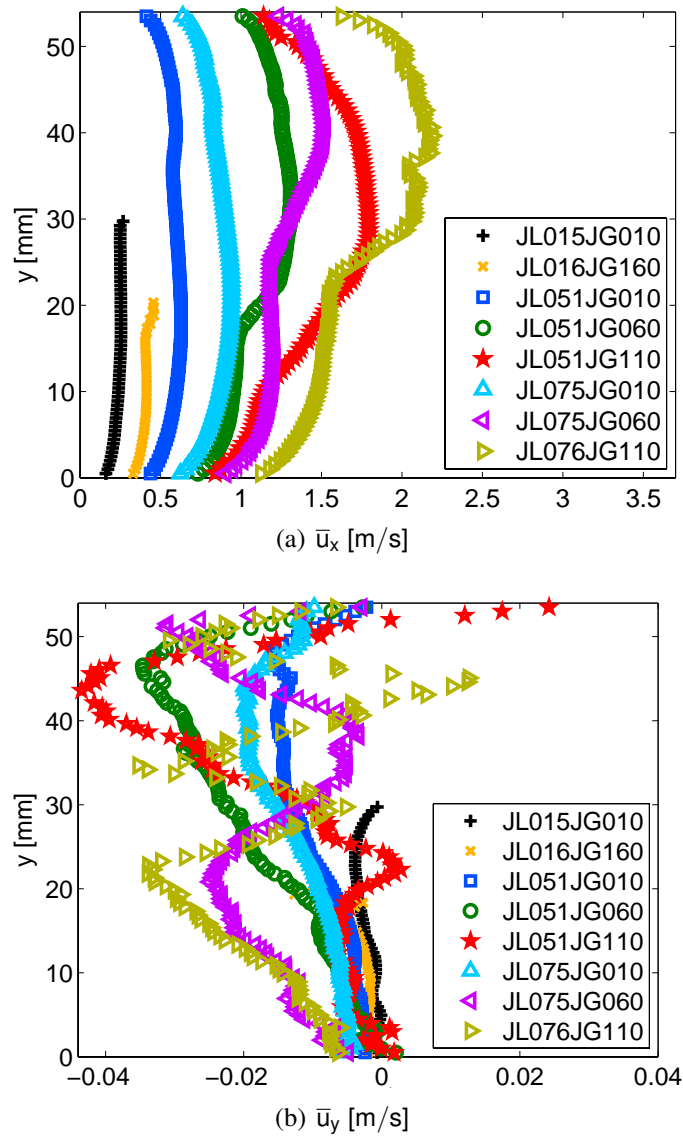
Figure 6.3: Mean velocity profiles.

of the liquid film. Figure 6.5(a) shows for this regime the expected secondary flow motion due to the cylindrical form of the pipe.

In wavy flow (*JL*016*JG*160), three zones can be distinguished (figure 6.3). One in the upper part of the pipe (gas zone with only air), another in the bottom part of the pipe (water zone; only water is present), and the last one near the interface (gas-liquid zone; depending on the wave position there is water or air; this data is conditional averaged). The width of the gas-liquid zone depends on the wave amplitude. This zone shows a direct influence from the air phase, which can be observed on the *x* component profile, where the mean
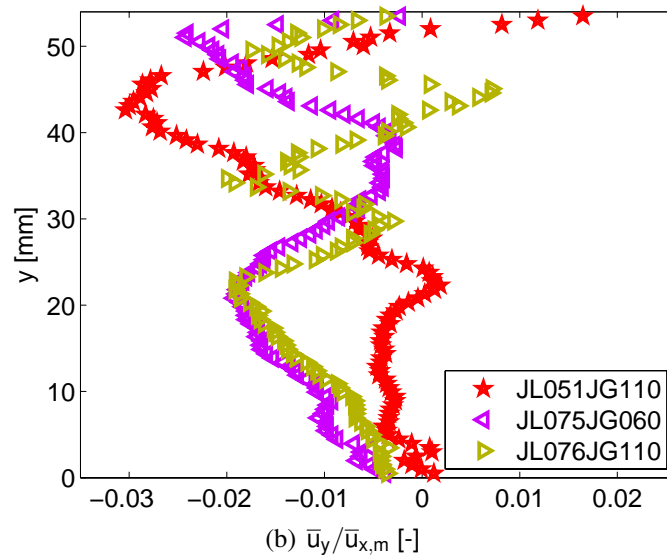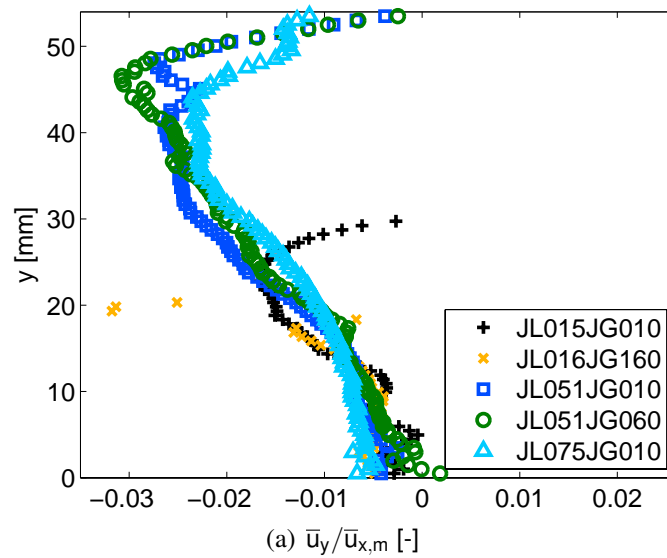
Figure 6.4: Profiles of the mean velocity of the *y* component $\bar{u}_y$ divided by the average value of the mean axial velocity $\bar{u}_{x,m}$.

(a) Stratified flows   (b) Plug flows
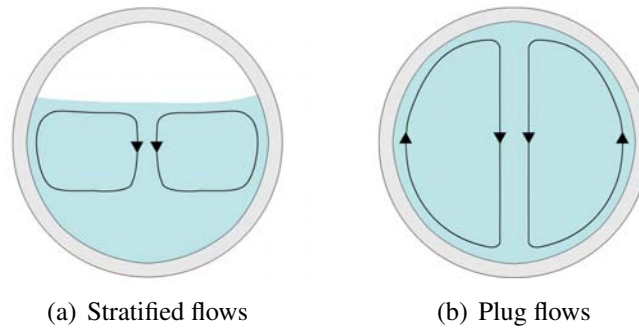
Figure 6.5: Mean motion of the secondary flow motion at the pipe cross section.

velocity increases in the gas-liquid zone. The y component of the mean velocity has a similar trend as for stratified flow.

In plug and slug flows (from $JL051JG010$ to $JL075JG110$), two zones appear (figure 6.3). One in the upper part of the pipe, where liquid and air flow alternatively (gas-liquid zone), and another in the bottom part of the pipe, where only water flows (liquid zone). The mean velocity in the gas-liquid zone represents the mean velocity of the upper part of the liquid slugs.

For operating points with very low air velocities ($JL051JG010$ and $JL075JG010$), the mean axial velocity in the gas-liquid zone is slightly lower than the velocity of the liquid zone figure 6.3). In these regimes, the elongated bubbles flow with slower velocities than the liquid average velocity. In the transitional regime between plug and slug flows and in slug flow regimes, the mean axial velocity in the gas-liquid zone has higher values than in the zone where only water flows.

In plug flow regimes, $Fr_M \leq 1.5$, ($JL051JG010$, $JL075JG010$ and $JL051JG060$), the y component of the mean velocity has a similar trend. The y component of the mean velocity is nearly zero at the pipe walls. Then, the vaue of the y component drops, increasing its negative tendency with increasing mixture velocities. Figure 6.5(b) shows the expected secondary flow motion due to the cylindrical form of the pipe for these regimes.

In the transitional regime between plug and slug flows, $Fr_{crit} > 1.5$ ($JL051JG110$, $JL075JG060$ and $JL075JG110$), the y component of the mean velocity oscillates in the gas-liquid zone. This behaviour is explained in detail in section 6.3, where the liquid flow motion at specific parts of the slug body is analysed.

6.2.2 Turbulence Quantities

Turbulence quantities are calculated on the basis of the fluctuating components of the velocity. Below, the intensity of the turbulent fluctuations is represented by root mean square quantities. Section 4.2.2.6 explains how the turbulence quantities have been obtained.

Time sequences of the instantaneous values of the fluctuating component of the velocity $u'(x,y,t)$ are shown in figure 6.6. The velocity fluctuations are calculated according to
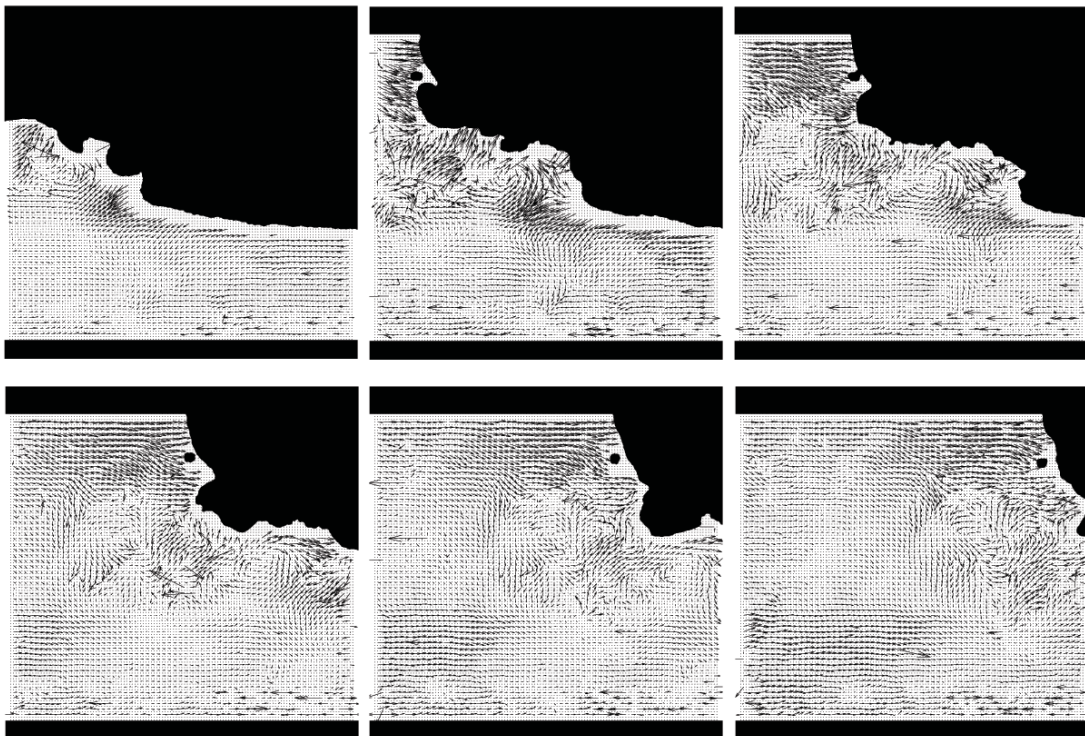
(a) Slug nose
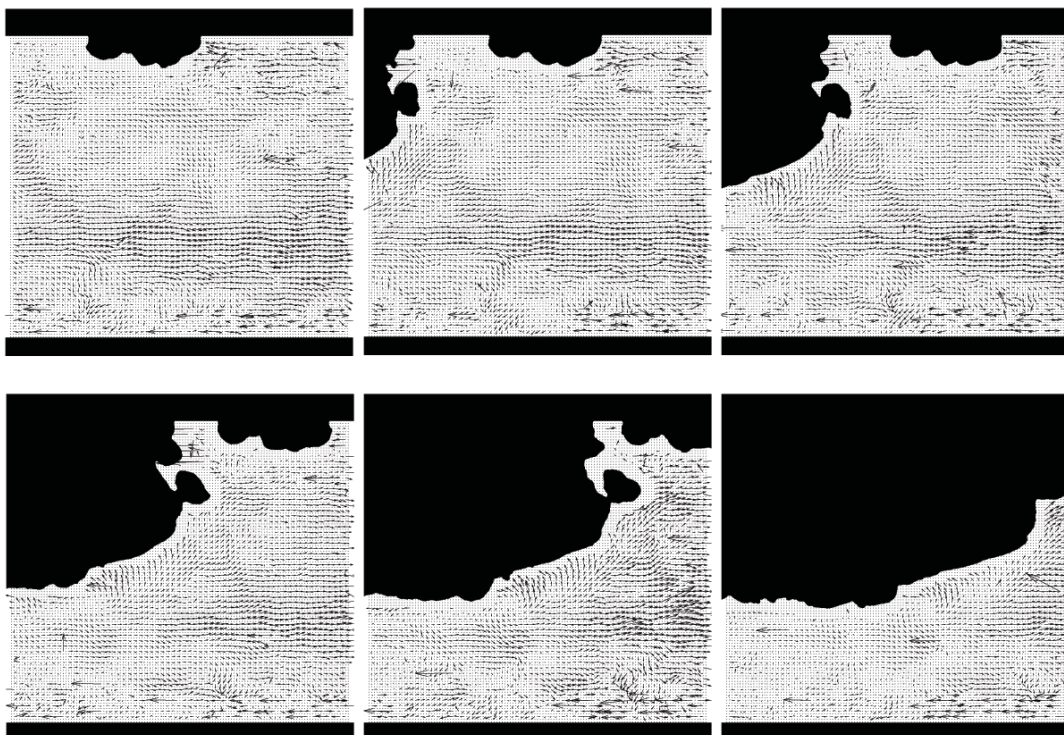
(b) Slug tail

Figure 6.6: Time sequence of the instantaneous values of the fluctuating component of the velocity field $u'(x,y,t)$ ($\Delta t = 0.8ms$).

equation 4.9. Both graphs show the same operating point (j_L =0.51 m/s, j_G =0.60 m/s), which corresponds to elongated bubble flow. Figure 6.6(a) shows the flow structure as the liquid is picked up from the preceding film. The highest instantaneous values of the fluctuating component of the velocity are to be found in the mixing region. Figure 6.6(b) shows the structure of the flow as the liquid is shed at the rear of the slug. It can be observed that the arriving elongated bubble overtakes the dispersed bubbles in the liquid slug. As previously mentioned in section 5.6.3, the average velocity of the bubbles is lower than the slug tail velocity.

The profiles of the root mean square values of the time series for each operating point are presented in figure 6.7. The upper graph shows the x component $u'_{x,rms}$ and the bottom

(a) $u'_{x,rms}$ [m/s]

(b) $u'_{y,rms}$ [m/s]

Figure 6.7: Profiles of the average fluctuating component of the velocity.

graph shows the y component $u'_{y,rms}$ (see equation 4.10). As expected, stratified and wavy flow have the lowest rms values. For these flows, the x component values are higher near the pipe walls and near the interface. The y component values are smaller near the pipe walls and near the interface. For wavy flow, the larger values of the y component are found in the gas-liquid zone.
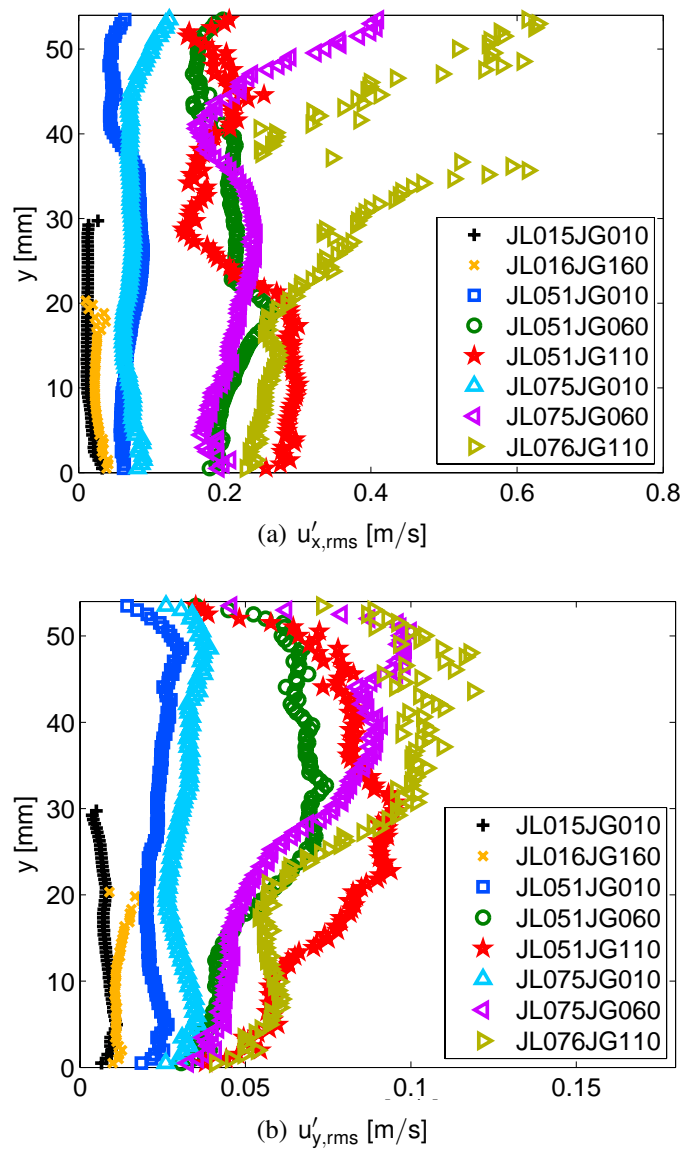
In general, for plug and slug flows, the rms values increase with increasing mixture velocities. For the operating points with very low air velocities (*JL*051*JG*010 and *JL*075*JG*010), the values of the x component in the central part of the pipe have almost the same values. However, the x component values near the pipe walls increase for the operating point with higher mixture velocity. For these operating points, the y component values have a similar trend. They decrease near the pipe walls and in the central part of the pipe. These values are always higher for the operating point with higher mixture velocity.

For the operating points with higher air velocities, it can be observed that near the pipe bottom, the rms values for the x and y component are similar for operating points with identical air velocities. Near the top of the pipe, these values are merely similar for operating points with the same liquid velocities. The y component profiles have higher values in the gas-liquid zone.

Figure 6.8 shows the profiles of the relative turbulence intensity I (given by equation 4.11). In general, the turbulence intensity is larger near the pipe walls. For plug and slug flows, these values are similar near the bottom of the pipe for operating points with identical water velocities. Near the top of the pipe, the values of the turbulence intensity are similar for the operational points with the same gas velocities.
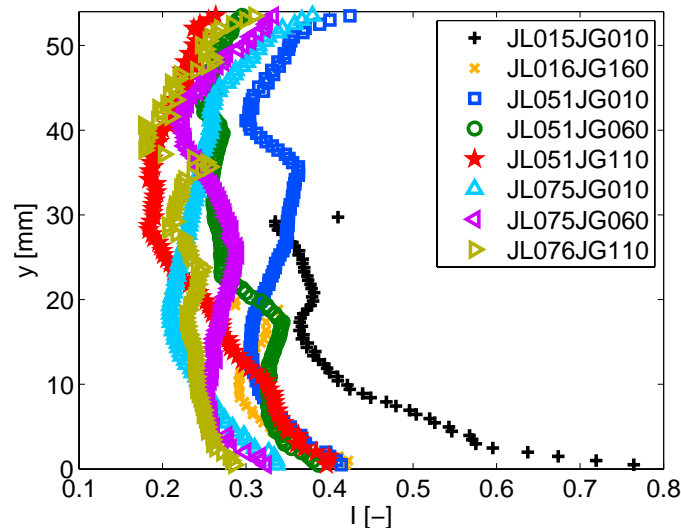
Figure 6.8: Turbulence intensity I.

Figure 6.9 shows the profiles of the mean integral turbulent length scale l_{tur} (given by equation 4.14). Physically, it represents the mean size of the large eddies in a turbulent flow, e.g. eddies with low frequency and large wavelength. It can be observed that the

lower values of the mean integral length scale are located near the pipe walls. For stratified and wavy flow, the mean integral turbulent length scale near the interface tends to zero. For elongated bubble and slug flows, the largest eddies are located in the central part of the pipe, achieving a value of about 30 mm ($\approx D/2$).
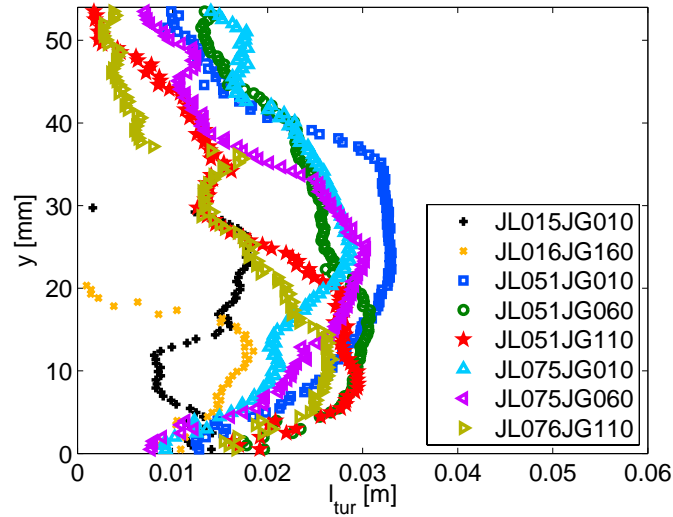
Figure 6.9: Integral turbulent length scale l_{tur}.

Figure 6.10 shows the influence of the inlet fluid velocities on the turbulence Reynolds number Re_{tur} (given by equation 4.13). The mean turbulence Reynolds number take the mean dimension of the turbulence structures and the intensity of the velocity fluctuations into account. The turbulence Reynolds number profiles show a smaller value near the
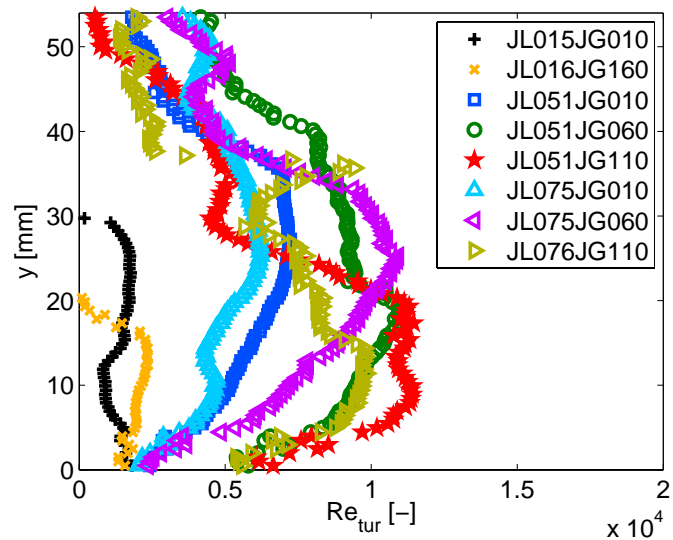
Figure 6.10: Turbulence Reynolds number Re_{tur}.

walls. For stratified and wavy flow, the turbulence Reynolds number tends to zero near the interface.

6.3 Moving Window Analysis

In order to understand the behaviour of the flow in different zones of a slug unit, data has been analysed with the so called "moving window" approach. This approach allows to study the flow field at specific zones of the slug unit. Data belonging to different parts of the slug region are put into separate bins. These are processed separately as already explained in section 4.2.2.7.

A total of 20 PIV/PS images have been processed in the same manner as for the "fixed window" analysis. Although the number of images is too limited to allow a statistical study, the results in this section nonetheless show the potential information that can be obtained with this analysis.

### 6.3.1 Velocity Quantities

Figure 6.11 shows how the velocity field develops through the slug region. The superficial liquid and gas velocities are $j_L =0.75$ m/s and $j_G =0.60$ m/s, respectively (which corresponds to plug-slug flow transition, $JL075JG060$). Every graph shows the mean axial velocity field $\overline{u}_x(x,y)$ at a different position from the slug nose (see equation 4.7). The first graph shows the mean axial velocity field at the slug tail, and the last one at the slug nose. In these images, the translational velocity of the leaving bubble tail and the arriving bubble nose have nearly the same value (approx. 1.8 m/s).

All the images of figure 6.11 show the impact of the pipe walls on the liquid flow. The mean axial average velocity is much smaller near the pipe walls than in the rest of the liquid field. The highest values of the mean axial velocity are found in the upper part of the pipe, behind the elongated bubble (see image $L = 0.0D$). The lowest values of the mean axial velocity are registered in the leaving film region. The liquid in this zone slows down due to the arriving liquid slug (pick-up process). Then, further down the liquid slug body, the mean velocity starts to drop in the upper part of the pipe and to increase in the bottom part of the pipe (see images $L = 0.6D$ and $L = 1.8D$) until the flow becomes fully developed (see image $L = 3.0D$). Then, the mean axial velocity increases in the central part of the pipe due to the arriving elongated bubble.

The profiles corresponding to figure 6.11 are shown in figure 6.12. The values for each profile have been picked in the center of the corresponding image. The graphs on the left show the x component, the graphs on the right show the y component.

At $L = 0.0D$, the x and the y components of the mean liquid velocity do not show any values at the position of the bubble. The mean axial velocity in the bottom part of the pipe (liquid zone) is two times smaller than the velocity in the upper region of the pipe
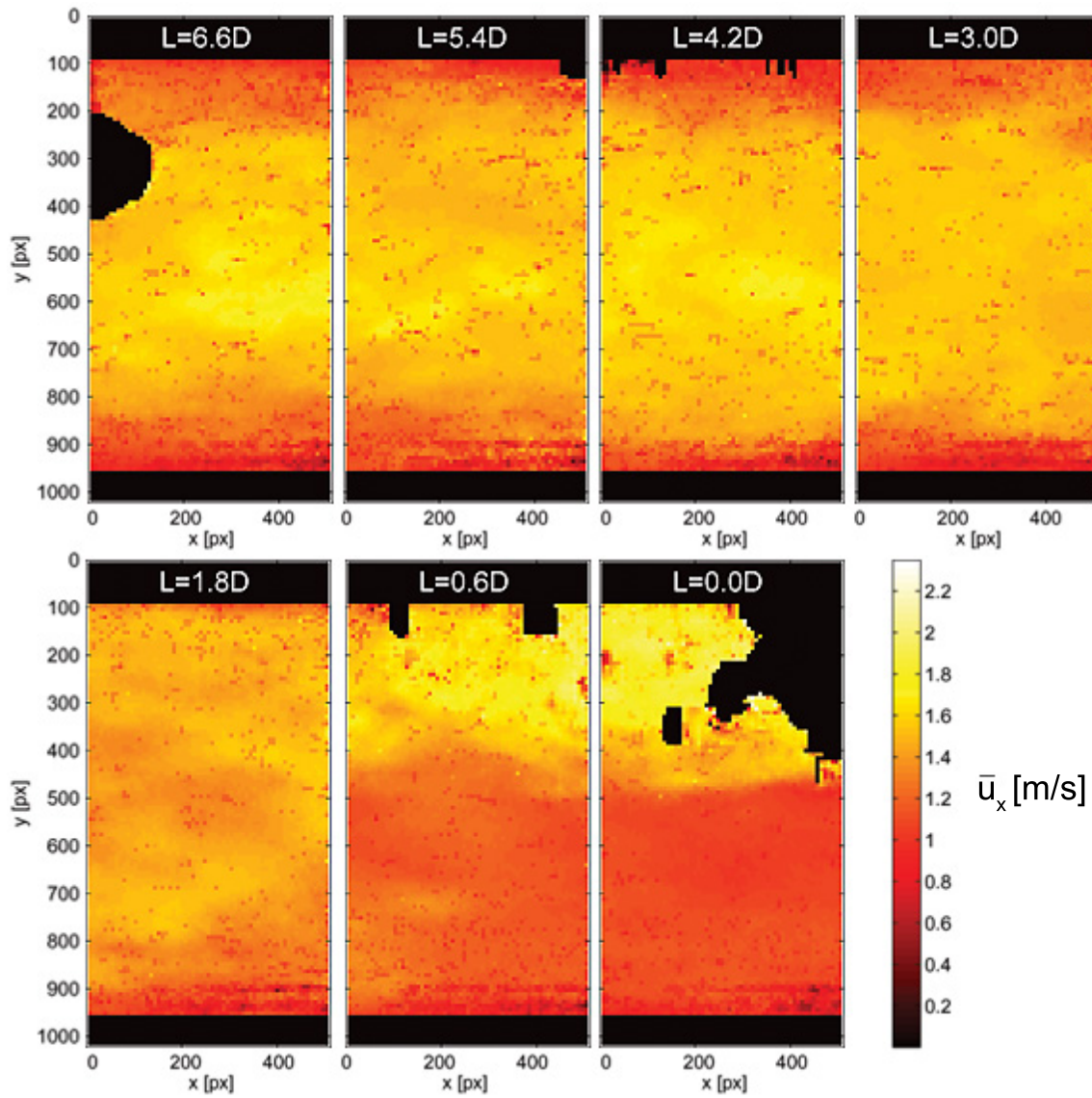
Figure 6.11: Development of the mean axial velocity field $\bar{u}_x(x,y)$ along the slug body.

(gas-liquid zone). The height of the preceding film has a value of around 36 mm. At the height of 28 mm, the axial velocity starts to increase, reaching the highest values in the central part of the gas-liquid region (45 mm). Below 28 mm, the vertical component of the velocity is close to zero. In the gas-liquid zone, the y component strongly oscillates between positive and negative values due to the arriving slug.

At $L = 0.6D$, the values of the mean axial velocity slightly increase in the bottom part of the pipe, and the values in the top region of the pipe decrease. The y component has negative values near the top of the pipe, reaching the highest negative value at 45 mm. At a height of 38 mm, the y component is zero and have a positive tendency towards the
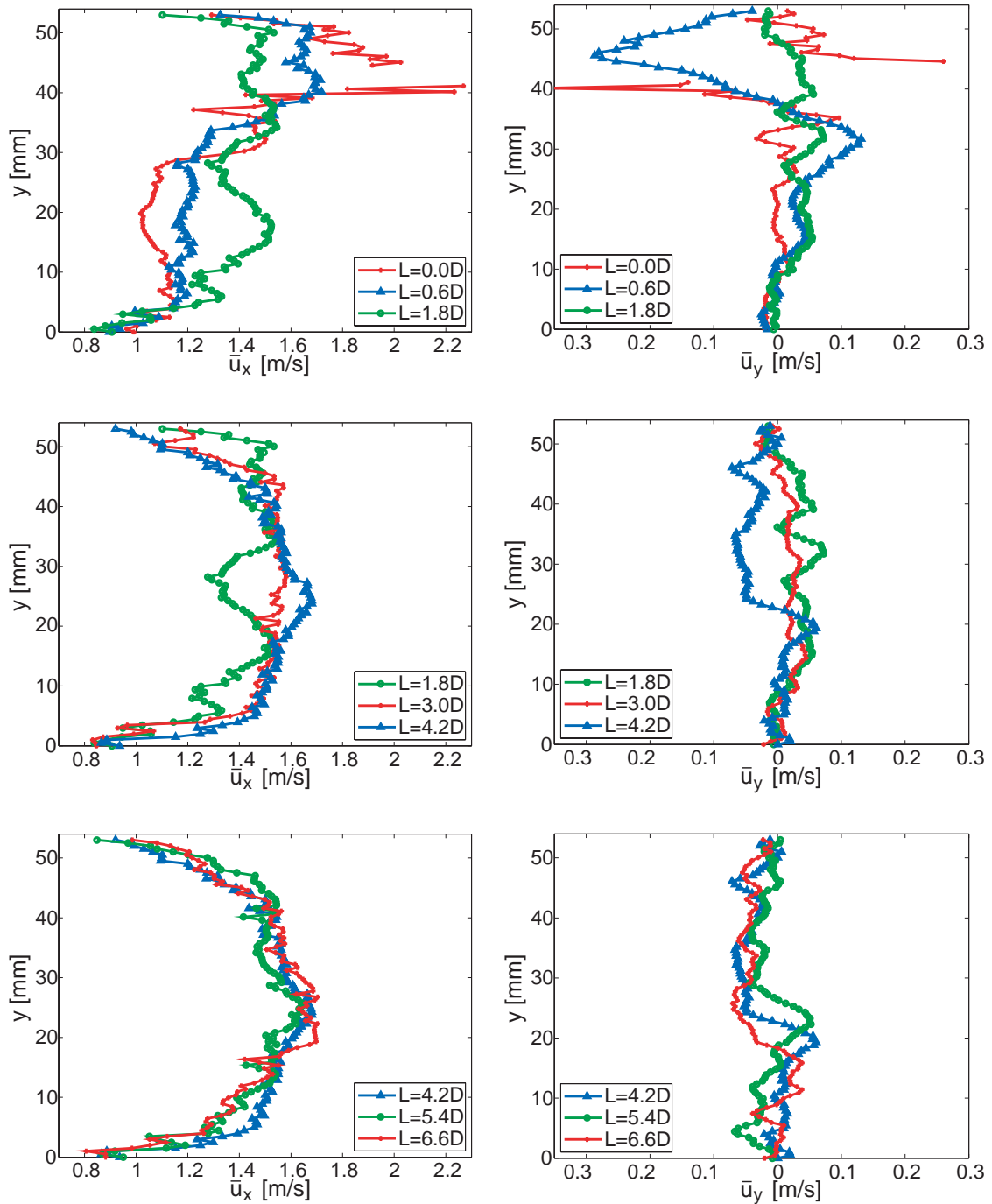
Figure 6.12: Mean velocity profiles along the slug body.

bottom. Below 12 mm, the vertical component of the mean velocity remains close to zero (this region is smaller at this position).

At $L = 1.8D$, the values of the axial velocity increase in the bottom part of the pipe, and the values in the top region of the pipe decrease even more than for the other profiles closer to the slug nose. However, the flow is not yet fully developed. The y component is positive above 8 mm. Above 8 mm, the vertical component of the mean velocity remains close to zero (this region becomes smaller).

At $L = 3.0D$, the profile of the mean velocity is fully developed for the x and y component. The axial mean velocity presents the typical turbulent profile. The vertical component of the mean velocity remains close to zero. Figure 6.13 shows the velocity profile at $L = 3.0D$ and the theoretical velocity profile for turbulent flows given by the following exponential relationship:

$$\bar{u} = \bar{u}_{max} \left(\frac{y}{R}\right)^n = \bar{u}_{max} \left(\frac{R-r}{R}\right)^n, \tag{6.1}$$

where the value of the exponent n depends on the Reynolds number ($n = 1/6$ for $Re = 4 \cdot 10^3$; $n = 1/7$ for $Re = 110 \cdot 10^3$; $n = 1/10$ for $Re = 3240 \cdot 10^3$ [Schlichting, 1982]). The relationship between the average value of the mean velocity $\bar{u}_m$ and the maximal value of the mean velocity $\bar{u}_{max}$ can be interpolated by:

$$\frac{\bar{u}_m}{\bar{u}_{max}} = \frac{2n^2}{(n+1)(2n+1)}. \tag{6.2}$$

For $n = 1/7$ is $\bar{u}_m = 0.816\,\bar{u}_{max}$. The mean velocity at $L = 3.0D$ shows a profile close to the $1/7$ potency law profile. This means that there is a zone after an entry length in the liquid slug, which does not notice the presence of the preceding elongated bubble or the arriving elongated bubble.

At $L = 4.2D$, the mean axial velocity increases near the central part of the pipe (between 20 mm and 30 mm), indicating that the flow starts to notice the arriving elongated bubble. The mean axial velocity drops slightly in the upper part of the pipe and increases in the bottom part of the pipe. The y component remains close to zero only below 10 mm, then the values become positive, having the biggest value at a height of 23 mm. Above 27 mm, the y component shows negative values.

At $L = 5.4D$ and $L = 6.6D$, the values of the mean axial velocity increase slightly in the upper part of the pipe and decrease in the bottom part of the pipe. The highest values of the mean axial velocity are still found near the central part of the pipe (region affected by the elongated bubble). The values of the y component are negative everywhere else.

It is observed that due to the pick-up process the y component of the mean velocity strongly oscillates behind the elongated bubble. For $L = 0.0D$ and $L = 0.6D$, the values of the y component of the mean velocity in the upper part of the pipe oscillate between positive and negative values and are much higher than all other values. This behaviour explains the
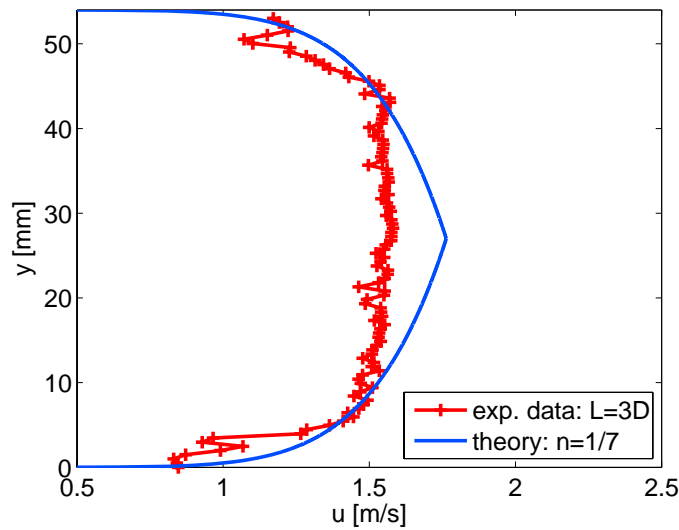
Figure 6.13: Turbulent velocity profile.

values of the *y* component obtained from the "fixed window analysis" (see section 6.2.1). The values of the *y* component behind the elongated bubble strongly affects the calculated mean vertical velocity for the operational points with $Fr_{crit} > 1.5$ (see figure 6.3).

Figure 6.14 and figure 6.15 show secondary velocity vectors at different positions from the slug nose. In these images, the liquid slug velocity ($u_{Ls} = U_M = 1.35$ m/s, see section 2.1) is subtracted from the mean liquid velocity ($\vec{u}(x,y) - \vec{U}_M$). The first graph of figure 6.14 shows the slug tail ($L = 6.6D$), and the last graph of figure 6.15 the slug nose ($L = 0.0D$).

In every image, the gaseous phase is covered with a mask. This mask represents the sum of all gas phase areas of every PIV/PS image which have been averaged. As mentioned in section 5.6.3, the bubbles move slower than the liquid in the slug. This can be seen in the images, especially at $L = 0.6D$. More or less, bubbles have a spherical form, but due to the lower velocity of the bubbles (the camera moves with the same velocity as the elongated bubble), the sum of the masks show an ellipsoidal form. The mask of image $L = 0.6D$ shows how the bouyancy forces cause the bubbles to migrate to the upper part of the pipe. The bubble velocity is lower than the liquid velocity, resulting the sum of the bubble masks in an ellipse.

In all the images, the impact of the pipe walls on the liquid flow is visible. As expected, the velocity vectors near the walls are negative, which means that the mean average velocity of the liquid flow near the walls is smaller than the mixture velocity. At $L = 0.0D$ and $L = 0.6D$, it can be clearly observed how the liquid is picked up from the preceding film. The velocity of the liquid in the film region has a lower velocity than the mixture velocity, so that the vectors shown in the image move towards the liquid slug. The liquid expands to the upper part of the pipe after a short entry length in the slug body. In the upper region of the pipe, the velocity of the liquid is much higher than the mixture velocity, so that all
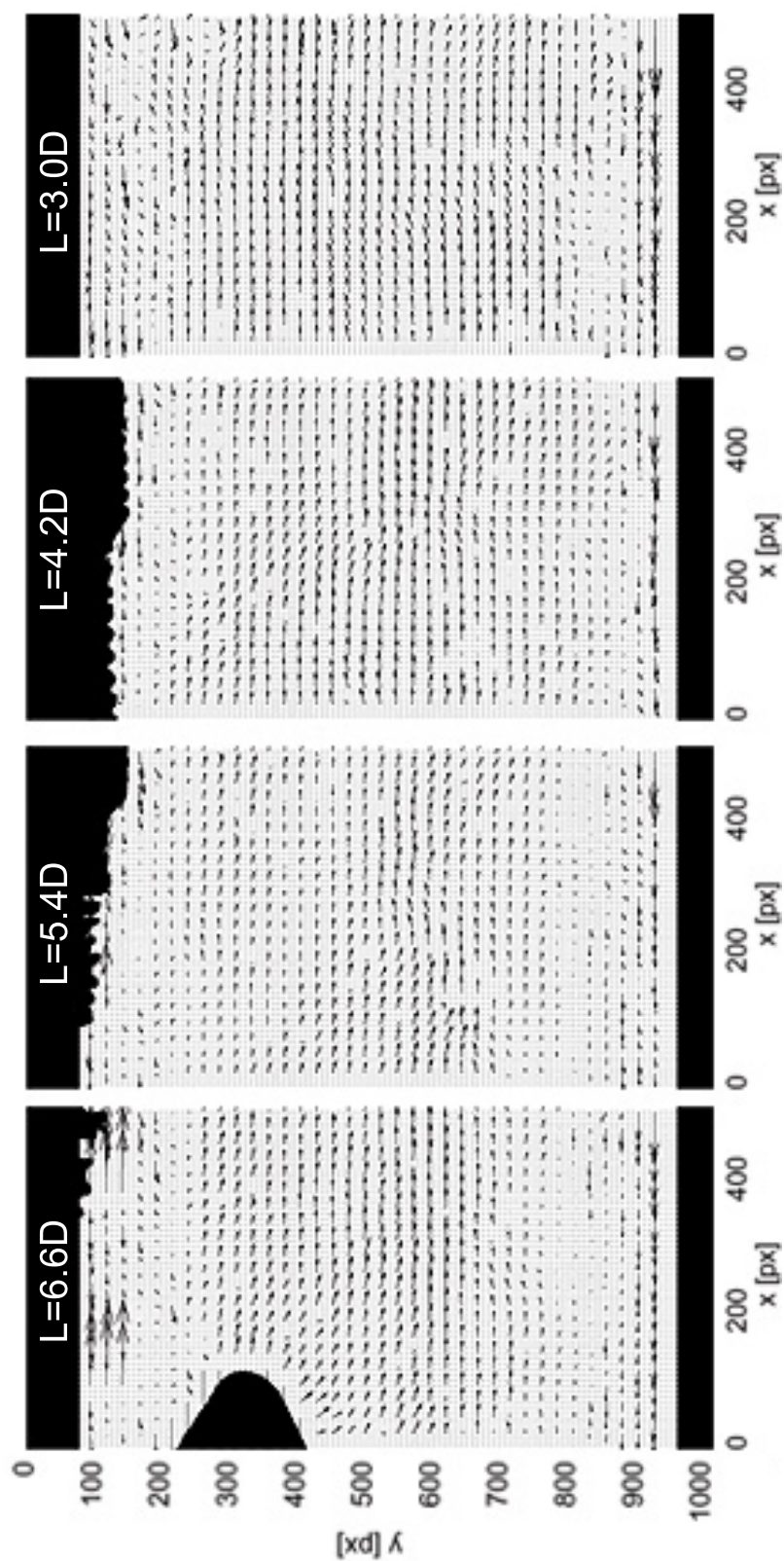
Figure 6.14: Secondary flow along the slug body: $\vec{\bar{u}} - \vec{U}_M$.
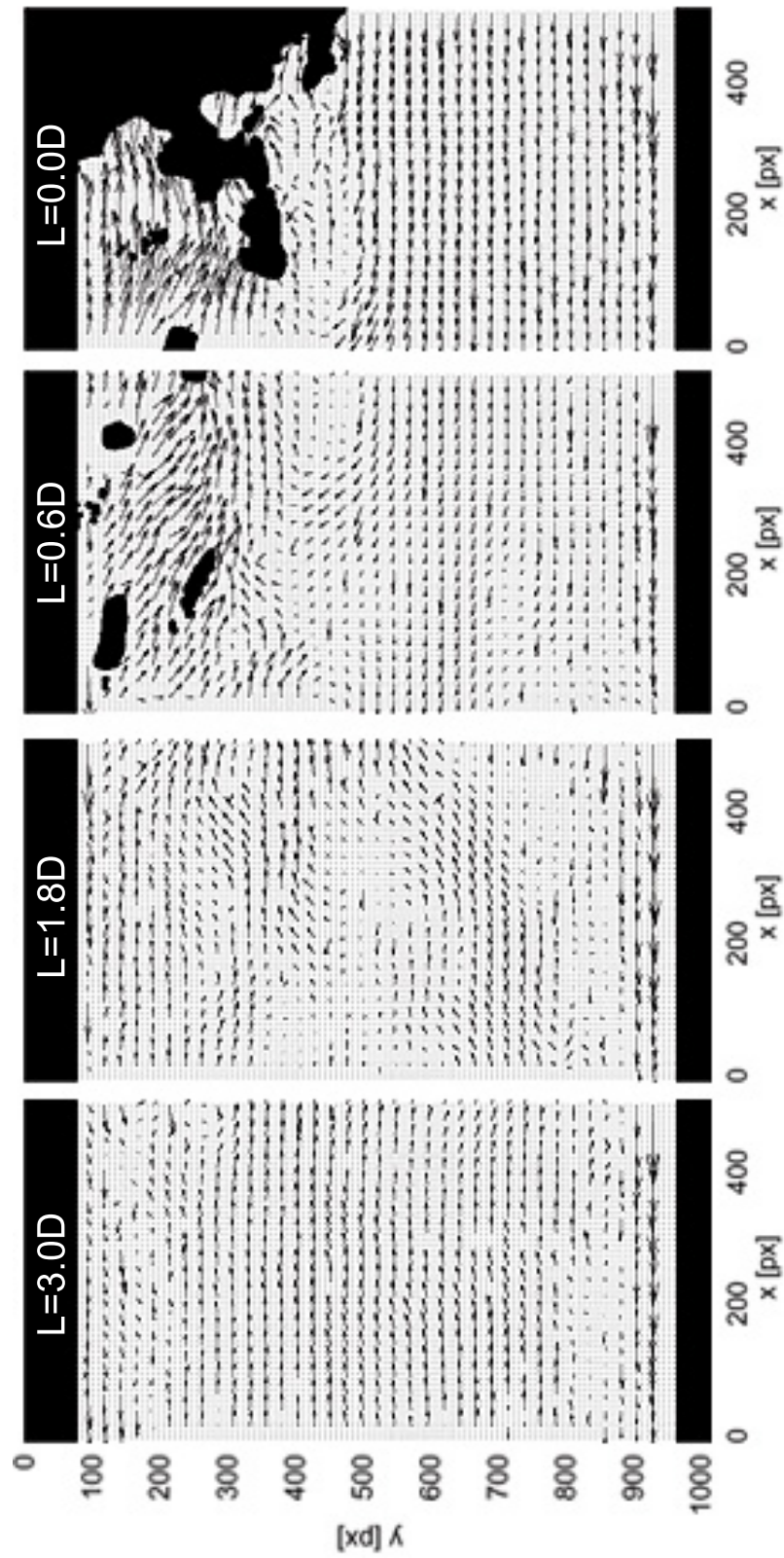
Figure 6.15: Secondary flow along the slug body: $\vec{u} - \vec{U}_M$.

vectors are positive in the axial direction. At $L = 1.8D$, there are still some structures to be seen, but from $L = 3.0D$ to $L = 6.6D$, all vectors of the liquid are positive in the axial direction. At this positions, the velocity of the liquid is larger than the mixture velocity.

7 Summary and Conclusions

The scope of this thesis is to gain insight into gas-liquid intermittent flows. The chaotic distribution of turbulent interfaces between the different phases and a full understanding of their nature make the prediction of the flow characteristics and the numerical modelling of such flows a difficult and challenging task for researchers. In this work, particular efforts have been devoted to the investigation of developing intermittent flows (plug and slug flows) in horizontal pipes in order to attain a thorough physical understanding of the internal structure of these two-phase flow patterns.

First, the modelling approaches existing in the literature were thoroughly reviewed and discussed.

An existing system code (ATHLET) for nuclear reactor analysis was applied for the prediction of different flow patterns, including stratified, wavy and intermittent flows, in an adiabatic horizontal pipe. The aim was to study the feasibility and accuracy of ATHLET simulations for an air-water two-phase flow in horizontal circular pipes. Using the ATHLET system code several simulations of the test facility were carried out.

A parametric study was executed on the regime boundaries. Different nodalisations were made depending on the flow characteristics. For intermittent flow, numerical instabilities were detected when the nodes were finer than 10 cm, probably due to the ill-posed nature of the equation set. For the prediction of intermittent flow, this means that the solution given by ATHLET is always sensitive to the size of the grid. However, in order to capture the patterns of the intermittent flow and its characteristics, a fine local nodalisation is strongly recommended if intermittent flow is present in the pipe.

The influence of steady/unsteady inlet boundary conditions on the flow characteristics was also studied. The results show that the boundary conditions have almost no influence on the slug characteristics. This result was to be expected, given that the onset of slug formation in the code depends on a critical value of the vapour phase velocity.

Several simulations were made in order to detect the transitions between stratified-wavy and intermittent flow. A discrepancy between the code predictions and the experimental data revealed that the correlation for the calculation of the interfacial shear stress coefficient was not correctly implemented in the code. The code was modified, thereby improving the prediction of the void fraction and the transition between stratified-wavy flow and intermittent flow.

The modified code is suitable to adequately predict the transition between stratified-wavy flow and intermittent flow for adiabatic flows. Under conditions promoting intermittent flow, continuous trains of slugs are predicted by the code if a sufficiently fine nodalisation is made. Transient phenomena such as slug growth, collapse or merging are captured by

the equations, but the inherent characteristics of intermittent flow, such as the slug frequency, the slug body lenght or the slug velocity are beyond the reach of the code. The code did not correctly predict neither the height of the film, nor the mean liquid fraction. These results were to be expected, since ATHLET 2.1A does not include models or closure relations to predict slug features. Moreover, the only flow pattern related constitutive model for adiabatic flows implemented in ATHLET is the interfacial shear force model. Although the flow pattern model implemented in ATHLET accounts for liquid entrainment into the gas phase, there is no correlation for the case of gas entrainment into the liquid phase. Bubble flow and intermittent flow in horizontal pipes are modelled in a similar manner. Better results might be achieved by means of a specific modelling of bubble entrainment into the liquid phase. A different modelling of the interfacial friction for bubble flow and for intermittent flows could lead to better agreement with the experimental data. Summarising, it can be stated that ATHLET 2.1A, though perfectly suited for the simulation of one-dimensional processes, proved insufficient for the representation of interactions of multiple factors, which determine not only the slug initiation, but also the inherent characteristics of intermittent flows.

Measuring techniques with high spatial and temporal resolution were used in the experimental part of this study in order to get detailed information on the behaviour of intermittent flows. Moreover, the experimental facility was carefully designed to fulfil the requirements of the study. The metering and controlling of the gas-liquid flow rates and the design of the two-phase mixing section, which define initial and boundary conditions of the experiment, were laid out with a view to clearly defined and quantified flow patterns. They allowed the boundary conditions of the different test cases to behave equally in the experiment and in the simulation. On the basis of the acquired data, an experimental database was created. It is suitable for the investigation of two-phase flows as well as for the validation of two-phase codes using already well-known models. Due to its detailed information on the two-phase flow field, the experimental data is particularly appropriate for the validation of 3D CFD codes.

Void fraction measurements were carried out by means of wire-mesh sensors. Four sensors were placed along the measuring test section to enable the study of the evolution of the flow pattern along the horizontal pipe. In order to further develop the physical understanding of intermittent flows, experimental data was acquired with careful attention to the boundaries between plug flow (also called elongated bubble flow) and slug flow. The literature usually differentiates plug and slug flow by the absence or presence of bubbles in the slug body. This work distinguishes within the intermittent regime between plug and slug flow depending on the shape of the bubble (nose and tail morphology) and the gas entrainment into the slug body. The transition from one regime to the other was studied, identifying two critical Froude numbers Fr_{crit} at which the slug morphology and the slug characteristics change.

For low mixture velocities ($Fr_{crit} \leq 1.5$), there is almost no aeration in the liquid slug and slugs are fairly large. The elongated bubble always presents a long thin tail. The slug drift velocity plays an important role for the calculation of the slug velocity. For $Fr_{crit} > 1.5$, the liquid slug starts to be aerated at the slug front and the thin tail dissapears.

The experimental data shows that there is a transition between plug and slug flow for $1.5 < Fr_{crit} < 3.0$. In this range, the drift velocity may be neglected. The length of the slug tends to decrease with increasing superficial liquid velocities. A higher superficial gas velocity also tends to produce shorter slugs. For $Fr_{crit} > 3.0$, the slug body starts to be strongly aerated. In this regime, the slug drift velocity should be taken into account for the calculation of the slug velocity. For $Fr_{crit} > 3.0$, the slug length approaches to a constant value with increasing mixture velocities.

As mentioned above, gas entrainment is an important factor for the determination of slug flow characteristics. In order to gain insight into the gas entrainment phenomenon, experimental data of the bubbles dispersed in the liquid slug was acquired by means of four wire-mesh sensors at two different positions from the inlet. Not only the behaviour of the dispersed bubbles was studied in detail along the slug body, but also their number, velocity and vertical average position were analysed for different groups of bubble sizes. Given that literature on the behaviour of bubbles dispersed in the slug body is scarce, it may be assumed that no prior experiment of the kind described in this work has yet been conducted.

The experimental data shows that the average number of bubbles generally increases with increasing mixture velocities. Independently of the inlet velocities, the highest number of bubbles is found in the mixing region. Moreover, higher gas velocities have a higher number of bubbles in the mixing region. At low mixture velocities, almost no bubbles are found at the slug tail. At higher inlet superficial velocities, the bubbles are better distributed along the slug body, nonetheless, a decrease in the number of bubbles occurs toward the slug tail.

In a water slug, bubbles move slower than the liquid. The average velocity of the bubbles is slightly slower than the slug tail velocity. This means that the dispersed bubbles in the liquid slug will be caught up by the arriving elongated bubble. The average axial velocity of the bubbles in the slug body increases with increasing mixture velocities.

Despite buoyancy, the bubbles move towards the bottom of the pipe due to the pick-up process in the mixing region. Afterwards, they start rising until a certain vertical position is reached. This position remains constant towards the end of the slug body. Operating points with the same inlet gas velocities reveal bubbles at similar positions along the slug body. The ascent velocity of the bubbles is similar for all the operating points.

The average size of the dispersed bubbles in the liquid slug also changes at a critical Froude number. For $Fr_{crit} < 3.0$, the average volume of the dispersed bubbles drops with increasing mixture velocities. The experimental data shows a transition between plug and slug flow for $1.5 < Fr_{crit} < 3.0$. For $Fr_{crit} > 3.0$, the average volume of the bubbles increases slightly with increasing mixture velocities. In the mixing region the bubbles are smaller. Towards the slug tail, they become larger due to coalescence.

The number of bubbles, their vertical average position and the bubble size versus the time show to be influenced by the mixture length (pick-up process). The number of bubbles is larger, and their vertical average position and the bubble size drop in this region (behind

the elongated bubble). The mixture length is not linked to the length of the slug body. It increases with increasing inlet gas velocities.

The number of bubbles in the liquid slug drops with increasing bubble sizes. Bubbles tend to coalesce along the liquid slug. The highest number of bubbles for all operating points is found for bubble volumes between 6.52 mm^3 and 11.07 mm^3, which corresponds to a diameter of 2.32 mm and 2.76 mm, respectively. Larger bubbles have slightly higher ascent and axial velocities. The velocity of the bubbles increases moderately with its size. Larger bubbles tend to be at higher vertical positions in the pipe cross section. This was to be expected, as buoyancy has a smaller influence on smaller bubbles.

The Particle Image Velocimetry (PIV) technique and Pulsed Shadowgraph (PS) technique were used simultaneously and adapted for horizontal two-phase pipe flows in order to get detailed information on the flow field in the liquid phase. The technical difficulties of this task as well as the limitations of these measuring techniques for horizontal two-phase flows are discussed. The velocity fields of stratified, wavy, plug and slug flows were extracted from PIV/PS images with high resolution and statistically analysed. Given that literature on velocity fields of intermittent flows is scarce, it may be assumed that no prior measurements of the kind described in this work has yet been conducted.

The experimental data shows also here that there is a transition between plug and slug flow near $Fr_{crit} = 1.5$. The y component of the mean velocity shows a different secondary flow at the vertical pipe cross section for operating points with $Fr_{crit} \leq 1.5$ and for operating points with $Fr_{crit} > 1.5$.

Two different approaches were carried out for the statistical calculations in elongated bubble flow. The "fixed window analysis" permits the study of the flow from the point of view of a static camera. The "moving window analysis" allows the study from the point of view of a virtual camera that moves at the same speed as the elongated bubble. Both approaches use the same conditional averaging method, but while the fixed window analysis processes the PIV/PS images containing different parts of a slug unit as a whole, the moving window analysis cuts these images in specific parts of the slug zones and studies them separately. The moving window analysis gives a better insight into the behaviour of the different zones of a slug unit. The evolution of the velocity profiles along the liquid slug was presented and the kinematics of the intermittent regime is elucidated, extending the physical understanding of these flows. The experimental data show a zone after an entry length in the liquid slug, which does not notice the presence of the preceding elongated bubble or the arriving elongated bubble. The measurement data showed that the mean velocity of the y component is close to cero and the mean axial velocity presents the typical turbulent profile. The mean velocity after aprox. $3.0D$ from the elongated bubble shows a profile close to the velocity profile given by the $1/7$ potency law.

Future research work in the field of transient intermittent flows may be conducted making vaster use of the simultaneous PIV/PS technique. It may be very interesting to measure the third component of the velocity by means of a simultaneous PIV/PS technique with two cameras. This would allow the study of the secondary flow which develops due to the cylindrical form of the pipe.

Bibliography

[Abdul-Majeed 2000] ABDUL-MAJEED, G. H.: Liquid slug holdup in horizontal and slightly inclined two-phase slug flow. In: *Journal of Petroleum Science and Engineering* 27 (2000), pp. 27–32

[Andreussi and Bendiksen 1989] ANDREUSSI, P. ; BENDIKSEN, K.: An investigation of void fraction in liquid slugs for horizontal and inclined gas-liquid pipe flow. In: *International Journal of Multiphase Flow* 15 (1989), No. 6, pp. 937–946

[Andreussi et al. 1993] ANDREUSSI, P. ; MINERVINI, A. ; PAGLIANTI, A.: Mechanistic model of slug flow in near-horizontal pipes. In: *AIChE Journal* 39 (1993), No. 8, pp. 1281–1291

[Austregesilo et al. 2006] AUSTREGESILO, H. ; BALS, C. ; HORA, A. ; LERCHL, G. ; ROMSTEDT, P.: *ATHLET Mod 2.1. Cycle A - Models and Methods*. GRS-P-1 / Vol. 4, July, 2006

[Baker 1954] BAKER, O.: Designing for simultaneous flow of oil and gas. In: *Oil and Gas Journal* 53 (1954), No. 12, pp. 185–195

[Barnea 1987] BARNEA, D.: A unified model for predicting flow-pattern transitions for the whole range of pipe inclinations. In: *International Journal of Multiphase Flow* 13 (1987), No. 1, pp. 1–12

[Barnea and Brauner 1985] BARNEA, D. ; BRAUNER, N.: Holdup of the liquid slug in two phase intermittent flow. In: *International Journal of Multiphase Flow* 11 (1985), No. 1, pp. 43–49

[Barnea and Taitel 1993] BARNEA, D. ; TAITEL, Y.: A model for slug length distribution in gas liquid slug flow. In: *International Journal of Multiphase Flow* 19 (1993), No. 5, pp. 829–838

[Barnea and Taitel 1994] BARNEA, D. ; TAITEL, Y.: Interfacial and structural stability of seperated flow. In: *International Journal of Multiphase Flow* 20 (1994), pp. 387–414

[Bendiksen and Espedal 1992] BENDIKSEN, K. ; ESPEDAL, M.: Onset of slugging in horizontal gas-liquid pipe flow. In: *International Journal of Multiphase Flow* 18 (1992), No. 2, pp. 237–247

[Bendiksen 1984] BENDIKSEN, K. H.: An experimental investigation of the motion of long bubbles in inclined tubes. In: *International Journal of Multiphase Flow* 10 (1984), No. 4, pp. 467–483

[Bendiksen et al. 1996]   BENDIKSEN, K. H. ; MALNES, D. ; NYDAL, O. J.:   On the modelling of slug flow. In: *Chem. Eng. Comm.* 141-142 (1996), pp. 71–102

[Bonizzi 2003]   BONIZZI, M.: *Transient one-dimensional modelling of multiphase slug flows*, Department of Mechanical Engineering, Imperial College London, Dissertation, 2003

[Brill et al. 1981]   BRILL, J. P. ; SCHMIDT, Z. ; COBERLY, W. A. ; HERRING, J. D. ; MOORE, D. W.:   Analysis of two-phase tests on large-diameter flow lines in Prudhoe Bay Field. In: *Society of Petroleum Engineers Journal* 21 (1981), pp. 363–378

[Broeder and Sommerfeld 2002]   BROEDER, D. ; SOMMERFELD, M.:   An advanced LIF-PLV system for analysing the hydrodynamics in a laboratory bubble column at higher void fractions. In: *Experiments in Fluids* 33 (2002), pp. 826–837

[Carpintero-Rogero et al. 2006]   CARPINTERO-ROGERO, E. ; KROESS, B. ; SATTEL-MAYER, T.:   Simultaneous HS-PIV and shadowgraph measurements of gas-liquid flows in a horizontal pipe. In: *13th Int. Symp. on Applications of Laser Techniques to Fluid Mechanics, Lisbon, Portugal, 26-29 June*, 2006

[Chisholm 1967]   CHISHOLM, D.:   A theoretical basis for the Lockhart-Martinelli correlation for two-phase flow. In: *International Journal Heat Mass Transfer* 10 (1967), No. 12, pp. 1767–1778

[Chisholm 1983]   CHISHOLM, D.: *Two-phase flow in pipelines and heat exchangers.* George Godwin, Longman Inc., New York, 1983

[Cook and Behnia 1997]   COOK, M. ; BEHNIA, M.:   Film profiles behind liquid slugs in gas-liquid pipe flow. In: *AIChE Journal* 43 (1997), No. 9, pp. 2180–2186

[Cook and Behnia 2000a]   COOK, M. ; BEHNIA, M.:   Pressure drop calculation and modelling of inclined intermittent gas-liquid flow. In: *Chemical Engineering Science* 55 (2000), pp. 4699–4708

[Cook and Behnia 2000b]   COOK, M. ; BEHNIA, M.:   Slug length prediction in near horizontal gas-liquid intermittent flow. In: *Chemical Engineering Science* 55 (2000), pp. 2009–2018

[De Henau and Raithby 1995a]   DE HENAU, V. ; RAITHBY, G. D.:   A transient two-fluid model for the simulation of slug flow in pipelines - I. Theory. In: *International Journal of Multiphase Flow* 21 (1995), No. 3, pp. 335–349

[De Henau and Raithby 1995b]   DE HENAU, V. ; RAITHBY, G. D.:   A transient two-fluid model for the simulation of slug flow in pipelines - II. Validation. In: *International Journal of Multiphase Flow* 21 (1995), No. 3, pp. 351–363

[Dukler and Hubbard 1975]   DUKLER, A. E. ; HUBBARD, M. G.: A model for gas-liquid slug flow in horizontal and near horizontal tubes. In: *Industrial and Engineering Chemistry Fundamentals* 14 (1975), No. 4, pp. 337–347

[Dukler et al. 1985]   DUKLER, A. E. ; MARON, D. M. ; BRAUNER, N.: A model for predicting the minimum stable slug length. In: *Chemical Engineering Science* 40 (1985), No. 8, pp. 1379–1385

[Fabre and Liné 1992]   FABRE, J. ; LINÉ, A.: Modelling of two phase slug flow. In: *Ann. Rev. Fluid Mech.* 24 (1992), pp. 21–46

[Fagundes Netto et al. 1999]   FAGUNDES NETTO, J. R. ; FABRE, J. ; PERESSON, L.: Shape of long bubbles in horizontal slug flow. In: *International Journal of Multiphase Flow* 25 (1999), No. 6-7, pp. 1129–1160

[Fujiwara et al. 2004]   FUJIWARA, A. ; DANMOTO, Y. ; HISHIDA, K. ; MAEDA, M.: Bubble deformation and flow structure measured by double shadow images and PIV/LIF. In: *Experiments in Fluids* 36 (2004), pp. 157–165

[Gregory et al. 1978]   GREGORY, G. A. ; NICHOLSON, M. K. ; AZIZ, K.: Correlation of the liquid volume fraction in the slug for horizontal gas-liquid slug flow. In: *International Journal of Multiphase Flow* (1978), No. 1, pp. 33–39

[Gregory and Scott 1969]   GREGORY, G. A. ; SCOTT, D. S.: Correlation of liquid slug velocity and frequency in horizontal cocurrent gas-liquid slug flow. In: *AIChE Journal* 15 (1969), No. 6, pp. 933–935

[Greskovich and Shrier 1972]   GRESKOVICH, E. J. ; SHRIER, A. L.: Slug frequency in horizontal gas-liquid slug flow. In: *Ind. Eng. Chem. Process Des. Develop.* 11 (1972), No. 2, pp. 317–318

[Griffith and Wallis 1961]   GRIFFITH, P. ; WALLIS, G. B.: Two-phase slug flow. In: *Journal of Heat Transfer* 83 (1961), pp. 307–320

[Grotjahn 2001]   GROTJAHN, K.: *Transienten zweiphasiger Schwallströmungen aus Gasen und Flüssigkeiten in horizontalen Rohren*, Universität Hannover, Dissertation, 2001

[Hale 2000]   HALE, C. P.: *Slug formation, growth and decay in gas-liquid flows*, Department of Chemical Engineering and Chemical Technology, Imperial College of Science, Technology and Medicine, University of London, Dissertation, 2000

[Hassan 2003]   HASSAN, Y. A.: Dancing bubbles in turbulent flows: PIV measurement and analysis / Department of Nuclear Engineering, College Station, Texas. 2003. – Technical report

[Hassan et al. 1998]   HASSAN, Y. A. ; SCHMIDT, W. ; ORTIZ-VILLAFUERTE, J.: Investigation of three-dimensional two-phase flow structure in a bubbly pipe flow. In: *Meas. Sci. Technol.* 9 (1998), pp. 309–326

[Hewitt 2002]   HEWITT, G. F.: Computer codes. In: *Short Course: Modelling and Computation of Multiphase Flows, Zurich, Switzerland, 18-22 March*, 2002

[Heywood and Richardson 1979]   HEYWOOD, N. I. ; RICHARDSON, J. F.: Slug flow of air-water mixtures in a horizontal pipe: determination of liquid holdup by y-ray absorption. In: *Chemical Engineering Science* 34 (1979), pp. 17–30

[Hughmark 1965]   HUGHMARK, G. A.: Holdup and heat transfer in horizontal slug gas-liquid flow. In: *Chemical Engineering Science* 20 (1965), pp. 1007–1010

[Hurlburt and Hanratty 2002]   HURLBURT, E. T. ; HANRATTY, T. J.: Prediction of the transition from stratified to slug and plug flow for long pipes. In: *International Journal of Multiphase Flow* 28 (2002), No. 5, pp. 707–729

[Issa and Kempf 2003]   ISSA, R. I. ; KEMPF, M. H. W.: Simulation of slug flow in horizontal and nearly horizontal pipes with the two-fluid model. In: *International Journal of Multiphase Flow* 29 (2003), No. 1, pp. 69–95

[Issa and Woodburn 1998]   ISSA, R. I. ; WOODBURN, P. J.: Numerical prediction of instabilities and slug formation in horizontal two-phase flows. In: *3rd Int. Conf. Multiphase Flow, ICMF'98, Lyon, France,6-10 June*, 1998

[Kitagawa et al. 2005]   KITAGAWA, A. ; HISHIDA, K. ; KODAMA, Y.: Flow structure of microbubble-laden turbulent channel flow measured by PIV combined with the shadow image technique. In: *Experiments in Fluids* 38 (2005), pp. 466–475

[Kolev 2007]   KOLEV, N. I.: *Multiphase flow dynamics*. Springer-Verlag Berlin Heidelberg, 2007

[Lin and Hanratty 1986]   LIN, P. Y. ; HANRATTY, T. J.: Prediction of the initiation of slugs with linear stability theory. In: *International Journal of Multiphase Flow* 12 (1986), No. 1, pp. 79–98

[Lin and Hanratty 1987]   LIN, P. Y. ; HANRATTY, T. J.: Detection of slug flow from pressure measurements. In: *International Journal of Multiphase Flow* 13 (1987), No. 1, pp. 13–21

[Lindken 2002]   LINDKEN, R.: *Ein kombiniertes PIV/LIF/Schatten-Verfahren für Turbulenzmessungen in Blasenströmungen*, Universität GH Essen, Dissertation, 2002

[Lindken and Merzkirch 2002]   LINDKEN, R. ; MERZKIRCH, W.: A novel PIV technique for measurements in multiphase flows and its application to two-phase bubbly flows. In: *Experiments in Fluids* 33 (2002), pp. 814–825

[Lockhart and Martinelli 1949]   LOCKHART, R. W. ; MARTINELLI, R. C.: Proposed correlation of data for isothermal two-phase, two-component flow in pipes. In: *Chem. Engng. Prog.* 45 (1949), No. 1, pp. 39–48

[Mandhane et al. 1974]   MANDHANE, J. M. ; GREGORY, G. A. ; AZIZ, K.: A flow pattern map for gas-liquid flow in horizontal pipes. In: *International Journal of Multiphase Flow* 1 (1974), pp. 537–553

[Martinelli and Nelson 1948]   MARTINELLI, R. C. ; NELSON, D. B.: Prediction of pressure drop during forced-circulation boiling of water. In: *Trans. ASME* 70 (1948), pp. 695–702

[Mayinger 1982]   MAYINGER, F.: *Strömung und Wärmeübergang in Gas-Flüssigkeitsgemischen.* Springer-Verlag Wien New York, 1982

[Mishima and Ishii 1980]   MISHIMA, K. ; ISHII, M.: Theoretical prediction of onset of horizontal slug flow. In: *Journal of Fluids Engineering* 102 (1980), pp. 441–445

[Moissis and Griffith 1962]   MOISSIS, R. ; GRIFFITH, P.: Entrance effects in a two-phase slug flow. In: *Journal of Heat Transfer* 84 (1962), pp. 29–39

[Nicholson et al. 1978]   NICHOLSON, M. K. ; AZIZ, K. ; GREGORY, G. A.: Intermittent two phase flow in horizontal pipes: predictive models. In: *The Canadian Journal of Chemical Engineering* 56 (1978), pp. 653–663

[Nicklin et al. 1962]   NICKLIN, D. J. ; WILKES, J. O. ; DAVIDSON, J. F.: Two-phase flow in vertical tubes. In: *Trans. Inst. Chem. Eng.* 40 (1962), pp. 61–68

[Nogueira et al. 2003]   NOGUEIRA, S. ; SOUSA, R. G. ; PINTO, A. M. F. R. ; RIETH-MULLER, M. L. ; CAMPOS, J. B. L. M.: Simultaneous PIV and pulsed shadow technique in slug flow: a solution for optical problems. In: *Experiments in Fluids* 35 (2003), pp. 598–609

[Nydal and Andreussi 1991]   NYDAL, O. J. ; ANDREUSSI, P.: Gas entrainment in a long liquid slug advancing in a near horizontal pipe. In: *International Journal of Multiphase Flow* 17 (1991), No. 2, pp. 179–189

[Nydal and Andreussi 1993]   NYDAL, O. J. ; ANDREUSSI, P.: Gas entrainment in liquid slugs. In: *Proceedings of the Third International Offshore and Polar Engineering Conference, Singapore, 6-11 June*, 1993

[Nydal and Banerjee 1996]   NYDAL, O. J. ; BANERJEE, S.: Dynamic slug tracking simulations for gas-liquid flow in pipelines. In: *Chem. Eng. Comm.* 141 (1996), pp. 13–39

[Nydal et al. 1992]   NYDAL, O. J. ; PINTUS, S. ; ANDREUSSI, P.: Statistical characterization of slug flow in horizontal pipes. In: *International Journal of Multiphase Flow* 18 (1992), No. 3, pp. 439–452

[Prasser et al. 1998]   PRASSER, H.-M. ; BOETTGER, A. ; ZSCHAU, J.: A new electrode-mesh tomograph for gas-liquid flows. In: *Flow Measurement and Instrumentation* 9 (1998), pp. 111–119

[Prasser et al. 2001]   PRASSER, H.-M. ; SCHOLZ, D. ; ZIPPE, C.: Bubble size measurement using wire-mesh sensors. In: *Flow Measurement and Instrumentation* 12 (2001), pp. 299–312

[Raffel et al. 1998]   RAFFEL, M. ; WILLERT, C. ; KOMPENHANS, J.: *Particle Image Velocimetry*. Springer-Verlag Berlin Heidelberg New York, 1998

[Renault 2007]   RENAULT, F.: *A Lagrangian slug capturing scheme for gas-liquid flows in pipes*, Norwegian University of Science and Technology, Faculty of Engineering Science and Technology, Department of Energy and Process Engineering, Dissertation, 2007

[Ruder et al. 1989]   RUDER, Z. ; HANRATTY, P. J. ; HANRATTY, T. J.: Necessary conditions for the existence of stable slugs. In: *International Journal of Multiphase Flow* 15 (1989), No. 2, pp. 209–226

[Ruder and Hanratty 1990]   RUDER, Z. ; HANRATTY, T. J.: A definition of gas-liquid plug flow in horizontal pipes. In: *International Journal of Multiphase Flow* 16 (1990), No. 2, pp. 233–242

[Schlichting 1982]   SCHLICHTING, H.: *Grenzschicht-Theorie*. G. Braun GmbH, Karlsruhe, 1982

[Taitel 1987]   TAITEL, Y.: Effect of gas expansion on slug length in long pipelines. In: *International Journal of Multiphase Flow* 13 (1987), No. 5, pp. 629–637

[Taitel and Barnea 1990a]   TAITEL, Y. ; BARNEA, D.: A consistent approach for calculating pressure drop in inclined slug flow. In: *Chemical Engineering Science* 45 (1990), No. 5, pp. 1199–1206

[Taitel and Barnea 1990b]   TAITEL, Y. ; BARNEA, D.: Two-phase slug flow. In: *Advances in Heat Transfer* 20 (1990), pp. 83–90

[Taitel and Barnea 1998]   TAITEL, Y. ; BARNEA, D.: Effect of gas compressibility in a slug tracking model. In: *Chemical Engineering Science* 53 (1998), No. 11, pp. 2089–2097

[Taitel et al. 1980]   TAITEL, Y. ; BORNEA, D. ; DUKLER, A. E.: Modelling flow pattern transitions for steady upward gas-liquid flow in vertical tubes. In: *AIChE Journal* 26 (1980), pp. 345–354

[Taitel and Dukler 1976]   TAITEL, Y. ; DUKLER, A. E.: A model for predicting flow regime transitions in horizontal and near horizontal gas-liquid flow. In: *AIChE Journal* 22 (1976), No. 1, pp. 47–55

[Taitel and Dukler 1977] TAITEL, Y. ; DUKLER, A. E.: A model for slug frequency during gas-liquid flow in horizontal and near horizontal pipes. In: *International Journal of Multiphase Flow* 3 (1977), No. 6, pp. 585– 596

[Taitel et al. 2000] TAITEL, Y. ; SARICA, C. ; BRILL, J. P.: Slug flow modelling for downward inclined pipe flow: theoretical considerations. In: *International Journal of Multiphase Flow* 26 (2000), No. 5, pp. 833–844

[Tokuhiro et al. 1998] TOKUHIRO, A. ; MAEKAWA, M. ; IIZUKA, K. ; HISHIDA, K. ; MAEDA, M.: Turbulent flow past a bubble and an ellipsoid using shadow-image and PIV techniques. In: *International Journal of Multiphase Flow* 24 (1998), No. 8, pp. 1383–1406

[Tomiyama 1998] TOMIYAMA, A.: Struggle with computational bubble dynamics. In: *Multiphase Science and Technology* 10 (1998), pp. 369–405

[Tronconi 1990] TRONCONI, E.: Prediction of slug frequency in horizontal two-phase slug flow. In: *AIChE Journal* 36 (1990), No. 5, pp. 701–709

[Ujang 2003] UJANG, P. M.: *Studies of slug initiation and development in two-phase gas-liquid pipeline flow*, Department of Chemical Engineering and Chemical Technology, Imperial College London, Dissertation, 2003

[Ujang et al. 2006] UJANG, P. M. ; LAWRENCE, C. J. ; HALE, C. P. ; HEWITT, G. F.: Slug initiation and evolution in two-phase horizontal flow. In: *International Journal of Multiphase Flow* 32 (2006), No. 5, pp. 527–552

[Wallis 1969] WALLIS, G. B.: *One-dimensional two-phase flow*. McGraw-Hill Book Company, New York, 1969

[Wallis and Dobson 1973] WALLIS, G. B. ; DOBSON, J. E.: The onset of slugging in horizontal stratified air-water flow. In: *International Journal of Multiphase Flow* 1 (1973), pp. 173–193

[Woods and Hanratty 1996] WOODS, B. D. ; HANRATTY, T. J.: Relation of slug stability to shedding rate. In: *International Journal of Multiphase Flow* 22 (1996), No. 5, pp. 809–828

[Woods and Hanratty 1999] WOODS, B. D. ; HANRATTY, T. J.: Influence of Froude number on physical processes determining frequency of slugging in horizontal gas-liquid flows. In: *International Journal of Multiphase Flow* 25 (1999), No. 6-7, pp. 1195–1223

[Zheng et al. 1994] ZHENG, G. ; BRILL, J. P. ; TAITEL, Y.: Slug flow behaviour in a hilly terrain pipeline. In: *International Journal of Multiphase Flow* 20 (1994), No. 1, pp. 63–79

[Zuber and Findlay 1965] ZUBER, N. ; FINDLAY, J. A.: Volumetric concentration in two-phase flow systems. In: *Journal of Heat Transfer* 87 (1965), pp. 453–468